Christopher Mosser, BSc

Numerical Study on the Behaviour of Soil Nails

MASTER'S THESIS

to achieve the university degree of

Diplom-Ingenieur

Master's degree programme: Civil Engineering, Geotechnics and Hydraulics

submitted to

Graz University of Technology

Supervisor

Ass.Prof. Dipl.-Ing. Dr.techn.

Franz Tschuchnigg

Institute of Soil Mechanics and Foundation Engineering

Second supervisor

Univ.-Prof. Dipl.-Ing. Dr.techn. Roman Marte

Graz, May 2016

Eidesstattliche Erklärung

Ich erkläre an Eides statt, dass ich die vorliegende Arbeit selbstständig verfasst, andere als die angegebenen Quellen/Hilfsmittel nicht benutzt, und die den benutzten Quellen wörtliche und inhaltlich entnommene Stellen als solche kenntlich gemacht habe.

Graz, am …… ……

(Unterschrift)

Statutory declaration

I declare that I have authored this thesis independently, that I have not used other than the declared sources / resources, and that I have explicitly marked all material which has been quoted either literally or by content from the used sources.

Graz, …… ……

(signature)

Preface of the author

I am using this opportunity to express my gratitude to all the people who contributed to the success of my studies and finally this master thesis.

I express my warm thanks to Univ.-Prof. Dipl.-Ing. Dr.techn. Roman Marte and Ass.Prof. Dipl.-Ing. Dr.techn. Franz Tschuchnigg for giving me the opportunity to pursue this thesis under their guidance and supervision. Special thanks are directed to Franz for his extraordinary support and the helpful discussions during the project work.

I want to thank all my friends and colleagues, especially those of the 'Geotechnik Zeichensaal'. You made every single term of my studies unforgettable and contributed to an amazing phase of my life.

Dear Jennifer, thank you for your endless patience and being my driving force to complete this thesis. I am also grateful for your excellent review of this work.

Finally, my biggest debt of gratitude goes to my mother, who enabled my life journey and supported my educational choice.

Kurzfassung

Diese Masterarbeit befasst sich mit einer numerischen Studie des Tragverhaltens von Bodennägel. Unter Bodenvernagelungen versteht man Maßnahmen zur Sicherung und Verstärkung von Böschungen und Baugruben. Zur Berechnung von Nagelwänden werden in der konventionellen Geotechnik häufig statische Nachweise geführt, die von einer Gleichgewichtsbetrachtung im Bruchzustand ausgehen. Die Standsicherheit ergibt sich dabei aus der Gegenüberstellung von Widerstandskräften und Einwirkungen.

Eine Literaturrecherche der geläufigsten Berechnungsmethoden und eine Vergleichsstudie von analytischen Programmen werden in dieser Arbeit durchgeführt, um die Implementierung der Nägel und die Verwendung mathematischer Ansätze zu verstehen. Ein Vergleich von analytischen und numerischen Berechnungsverfahren, bezüglich der Standsicherheit von Nagelwänden, wird ebenfalls durchgeführt. Zusätzlich werden Parameterstudien hinsichtlich implementierbarer Nagelarten, elasto-plastischem Materialverhalten und verschiedener Nagelneigungen untersucht.

Nägel stellen in der Regel dreidimensionale Objekte dar, womit es schwierig ist diese in ein ebenes Verformungsmodell zu verpacken. Stäbe werden üblicherweise in zweidimensionalen Modellen als Plattenelemente dargestellt. Ein Hauptaugenmerk dieser Arbeit liegt darin, den Einfluss des Abstandes der Nägel in die Tiefe zu erforschen. Mittels numerischer 2D Berechnungen ist es mittlerweile möglich 3D Effekte von Stabelementen zu berücksichtigen. Eine Validierung der 2D Analysen wird anhand von 3D FE Berechnungen geliefert.

Abstract

In this thesis, a numerical study on the behaviour of soil nails is conducted. Soil nails have been widely used as an in-situ reinforcement procedure to stabilise slopes and excavations. In practical geotechnical engineering, the design of soil nailed structures is done by means of limit equilibrium approaches. The factor of safety is determined with a comparison of driving forces and resisting forces at limit state.

A comprehensive review of current calculation methods and implementation of soil nails in analytical programs is made. One purpose of this work is to compare the two-dimensional (2D) finite element (FE) approach with the limit equilibrium approach. Evaluations are done on support types, elastoplastic material behaviour and the effects of nail inclination.

Since soil nails are real three-dimensional (3D) objects, they are difficult to design in a 2D model. Parametric studies are performed to investigate the influencing factors on the overall stability of reinforced slopes. One main objective of this work is to study a simplified 2D plane strain FE analysis, which is able to consider 3D characteristics. Embedded beam rows are used in the 2D model to consider 3D effects.

Table of contents

List of figures

List of tables

List of symbols and abbreviations

Capital letters

A	[%]	cross section area
D	[m]	diameter soil nail
E	[kN/m²]	Young's modulus
F_{max}	[kN]	maximum base resistance of embedded beam row
L_N	[m]	nail length
L_p	[m]	pull-out length of soil nail
L_s	[m]	out-of-plane spacing of nail
M	[kN]	bending moment
M_p	[kN]	maximum bending moment (elastoplastic)
N	[kN]	axial force
N_p	[kN]	maximum axial force (elastoplastic)
Q	[kN]	shear force
R_P	[kN]	plate capacity
R_T	[kN]	tensile capacity
R_{inter}	[-]	interface reduction factor
T_{lat}	[kN/m]	lateral skin resistance of embedded beam row
T_m	[kN/m]	bond strength
$T_{m,mob}$	[kN/m]	mobilised skin force along nail
T_N	[kN/m]	resistant soil friction (caused by nail)
T_S	[kN/m]	restraining tensile force of nail
T_{skin}	[kN/m]	axial skin resistance of embedded beam row
Z_g	[kN]	available nail traction
Z_{mob}	[kN]	mobilised nail traction

Small letters

c	[kN/m²]	cohesion
c_∞	[kN/m²]	cohesion $\sigma_n = \infty$
c'	[kN/m²]	effective cohesion
c'_{mob}	[kN/m²]	mobilised cohesion
d	[m]	equivalent thickness of plate
h	[m]	slope height
w	[kN/m/m]	plate weight

Greek letters

α_s	[°]	slope inclination
γ	[kN/m³]	unit weight
γ_{sat}	[kN/m³]	unit weight of soil below ground water table
γ_{unsat}	[kN/m³]	unit weight of soil above ground water table
ε	[°]	nail inclination
η	[-]	safety factor
θ	[°]	inclination of slip surface
ν'	[-]	Poisson's ratio
σ'_n	[kN/m²]	effective normal stress
τ	[kN/m²]	shear stress
τ_m	[kN/m²]	available skin friction
τ_f	[kN/m²]	shear stress at failure
φ	[°]	friction angle
φ'	[°]	effective friction angle
φ_0	[°]	effective friction angle at $\sigma_n=0$
φ'_{mob}	[°]	mobilised friction angle
ψ	[°]	dilatancy angle

Abbreviations

CFS	Critical Failure Surface
EB	Embedded Beam (3D)
EBR	Embedded Beam Row (2D)
FE	Finite Element
FEM	Finite Element Method
FOS	Factor of Safety
FOS_{FE}	Factor of Safety (calculated with finite element approach)
GLE	General Limit Equilibrium
LE	Limit Equilibrium
MC	Mohr Coulomb
USC	Unified Strength Criterion
VE	Volume Element

1 Introduction

The principle of soil nailing is to stabilise and reinforce landslides, slopes or excavations by means of installed steel bars, called ‘nails’. In general, the nails are arranged in form of a grid-shaped pattern and installed with the same inclination. A monolithic body is formed as a result of group interaction of the nails. Soil nail wall is a construction technique, which refers in general to an unstable natural soil slope stabilised by means of soil nails and rigid facing. The construction process of this technique proceeds from the top down. Steel bars are installed through a drill and grouting procedure. A rigid facing (often applied by shotcrete reinforced with welded wire meshes) or soil nail head plates are used to stabilise the slope surface.

The soil nails are considered ‘passive’, developing tensile capacity only in case of deformations. Soil nails primarily receive traction due to a nail – ground interaction. Further, the nails receive shear and bending stresses caused by movements of the soil mass.

In chapter 2, a theoretical background is given on the load transfer concept of soil nail structures. A literature research of the current analytical calculation methods and a comparative study on limit equilibrium (LE) based software can be found in chapter 3. The analytical programs SLIDE (SLIDE, 2016) and GGU (GGU, 2014), which are explained in more detail in chapter 4, are used for verification of the implemented equations, employed for safety analysis.

To approach practical geotechnical problems the conventional LE method is typically used to determine the factor of safety (FOS). Chapter 4 represents a validation of the finite element (FE) based program PLAXIS 2D (Brinkgreve & et al., 2015). A comparative study on LE and FE is provided. Further, parametric studies are carried out to investigate influence factors on the overall stability of soil nail structures. In reality, a nail is surrounded by ground (3D characteristics) which is difficult to model in a 2D approach. Thus, also 3D effects with a simplified 2D plane strain FE approach are studied.

A verification of the 2D results is given in chapter 5 by means of a 3D computation. The 3D simulations are performed with PLAXIS 3D (Brinkgreve & et al., 2015).

2 Load transfer concept in soil-nailed structures

Soil nails are considered 'passive', developing tensile capacity only in case of deformation. The behaviour of 'passive' reinforcements depends on the following two fundamental mechanisms: The dominant mechanism is the generation of tensile load as a result of frictional interaction between the ground and the soil nail. The second mechanism is the development of shear stress and bending stiffness in the nails caused by movements of the soil mass. A critical failure surface (CFS) divides the ground into a passive (resistant) and an active zone, as illustrated in Fig. 3.

2.1 Nail tension distribution

2.1.1 Stress-transfer mechanism

As the soil mass deforms laterally towards the wall facing, the nail gathers resistance against the expansion. Within the anchored zone the nail is pulled out of the slope. As depicted in Fig. 1, the direction of the shear stress is changing at the appearance of the maximum tensile force (T_{max}) in the nail. T_0 represents the tensile force at the nail head.

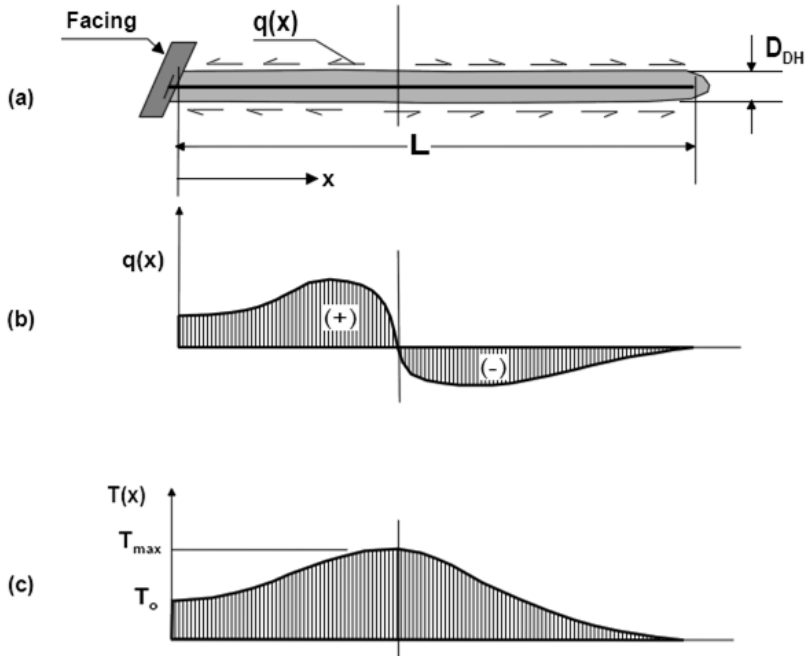

Fig. 1 Shear stress and tensile force distribution in a nail (FHWA, 2003)

2.1.2 Simplified Distribution of Nail Tensile Forces

A simplified model of tensile force distribution has been introduced for designing soil nail structures.

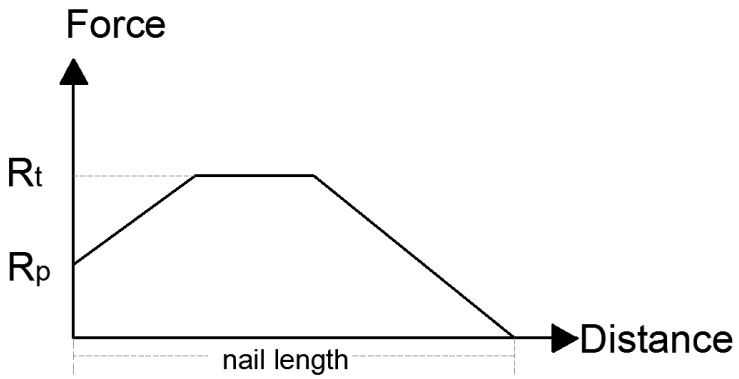

Fig. 2 Simplified tensile force distribution in a nail

As illustrated Fig. 2, R_t represents the tensile capacity and R_p the plate capacity. The gradient of the line is depending on the bond strength between grout body and soil. This simplified distribution model is the basis for several limit equilibrium based computations.

2.1.3 Maximum Tensile Force Distribution

The tensile force is a function of the intersection between the soil nail and the failure surface. Due to a complex load transfer within particular nails, the line of the maximum tensile force does not coincide with the critical failure surface (if failure occurs within nails). As shown in Fig. 1 the distribution of tension along the nails changes. The location of the critical failure surface (CFS) is controlled by global stability analysis. According to measurements of on-site tests, the maximum tensile force occurs in the region of 0.3 H to 0.4 H in the upper portion of the wall, behind the wall facing (Plumelle et al., 1990; Byrne et al, 1998).

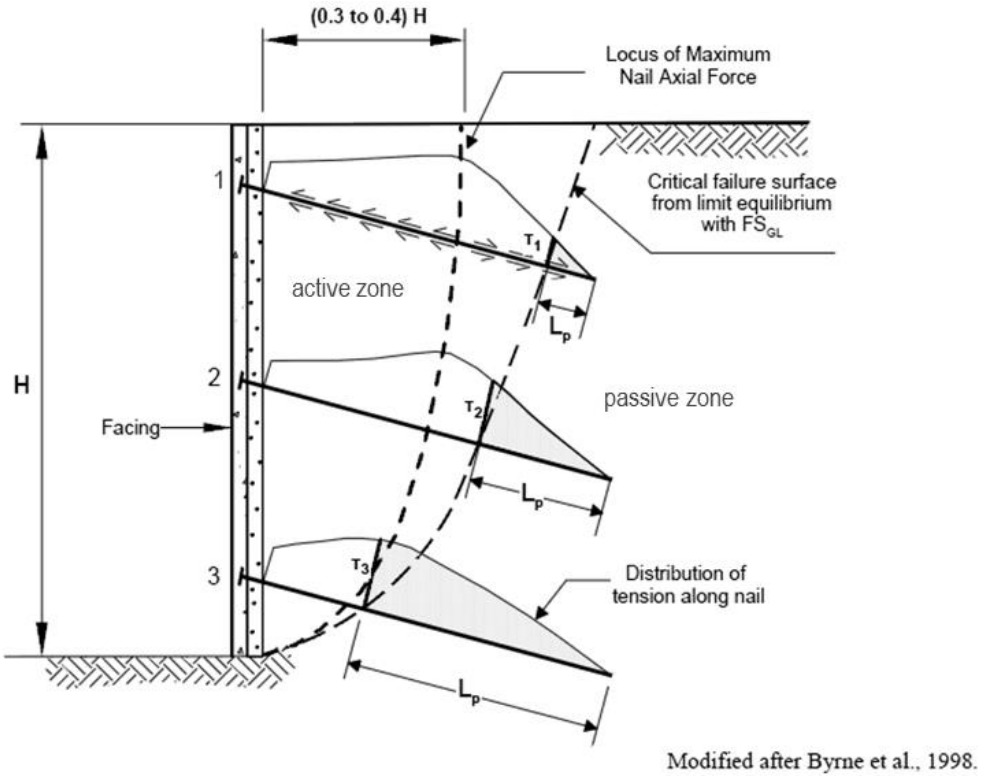

Fig. 3 Schematic location of maximum tensile force in particular soil nail (FHWA, 2003)

The pull-out length of the nails (L_p) are governed by the location of the failure surface. Hence it has to be considered that the stability contribution of the upper soil nail (T_1) is minor since the nail length behind the CFS is too short to reach the maximum potential of the pull-out capacity. In this example, the deepest soil nail T_3 is capable of mobilising the full pull-out capacity.

2.2 Bending stiffness and shear stress in nails

When the active block begins to move along the slip surface a shear zone is mobilised. As a reaction to the slope movement, soil nails sustain shear forces and bending moments. The nails originate such loads before and during a slope failure. The mechanism of bending stiffness and shear stress is shown in Fig. 4. Several models for shear force in soil nails and an analysis for bending stiffness, concerning its influence on slope stability, are represented by Jewell and Pedley (1990, 1992).

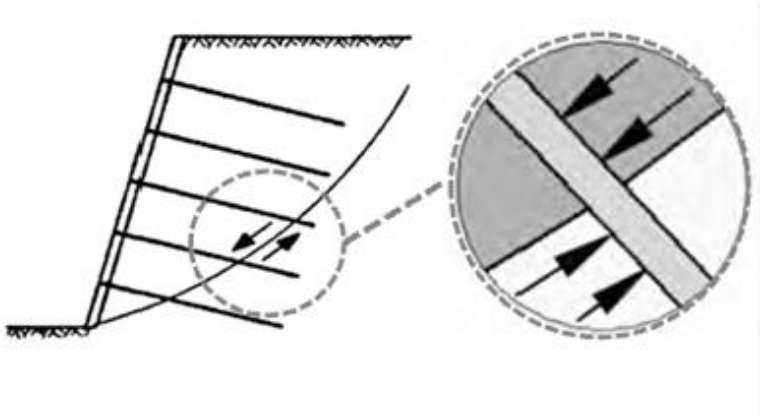

Fig. 4 Mechanism bending stiffness and shear stress (Marte, 2014)

2.3 Failure modes of soil nailed structures

According to Byrne et al. (1998) three failure modes of soil-nailed structures (see Fig. 5) can be identified as such:

- External failure mode (i.e., failure surface is not cutting the nails)
- Internal failure mode (i.e., failure surface is cutting the nails)
- Mixed failure mode (i.e., failure surface is cutting some nails)

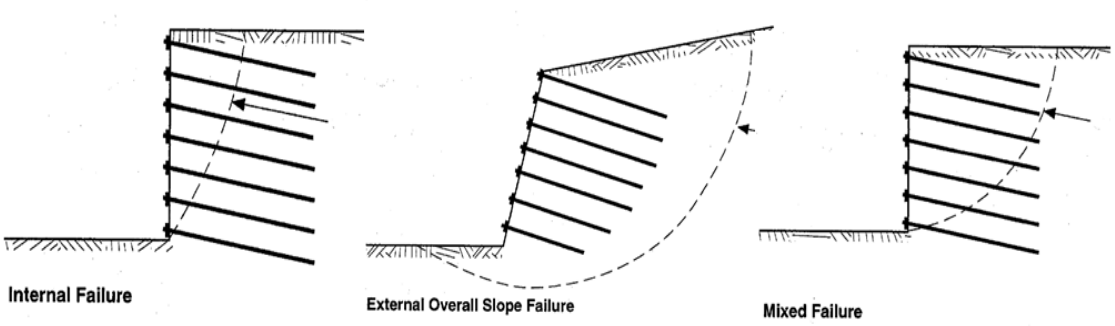

Fig. 5 Failure modes in soil nail walls (Modified after Byrne et al., 1998)

Considering a limit equilibrium approach, the soil mass of a failure mode is treated as a block. For safety calculations, only intersected soil nails are taken into account as an additional soil resisting force. An evaluation of stability analyses is performed for each potential failure mode to guarantee that the soil nail walls are able to resist any destabilisation caused by service loads, extreme loads or excavations. Influencing factors of external stability can be named as soil stratigraphy, i.e., wall height, width of nailed area and the soil resistance, nail resistance and interface resistance.

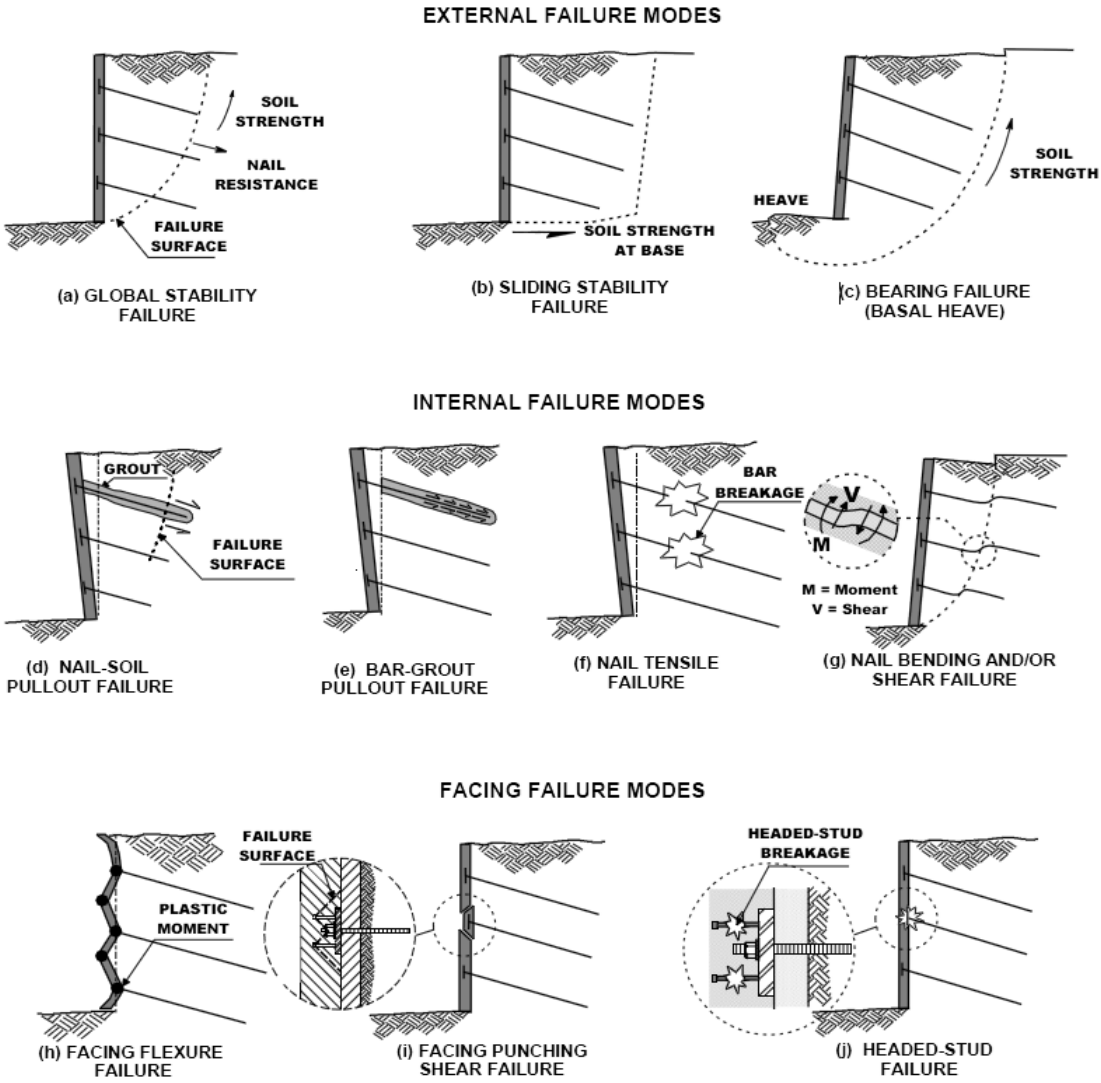

Fig. 6 Potential failure modes of soil nail walls (FHWA, 2003)

The failure modes as well as the state of the slope (service state, limit state) control the distribution of tension along soil nails. Regarding external failure modes, the position of maximum axial force (within the nail) never coincides with the CFS. Fig. 6 depicts the potential failure modes of soil nail walls, considering internal, external and facing failure modes. Regarding internal failure modes, the position of maximum axial force is usually found behind the CFS. If pull-out failure occurs, the position of maximum axial force is located in front of the CFS. While for a nail tensile failure, the position of maximum axial force will coincide with the CFS.

2.3.1 External failure modes

These failures develop due to a slip surface outside the soil-nailed ground mass. External failure can be generated by:

- sliding
- rotation
- bearing capacity
- other overall slope failures

2.3.2 Internal failure modes

Internal failure modes are usually classified into three different types, as illustrated in Fig. 7.

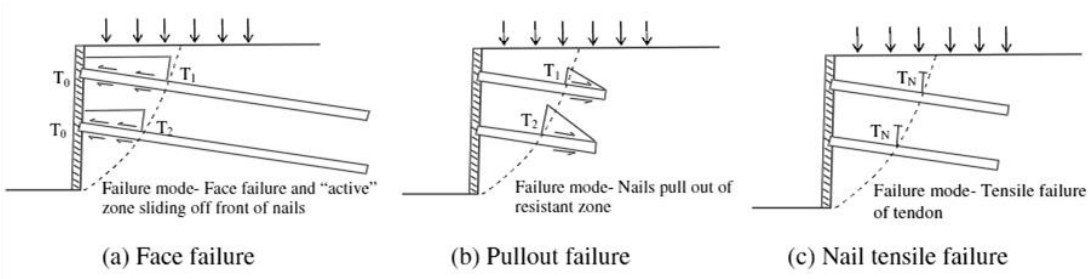

Fig. 7 Internal failure modes (Byrne, 1998)

- Face failure

Face failure can occur due to inappropriate structural design like punching shear failure of the face, headed-stud failure or flexural failure (bending moment exceeds the section modulus of face) (see Fig. 6 – facing failure modes).

- Pull-out failure

This failure results from inadequate soil nail length embedded into the resistant zone. The pull-out resistance is governed by the location of CFS, the diameter of the grouted body (nail) and the interaction between the ground and the nail (ground/soil nail bond stress).

- Nail tensile failure

In the case of nail tensile failure, the applied load exceeds the maximum nail capacity. Usually this type of failure happens abrupt without any previous warnings. The failure can occur due to corrosion of the steel bars, water infiltration, excessive surcharge, or selection of too little nail cross section.

3 Validation of analytical calculation methods

Every existing limit equilibrium method uses a failure mechanism of rigid bodies to describe slope failures. Thereby sliding of rigid blocks in the state of failure is assumed. These blocks are sliding along a slip surface. If a shear joint is generated spontaneously, the system fails and cannot gather any additional load.

Equilibriums between driving forces and mobilised resisting forces are applied at a state of failure. If the resistance is bigger than the driving forces, the system is in a stable state. Most approaches for reinforced slope-stability-analysis are based on these principles.

Besides soil resistance, soil nails are set as resistant in safety equations. Once the slip surface intersects the soil nail, nails obtain stabilising effects. A majority of approaches consider only axial traction in nails (e.g., Gässler, 1987; Clouterre, 1991). Some also consider generation of shear stresses and bending moments of the nails (e.g., Clouterre 1991; Juran 1990; Bridle and Barr 2009).

The established approaches differ regarding the shape of the failure mechanism (rotation or translation), the considered force equilibrium (equilibrium of moments or forces) and the definition of safety.

In the following sections, the current approaches for calculating soil nailed structures are represented. A software analysis of the analytical programs SLIDE (SLIDE, 2016) and GGU (GGU, 2014) is carried out to investigate the implementation of soil nails in such programs.

3.1 Description of current approaches

Usually the shear stress (τ_f) of the ground is expressed by the Mohr-Coulomb strength model, where τ_f and τ are defined as follows:

$$\tau_f = c' + \sigma'_n * tan\varphi' \tag{3.1}$$

$$\eta_1 = \frac{\tau}{\tau_f} \tag{3.2}$$

τ_f	[kN/m²]	shear stress at failure
c'	[kN/m²]	effective cohesion

φ'	[°]	effective friction angle
σ'_n	[kN/m²]	effective normal stress
τ	[kN/m²]	mobilised shear stress
η_1	[-]	safety factor (after Mohr-Coulomb)
η_2	[-]	safety factor (after Fellenius)

The available shear strength depends on the effective soil strength parameters (*φ' and c')* and the effective normal stress. The mobilised shear strength, however, depends on the driving forces acting on the soil mass. The FOS is gained through resisting forces divided by driving forces.

Tab. 1 Limit equilibrium methods (Krishna Prasad Aryal 2006, Abramson et al. 2002)

Methods	Circular	Non-cir.	ΣM = 0	ΣF = 0	Assumptions for T and E
Ordinary	√	-	√	-	Neglects both E and T
Bishop simplified	√	(*)	√	(**)	Considers E, but neglects T
Janbu simplified	(*)	√	-	√	Considers E, but neglects T
Janbu GPS	√	√	(***)	√	Considers both E and T, act at LoT
Lowe-Karafiath	-	√	-	√	Resultant inclines at, $\theta = \frac{1}{2}(\alpha + \beta)$
Corps of Engrs.	-	√	-	√	Resultant inclines at, $\theta = \frac{1}{2}(\alpha_1 + \alpha_2)$
Sarma	√	√	√	√	Interslice shear, $T = ch + E \tan\phi$
Spencer	√	(*)	√	√	Constant inclination, T =tanθ E
Morgenst.-Price	√	√	√	√	Defined by f(x), T = f(x).λ..E

(*) Can be used for both circular and non-circular failure surfaces,

(**) satisfies vertical force equilibrium for base normal force, and

(***) satisfies moment equilibrium for intermediate thin slices (Janbu 1957, Grande 1997)

A detailed illustration of all the LE methods, mentioned in Tab. 1, can be found in Krishna Prasad Aryal (2006). This thesis describes methods which are commonly used in practice for reinforced soil wall design.

Independent of the calculation method, a definition of the FOS is applied after Fellenius:

$$\eta_2 = \frac{tan\varphi'}{tan\varphi'_{mob}} = \frac{c'}{c'_{mob}} \geq 1.0 \tag{3.3}$$

This formula implies an iterative process, whereas the friction angle and cohesion are de- or increased until η_2 corresponds to $\frac{tan\varphi\prime}{tan\varphi\prime_{mob}}$ or $\frac{c\prime}{c\prime_{mob}}$.

3.1.1 Approach by Gässler

According to Renk (2011) the stability analysis made by Gässler can be simplified by the following assumptions:

- The nails are axially loaded, not lateral to their axis (only traction).
- According to Gässler's measurements, an averaged constant limit shear force T_m can be applied along the nails. The size of the skin friction within the nail must be obtained by pull-out attempts in situ.

Gässler introduced a translational mechanism with one or two rigid bodies, as well as a rotational mechanism with one rigid body as possible types of failure. These methods are illustrated in more detail in Renk (2011).

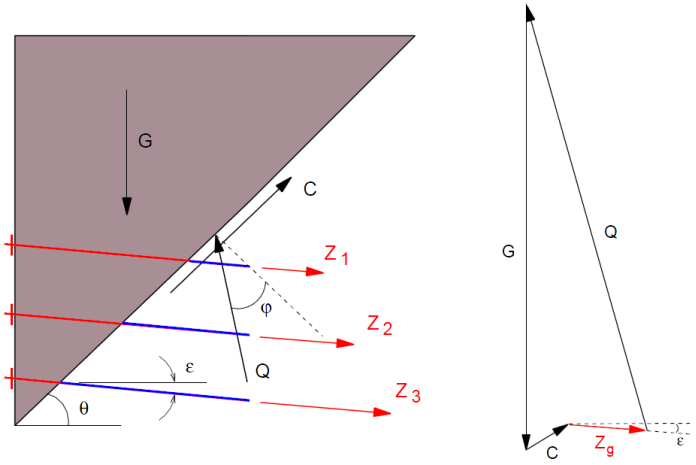

Fig. 8 Translational mechanism with one rigid body; polygon of forces (Renk 2011; Gässler 1987)

Fig. 8 shows an example of a translational mechanism with one rigid body (Renk 2011; Gässler 1987). For an assumed slip surface inclination θ, the available nail traction Z_g can be calculated by means of known values C (cohesion of soil along the slip surface) and G (self-weight of slipping body). The maximum mobilised nail traction Z_{mob} can be determined with the following equation:

$$Z_{mob} = T_{m,mob} \frac{\Sigma L_{p(\theta)}}{L_s} \tag{3.4}$$

$T_{m,mob}$ [kN] skin friction force along the nails

ΣL_p [m] sum of pull-out lengths of nails in passive zone

L_s [m] out-of-plane spacing of the nails

Hence a factor of safety η implies according to Gässler as:

$$\eta_{GÄSS.} = \frac{Z_{mob}}{Z_g} \tag{3.5}$$

A variation of the slip surface inclination θ gives the least value of $\eta_{GÄSS}$. Thus, the safety against failure is gained (no Fellenius rule is applied).

3.1.2 Simplified approach by Bishop

The following description of this approach refers to the dissertation of Renk (2011).

The simplified Bishop's method is a more accurate method than Gässler's approach. Like Gässler, Bishop assumes the formation of a slip surface in the state of failure, whereby simplified assumptions are made:

- nails only receive tension forces
- resultant inter-slice forces E_l and E_r are horizontal
- vertical inter-slice shear forces T_l, T_r and their pore-water pressure are ignored
- does not satisfy horizontal force equilibrium

The maximum available tensile capacity T_m can be obtained by the available skin friction τ_m, the nail diameter D, the pull-out length L_p and the out-of-plane spacing L_s.

$$T_m = \tau_m * \pi * D * L_p / L_s \tag{3.6}$$

A separation of the rigid body into different slices and established equilibrium conditions leads to a mathematical solution. Bishop's method satisfies moment equilibrium for FOS and vertical force equilibrium for N_i (resistant forces at the slip surface, Fig. 10). However, the approach by Renk contains a different definition of safety reduction of nail forces compared to DIN 4084. The following equations are based on DIN 4084, whereby pore-water pressure and other external forces are neglected.

$$N_i = \Sigma \frac{((G_i + \frac{T_N}{\eta_{BISH.}}) * tan\varphi'_i + b_i * c')}{cos\vartheta_i + \frac{tan\varphi'}{\eta_{BISH.}} * sin\vartheta_i} + \Sigma T_S \tag{3.7}$$

i	[-]	slice index
b	[m]	width of each slice
G	[kN/m]	self-weight of each slice
ϑ	[°]	inclination of each slice
ε	[°]	nail inclination

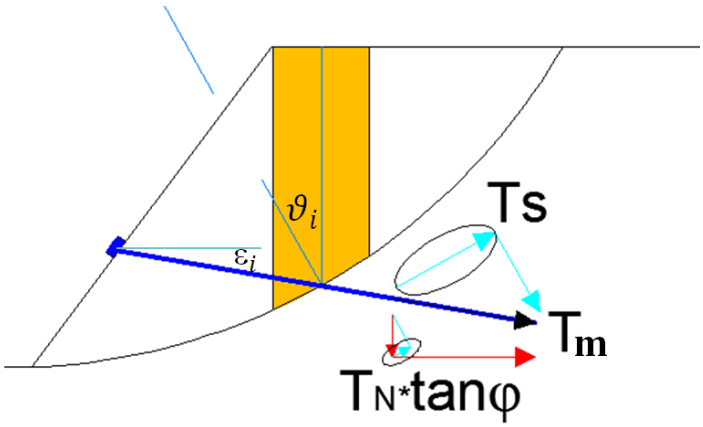

Fig. 9 Force conditions of a particular soil nail

$$T_S = T_{mi} * cos(\vartheta_i + \varepsilon_i) \tag{3.8}$$

$$T_N = T_{mi} * sin\varepsilon_i \tag{3.9}$$

Referring to equations (3.8) and (3.9) T_S represents the restraining tensile force of the nail and T_N is acting as the resistant soil friction caused by the nail.

$$\eta_{BISH.} = \frac{N_i}{\Sigma G_i * sin\vartheta_i} \tag{3.10}$$

Where $\Sigma G_i * sin\vartheta_i$ represents the driving forces indicated in equation (3.10).

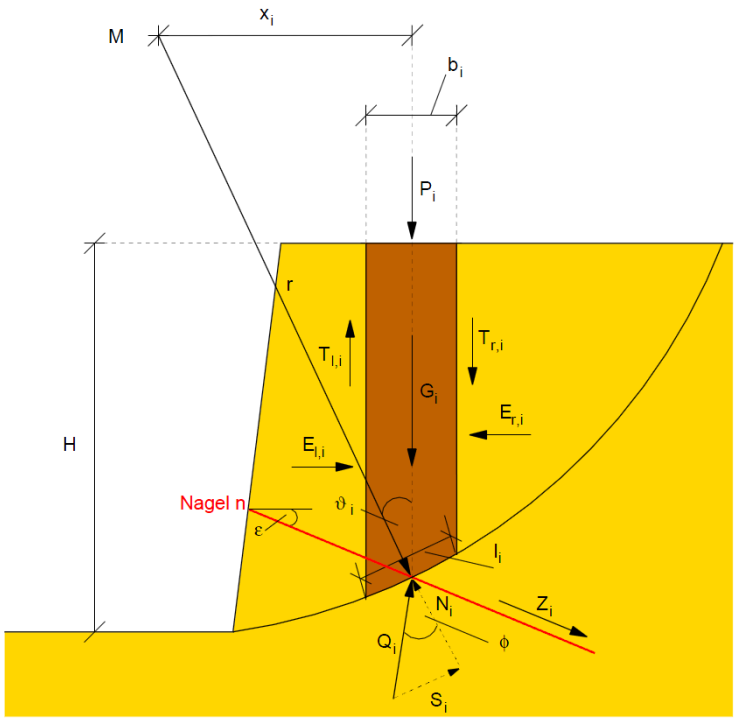

Fig. 10 Force conditions at a particular slice considering nails (Renk, 2011)

3.1.3 Simplified approach by Janbu

Janbu's simplified method is introduced in this section. The following description of this approach refers to the dissertation of Renk (2011). It deals with a translational rigid body failure mechanism at limit state. The failure occurs on a polygonal slip surface (non-circular) and is thus used for composite shear surfaces. A separation of the rigid body into *n* different slices is made for safety calculation. Unlike Bishop's method, Janbu's method considers the equilibrium of horizontal and vertical forces at each slice, satisfying the FOS. In addition, the following simplified assumptions are made:

- nails only receive tension forces
- resultant inter-slice forces E_l and E_r are horizontal
- vertical inter-slice shear forces T_l, T_r and their pore-water pressure are ignored
- does not satisfy moment equilibrium

The following equations are also based on the DIN 4084, whereby pore-water pressure and other external forces are neglected. Where b_i represents the width of each slice and N_i is the resistant force at the slip surface.

$$N_i = \Sigma \frac{((G_i + \frac{T_N}{\eta_{JAN.}}) * tan\varphi'_i + b_i * c')}{cos^2\vartheta_i * \left(1 + \frac{tan\varphi_i}{\eta_{JAN.}} * tan\vartheta_i\right)} + \Sigma T_S \tag{3.11}$$

$$T_S = T_i * \frac{cos(\vartheta_i + \varepsilon_i)}{cos\vartheta_i} \tag{3.12}$$

$$T_N = T_i * sin\varepsilon_i \tag{3.13}$$

Referring to equations (3.12) and (3.13), T_S represents the restraining traction of the nail and T_N is acting as the friction resistance of the soil caused by the nail.

$$\eta_{JAN.} = \frac{N_i}{\Sigma G_i * tan\vartheta_i} \tag{3.14}$$

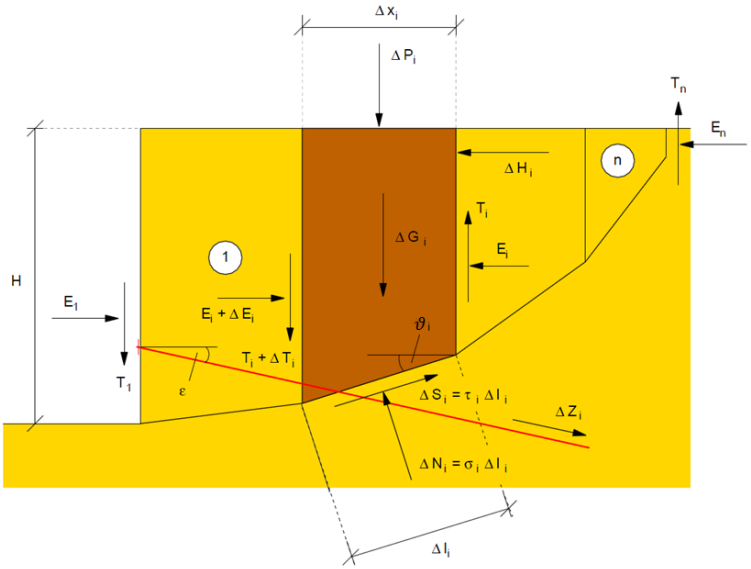

Fig. 11 Force conditions at a particular slice according to Janbu (Renk, 2011)

3.1.4 General limit equilibrium approach

The general limit equilibrium (GLE) method is discussed only briefly, since it is based on the same principles as Janbu's and Bishop's method. However, it is more accurate and thus important. This method combines all assumptions and benefits of the previously developed LE approaches. It satisfies both, force and moment equilibriums and does not ignore inter-slice forces. The inclination of the horizontal inter-slice forces is considered by means of a mathematical procedure (no assumptions are necessary). A more detailed description can be found in the dissertation of Krishna Prasad Aryal (2006).

3.1.5 Approach by Renk

In contrast to the other approaches which assume rigid body failure mechanisms, Renk's soil nail-wall design is based on the consideration of deformation in the serviceability state. In LE methods, a failure occurs without any deformation of the soil body. However, a generation of traction along the nails can only appear due to movements. Thus, Renk developed a method, which considers a mobilisation of nail forces via deformation planes.

One of Renk's theories is based on the comparison of dissipation between soil nail interaction and the work of external loads. Soil nails have a much higher stiffness, related to the ground. Their stiffness is activated, if the soil moves relative to the nail, resulting in shear stresses along the surface of the nails.

If a retaining wall is burdened by earth pressure, shearing occurs. Under the approximation of a constant volume, horizontally installed nails experience no load transfer (see Fig. 12).

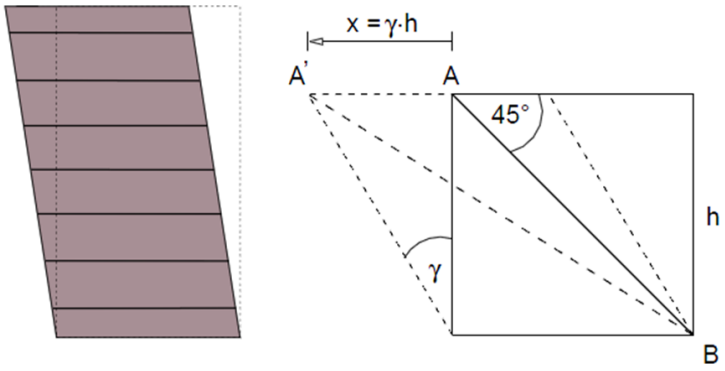

Fig. 12 Shearing under constant volume (Renk, 2011)

The figure above exhibits the ideal inclination of nails under such conditions. The emergence of maximum strains occurs under an inclination of 45°.

The energy caused by friction (dissipation) divided by the earth pressure (external work) reveals the FOS and is composed as follows:

$$D = D_0 + D_n = \frac{1}{2}\gamma \, tan\varphi \, \rho \, g \, h^2 + n \, \frac{1}{2} \, \tau_m \, U \, \gamma \, b^2 \tag{3.15}$$

$$\eta = \frac{D}{A} \tag{3.16}$$

The derivatives of equation (3.15) and (3.16) can be found in the dissertation of Renk (2011).

3.2 LE software used for soil nail walls

In this chapter, a software analysis of the analytical programs GGU (GGU, 2014) and SLIDE (SLIDE, 2016) is performed in order to investigate how soil nails are implemented. The implementation of equations and the used parameters are verified. This analysis serves as a basis for a comparative study on LE methods.

3.2.1 SLIDE

The SLIDE 6.0 software is a limit equilibrium program for groundwater and slope stability analyses, developed by Rocscience Inc Toronto Canada. It is a 2D-LE based software, which can evaluate circular and non-circular failure surfaces.

3.2.1.1 *Design standard*

Eurocode 7 and British Standard 8006 are available in SLIDE. For the following calculations, all design factors are set to 1 to enable reasonable comparisons.

3.2.1.2 *Input soil parameters*

Depending on the applied strength type, the used soil parameters (for MC-model) are the following:

- γ unit weight
- c cohesion
- φ friction angle

The input of the water-surface feature is neglected.

3.2.1.3 *Strength type (soil)*

SLIDE provides several strength type models. The most important models are briefly described within this section.

- **Mohr-Coulomb (MC)**

The MC model exhibits linear-elastic and perfectly-plastic soil behaviour. It is a first order model for soils which requires an input of three parameters in SLIDE (see chapter 3.2.1.2).

$$\tau = c' + \sigma'_n * tan\varphi' \tag{3.17}$$

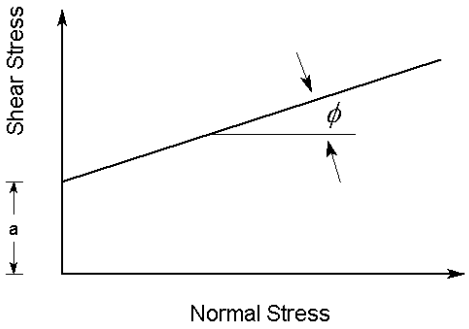

Fig. 13 Mohr-Coulomb failure envelope (SLIDE, 2016)

- **Undrained (φ=0)**

For this strength model, the shear strength is defined by cohesion. In case '*constant'* is selected (τ=*c*) as cohesion type, shear strength is constant throughout the material. A selection of cohesion type '*F(depth)'* and *'F(datum)'* induce a shear strength with a function of depth (see equation (3.18)). These two options only differ in the datum at which the depth is measured.

$$\tau = c_t + (y_t - y)\delta_c \tag{3.18}$$

- **Hoek-Brown**

The Hoek-Brown failure criterion is widely used for rock masses. It considers the properties of intact rock and the influence of joints. SLIDE requires three input parameters to fulfil the Hoek-Brown criterion, namely the unified strength criterion USC (σ'_{ci}) and two material constants *m* and *s*. These input parameters are expressed by the following equation:

$$\sigma'_1 = \sigma'_3 + \sigma'_{ci}\sqrt{m_b\sigma'_3/\sigma'_{ci} + s} \tag{3.19}$$

Detailed information about the Hoek-Brown criterion and its correct implementation can be found in the manuals of Rocscience (SLIDE, 2016).

- **Hyperbolic**

The hyperbolic shear strength model characterises an interface between materials such as concrete and soil. The materials are defined by the input parameters c_∞ and φ_0. The cohesion c_∞ defines the shear strength at σ_n=∞ and φ_0 represents the friction angle at σ_n=*0*.

$$\tau = \frac{c_\infty * \sigma_n tan\varphi_0}{c_\infty + \sigma_n tan\varphi_0} \tag{3.20}$$

This equation is derived from the study of Esterhuizen, Filz and Duncan (2001) and is shown in Fig. 14.

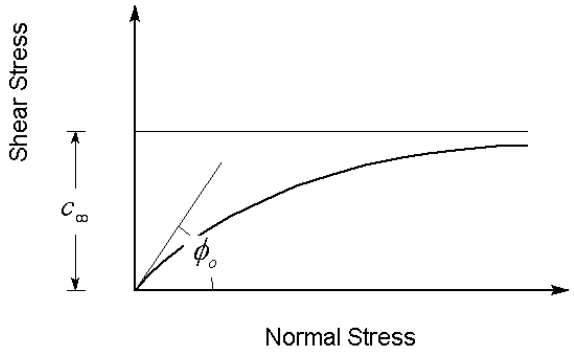

Fig. 14 Hyperbolic shear strength envelope (SLIDE, 2016)

Additional strength models implemented in SLIDE:

- no strength (i.e. water)
- infinite strength ($\tau = \infty$)
- anisotropic strength
- shear/Normal function
- anisotropic function
- generalised Hoek-Brown
- vertical stress ratio
- Barton-Bandis
- Power-Curve
- discrete function
- drained-undrained
- anisotropic linear
- generalised anisotropic
- Snowden mod. anisotropic linear

More detailed information of all previously mentioned strength models can be found in the manuals of Rocscience (SLIDE, 2016).

3.2.1.4 *Calculation methods*

The following LE analysis methods are available in SLIDE:

- Ordinary / Fellenius
- Bishop Simplified
- Janbu Simplified
- Janbu Corrected
- Spencer
- Corps of Engineers #1
- Corps of Engineers #2
- Lowe-Karafiath
- GLE (General Limit Equilibrium) / Morgenstern-Price

The most significant methods are discussed in chapter 3.1.

3.2.1.5 *Support types*

SLIDE provides the modelling of various types of slope reinforcements including geo-textiles, soil nails, tiebacks (anchors) and rock bolts. Inclination, bar length and out-of-plane distance can be entered for each support element. The force application of each support type can be set to *'active (method A)'* or *'passive (method B)'.* Active support (3.21) can be applied for pre-stressed reinforcements (anchors) and passive support (3.22) for non-tensioned reinforcements (soil nails). Method A decreases the driving force during FOS calculation (see equation), whereas method B increases the resisting force provided by shear restraint. The following equations are referred to method A and B in SLIDE:

$$\eta_A = \frac{resisting\ force + T_N * tan\varphi}{driving\ force - T_S} \tag{3.21}$$

$$\eta_B = \frac{resisting\ force + T_N * tan\varphi + T_S}{driving\ force} \tag{3.22}$$

As illustrated in Fig. 9, T_S represents the restraining traction of the nail and T_N acts as the friction resistance of the soil caused by the nail. Active support always gives a higher FOS than passive support.

Available support types:

- **End anchored**

The end anchored support type represents an anchor with a free tendon length. As a value for support, the *Anchor capacity* has to be entered. The end anchored support is only examined by its tensile strength. The applied force to the slip surface is constant and equal to the anchor capacity divided by the out-of-plane spacing. The internal stability is only governed by the tensile failure of the anchor.

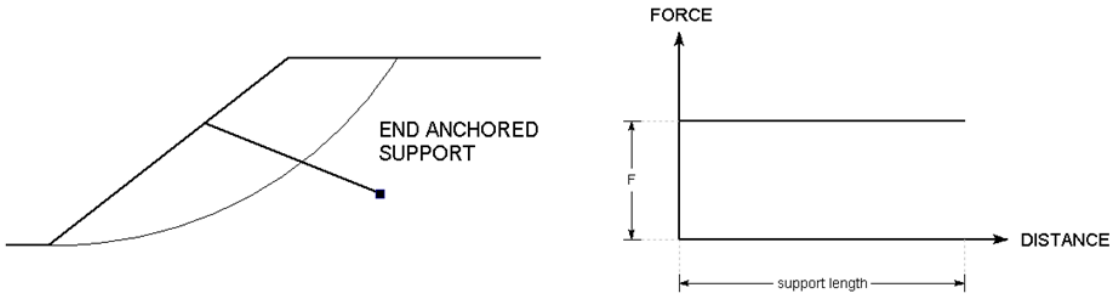

Fig. 15 End anchored support with force diagram (SLIDE, 2016)

- **Geotextile**

This term can be correlated to all types of planar reinforcements, such as, geogrids, geotextiles or geosynthetics. However, it can also be used to model soil nails. For the strip properties, *strip coverage* and *tensile strength* are required. The strips have a certain width with predefined gaps. If the strip coverage is set to 100%, there are no gaps between the strips. Since the material is flexible, the force orientation can also be non-parallel. Further, it can be manipulated within SLIDE. The shear strength option allows choosing between a linear (MC) and hyperbolic geotextile/soil interface behaviour. Thus, the shear strength will vary along the geotextile length.

Different types of anchorage can be chosen, where none, both or only one end of the geotextile are fixed and immovable. The selected type of anchorage governs the potential failure modes and consequently the resistant capacity (force diagram). For the *pull-out strength* option, the adhesion and friction angle have to be entered, controlling the stripping force and / or the pull-out failure.

The internal stability is controlled by pull-out (3.23), tensile (3.24) and stripping failure (3.25).

$$F_1 = 2 * L_0 * A * \tau/100 \quad (3.23)$$

$$F_2 = R_T * A/100 \quad (3.24)$$

$$F_3 = 2 * L_i * A * \tau/100 \quad (3.25)$$

A	[%]	strip coverage
L_0	[m]	pull-out length of nail
L_i	[m]	length of nail in active zone
R_T	[kN]	tensile capacity

Since the soil has two interfaces for the geotextile, a factor of two is included in the force calculation. The force applied to the slip surface is given by the minimum of *F1, F2,* and *F3*.

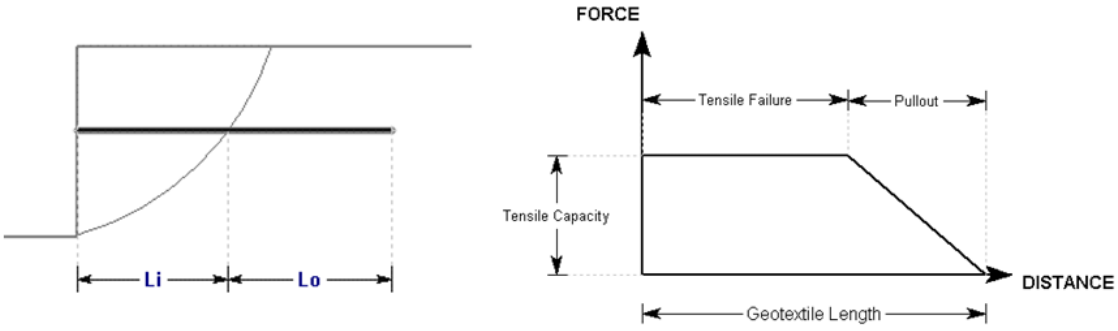

Fig. 16 End anchored support with force diagram (SLIDE, 2016)

- **Grouted tieback**

The grouted tieback feature can be used to model ground anchors with a free tendon length or soil nails. There is no stress dependency of the soil/grout interface. The resistant capacity is defined by entering *tensile capacity, plate capacity* and *bond strength*. Optionally a *shear* and *compression capacity* can also be chosen. The essential difference to other features is the input of the *bond length*. If the bond length input is 100% the grouted tieback option is equal to the soil nail option.

The implementation of support is controlled by pull-out failure (3.26), tensile failure (3.27) and stripping failure (3.28).

$$F_1 = T_m * L_0/L_s \tag{3.26}$$

$$F_2 = R_T/L_s \tag{3.27}$$

$$F_3 = (R_P + T_m * L_i)/L_s \tag{3.28}$$

T_m [kN/m] bond strength

L_s [m] out-of-plane spacing

R_P [kN] plate capacity

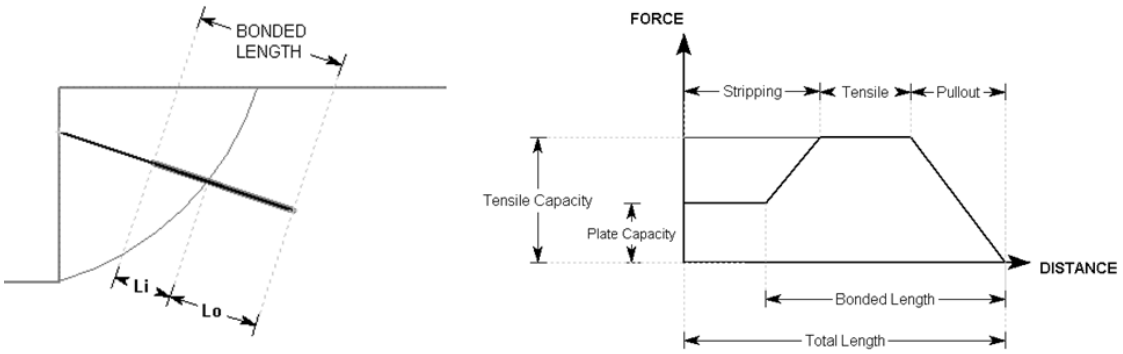

Fig. 17 Grouted tieback with force diagram (SLIDE, 2016)

- **Grouted tieback (with friction)**

This method possesses in general the same features as the grouted tieback (Fig. 17), however, there is one important difference. The specification of a selectable shear strength model (hyperbolic or linear) allows users to consider stress dependency (frictional strength τ) of the soil/grout interface. Instead of *bond strength*, the entered value of *adhesion* and *friction angle* is governing the pull-out strength. Pull-out (3.29), tensile failure (3.30) and stripping failure (3.31) characterise the implementation of support.

$$F_1 = \pi * D * \tau * L_0/L_s \tag{3.29}$$

$$F_2 = R_T/L_s \tag{3.30}$$

$$F_3 = R_P/L + (\pi * D * \tau * L_i)/L_s \tag{3.31}$$

D [m] grout diameter

- **Soil nail**

A grouted tieback support type with a determined bond length of 100% is equivalent to the soil nail feature. The used parameters and equations are stated above (3.29 – 3.31).

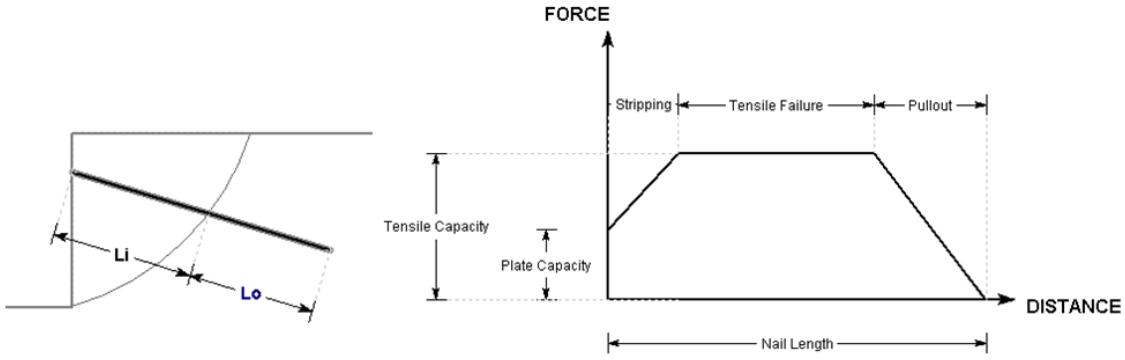

Fig. 18 Soil nail with force diagram (SLIDE, 2016)

The bond strength defines the gradient of the force diagram as shown in Fig. 18.

- **Micro pile**

This type of support only considers a shear failure which is tangential to the slip surface. The load acts transverse to the support direction (no traction in axial direction). Therefore, the support type is not appropriate for modelling soil nails. To have an effect on the FOS, the slip surface has to intersect the micro pile. By using the input of the *pile shear strength,* the resistant capacity can be controlled.

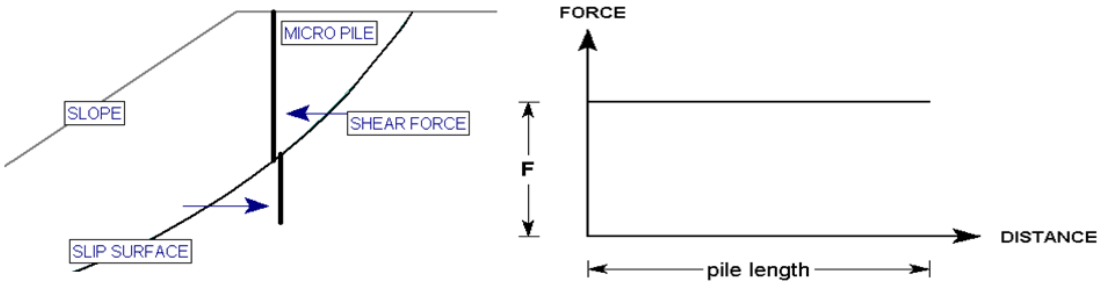

Fig. 19 Micro pile with force diagram (SLIDE, 2016)

Based on the studies above, it is recommended to use the support type *soil nail* or *grouted tieback (with friction)* for modelling soil nails in SLIDE.

3.2.2 GGU-Stability

The GGU software is a limit equilibrium program for slope failure investigations of soil nail walls and mechanically stabilised earth developed by Civilserve GmbH. The software is also 2D-LE based and is able to evaluate circular and polygonal failure surfaces.

3.2.2.1 *Design standard*

GGU-Stability enables a stability analysis according to Eurocode 7 and German Standard DIN 4084. For the following calculations all design factors are set to 1 to make reasonable comparisons. A definition of the FOS is applied according to Fellenius (see equation (3.3)).

3.2.2.2 *Input soil parameters*

The used soil parameters (for MC-model) are the following:

- γ unit weight
- c cohesion
- φ friction angle

The input for the water surface features is neglected. As an additional soil parameter, the angle *max psi(A)* can be entered to consider a 'passive anchor', introduced by DIN 4084:2009. The soil parameter $q_{s,k}$ refers to the skin friction and is equal to bond strength divided by circumference of a tension member.

3.2.2.3 *Strength type (soil)*

GGU-Stability only provides the MC-model as a failure criterion, which is briefly described in chapter 3.2.1.3.

3.2.2.4 *Calculation methods*

The following LE analysis methods are available in GGU-Stability:

- Krey
- Bishop Simplified
- Janbu Simplified
- general wedge method
- vertical slice method

The general wedge and the vertical slice method can be compared with the approach by Gässler, where polygons of forces are built to determine a FOS. The program de- and increases the strength parameters φ' and c' until the polygon forces are closed. In contrast to the calculations of Janbu and Bishop, these approaches consider vertical inter-slice forces. The difference between these two methods is the inclination of the inter-slice areas. Only vertical inter-slice areas are modelled in the vertical slice method. A description of the most significant calculation methods can be found in chapter 3.1.

3.2.2.5 *Support types*

Like SLIDE, GGU-Stability provides various types of slope reinforcements, such as soil nails, geosynthetics and anchors. The inclination, bar length and out-of-plane distance can be implemented for the pattern of each support type. The available support types are listed below.

- **Anchors**

This tool models an anchor with a free tendon length by defining a grouted section. The size of the design force $R_{,d}$ (tensile capacity) has to be specified. Anchor forces are only obtained if the anchor foot lies outside the moving slip body. It is possible to select pre-stressed anchors that consider the friction force in the slip surface due to applied pre-stressing. If non-pre-stressed and a grouted length identical to the anchor length is chosen, the support type is equivalent to a soil nail. The advantage of using this tool for modelling soil nails is the consideration of potential pre-stress forces.

- **Dowels**

This feature is similar to the micro pile option in SLIDE. Detailed information about this tool can be found in the GGU-Stability manual (GGU, 2014).

- **Soil nails**

The soil nail support type does not consider pre-stressing. A specification of a linearly variable skin friction is implied by the design values f_{1d} and f_{2d}. These two values represent the bond strength transferred along the soil nail. R_d constitutes the magnitude of the tensile capacity.

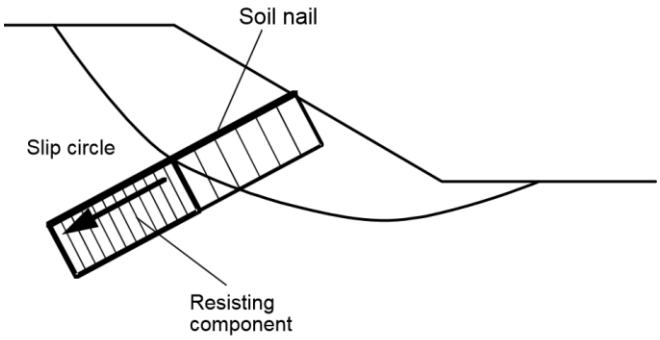

Fig. 20 Soil nail (GGU, 2014)

- **Geosynthetics**

Geosynthetics have similar properties as soil nails. A database allows choosing geosynthetic products from different manufacturers. By selecting a product, the design values *A1* (creep), *A2* (transport, installation and compaction), and *A4* (environmental influences) are defined by default. The bond strength is also computed automatically.

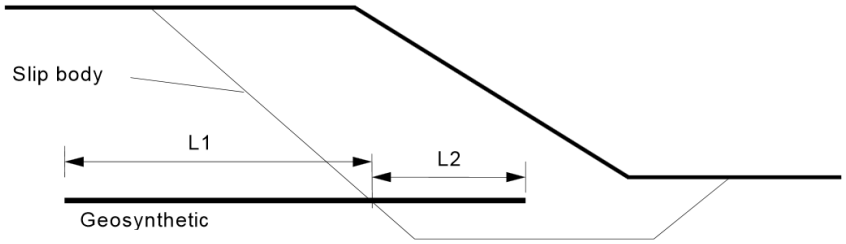

Fig. 21 Geosynthetic (GGU, 2014)

Knowing the lengths *L1* outside and *L2* inside the slip body, the program computes the resulting forces *F1* and *F2*. *F1* represents the pull-out strength, *F2* the stripping resistance and R_d the tensile strength. The smallest value among *F1, F2* and R_d is used for the safety calculations.

- **Tension members**

Tension members are a universal tool for modelling soil nails and anchors. It combines the features of the above mentioned structural elements. The resistant capacity is controlled by defining a *tensile capacity* (R_d) and a *characteristic shaft friction* ($q_{s,k}$). Further, the diameter of the tension member is required. In contrast to the 'soil nails' feature, linearly variable bond strength is not available.

Based on the studies above, it is recommended to use the support type *soil nails* or *tension members* for modelling soil nails in GGU.

3.3 Comparative study on LE methods

The objective of this comparison is the verification of the implemented formulas in the LE programs SLIDE and GGU. To verify the same results, an additional hand calculation is performed. To enable a comparison of the LE methods, the same input parameters for the two programs are used. Fig. 22 provides an overview of the used models.

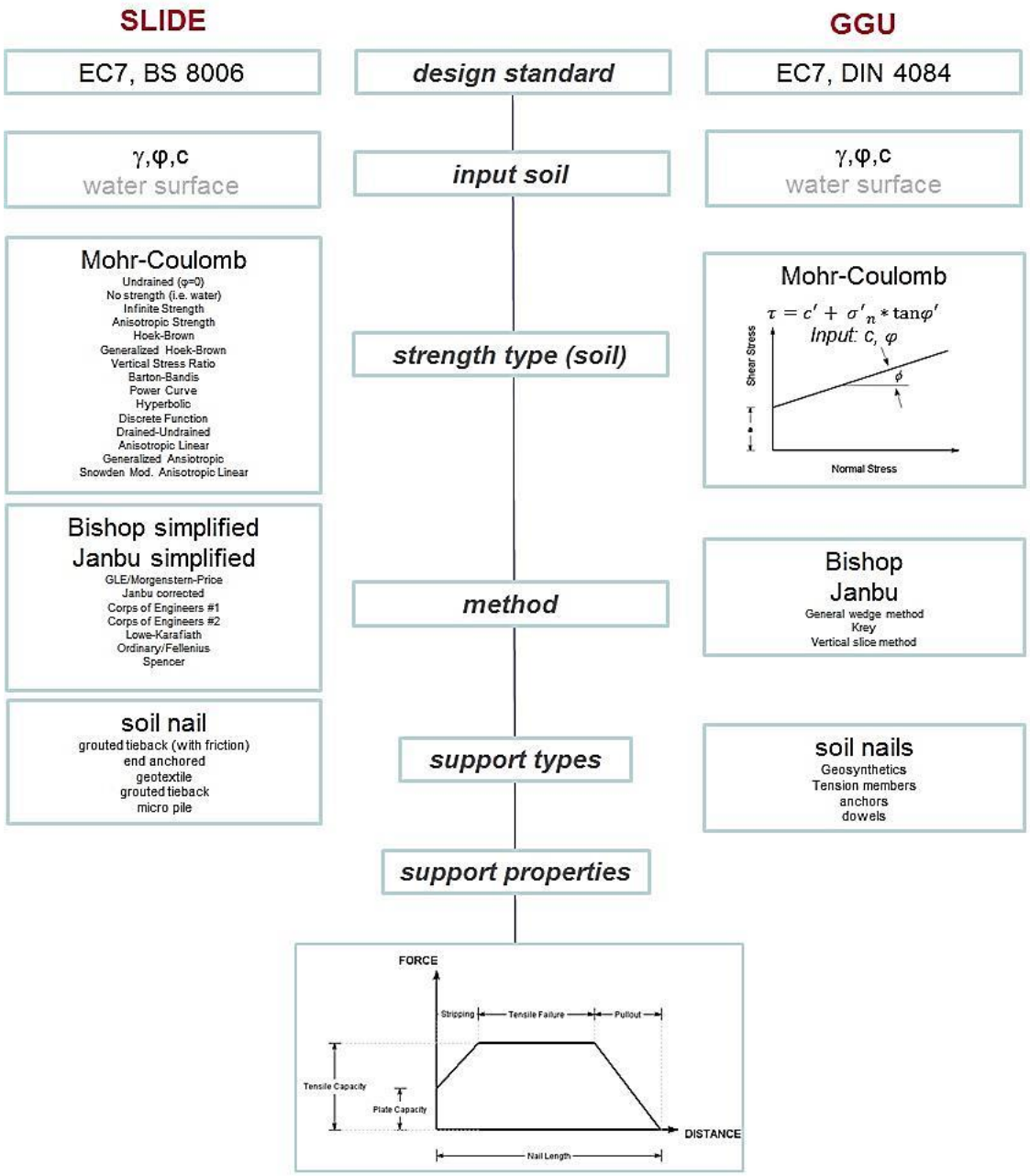

Fig. 22 Summary of comparative parameters

Since the design values are set to 1.0, the chosen design standard has no influence on the calculations. The MC strength model and the calculation methods of Bishop and

Janbu are selected. The support type *soil nail* exhibits the same features in both programs. A homogeneous soil without any pore-water-pressures is chosen.

3.3.1 Validation using the simplified Bishop method

3.3.1.1 *Geometry and material parameters*

Fig. 23 shows the homogeneous slope of 4 m height with an inclination of 53° (3:4) plotted by SLIDE. Two cases with different material sets are computed. The complete set of material parameters is given in Tab. 2 (soil) and Tab. 3 (soil nail). Material set 1 represents a frictional soil and set 2 a cohesive-frictional soil. Fig. 24 illustrates the resistant capacity of the reinforcements.

Tab. 2 Soil material parameters - case Bishop

Parameter	Symbol	Unit	Mat. Set 1	Mat. Set 2
Strength model	-	-	MC	MC
Friction angle	φ'	°	35	27
Cohesion	c'	kN/m²	0.1	10
Unit weight	γ	kN/m³	20	19

Tab. 3 Soil nail parameters - case Bishop

Parameter	Symbol	Unit	Mat. Set 1	Mat. Set 2
Bond strength	T_m	kN/m	50	50
Tensile capacity	R_T	kN	100	100
Plate capacity	R_P	kN	100	50
Nail inclination	ε	°	10	15
Nail length	L_N	m	4	4
Out-of-plane spacing	L_s	m	1	1

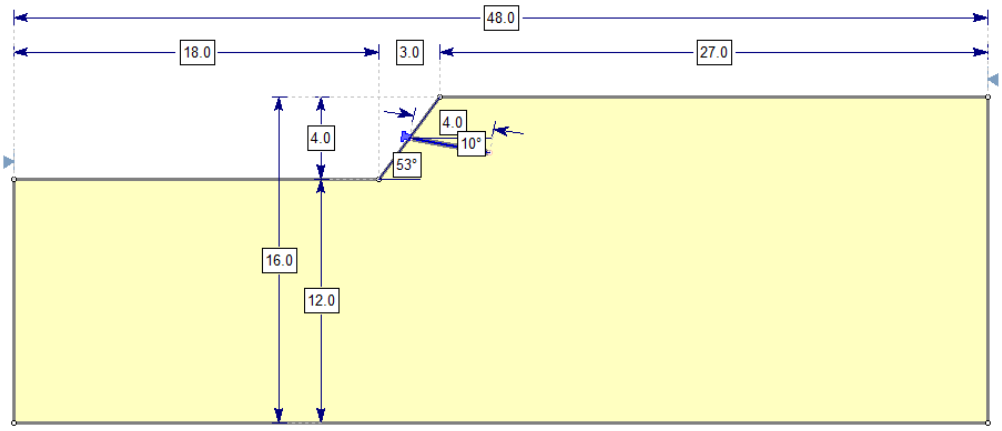

Fig. 23 Homogeneous slope geometry for validation with Bishop

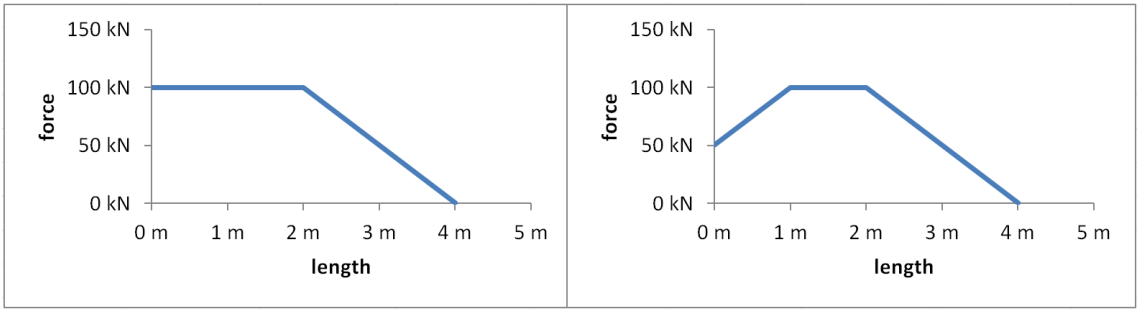

Fig. 24 Force diagrams of material set 1 and set 2

3.3.1.2 *Results 'Bishop'*

For this calculation, it is necessary to create an identical failure surface. SLIDE and GGU enable to define the radius and position of the failure circle. According to Tab. 4 GGU and SLIDE give the same results for the FOS. Fig. 25 shows a sketch of the employed measurements. The hand calculation is performed according to DIN 4084 (see equations in chapter 3.1.2). Additionally, the approach of Renk is evaluated since it contains a different definition for safety reduction of nail forces.

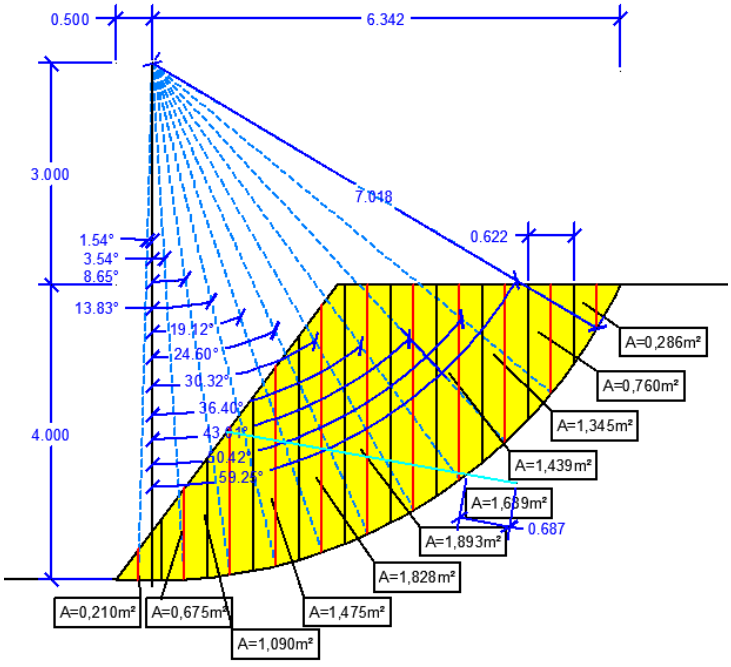

Fig. 25 Sketch of Bishop's failure surface

For material set 1, the slope collapses and exhibits a FOS of 0.59 without a supportive nail. Stable conditions are the result for material set 2 without reinforcements (FOS = 1.52). The results with an installed nail are listed in Tab. 4.

Tab. 4 Results for calculation with simplified Bishop method

	unit	SLIDE	GGU	Manual	Renk
$\eta_{BISH.}$ of material set 1	-	1.83	1.82	1.83	2.10
F of material set 1	kN	35.04	34.40	34.50	34.50
$\eta_{BISH.}$ of material set 2	-	2.42	2.43	2.43	7.42
F of material set 2	kN	100	100	100	100

The results of axial forces do not differ, since a consistent implementation of the slip surface is applied. Concerning material set 2, a tensile force transfer of 100 kN is applied, as the limited tensile capacity (100 kN) is reached. This validation proves that GGU and SLIDE use the formulas according to DIN 4084. Renk's approach gives a noticeable overestimation of the FOS, especially for the cohesive soil.

3.3.2 Validation using the simplified Janbu method

3.3.2.1 *Geometry and material parameters*

For the validation of Janbu's approach, another model with different geometry and material parameters is introduced. Fig. 26 visualises the homogeneous slope with 6 m height and an inclination of 85° (plotted from SLIDE). For this validation a pattern of 6 soil nails (Tab. 5) and only one material set (Tab. 6) is investigated.

Tab. 5 Soil material parameters - case Janbu

Parameter	Symbol	Unit	Mat. Set
strength model	-	-	MC
Friction angle	φ'	°	35
Cohesion	c'	kN/m²	0.1
Unit weight	γ	kN/m³	20

Tab. 6 Soil nail parameters - case Janbu

Parameter	Symbol	Unit	Mat. Set
Bond strength	T_m	kN/m	50
Tensile capacity	R_T	kN	100
Plate capacity	R_P	kN	100
Nail inclination	ε	°	10
Nail length	L_N	m	3
Out-of-plane spacing	L_s	m	1

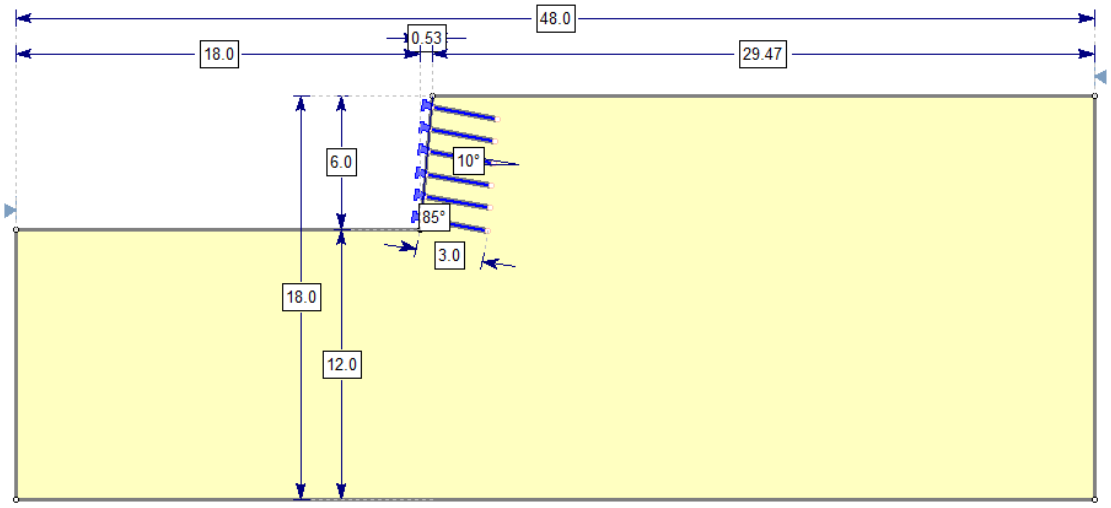

Fig. 26 Homogeneous slope geometry for validation with Janbu

3.3.2.2 *Results for Janbu*

Due to a polygonal failure surface, a planar slip surface is chosen (see Fig. 27). The manual calculation is performed according to DIN 4084 (see equations in chapter 3.1.3) and the approach by Renk is investigated.

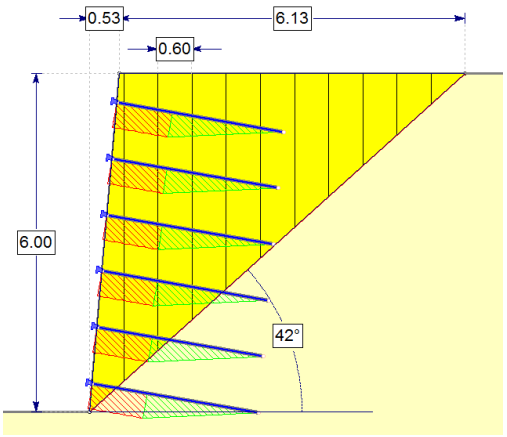

Fig. 27 Sketch of Janbu failure surface

Without any support, the FOS is 0.78, thus the system is in unstable conditions. The results for the factor of safety (with support) are listed in the table below.

Tab. 7 Results for calculation using simplified Janbu method

	unit	SLIDE	GGU	Manual	Renk
η	-	1.66	1.64	1.66	3.00

Only soil nails with an intersection of the failure surface experience a force transfer. For each of the calculations, similar results are obtained by SLIDE and GGU. Such evaluations ensure that both programs use the formulas according to DIN 4084. Further, Renk's approach gives a noticeable overestimation of the FOS.

4 Finite element investigations using PLAXIS 2D

For practical geotechnical problems the conventional limit equilibrium (LE) method is typically used to determine the factor of safety. In recent years the practical use of finite element methods (FEM) is on the rise and is adduced to face plenty of boundary value problems.

For the numerical performance, the two-dimensional FE program PLAXIS 2D version 2015.02 (Brinkgreve & et al., 2015) is used for this study. The main focus of this chapter is to compare LE with FE methods and investigate the opportunities of modelling nails in PLAXIS 2D. A comparison of the useable elements with a parameter study is presented. Thereby, the main attention is concentrated on the FOS, the incremental shear strains and the inner nail forces. The comparative studies are carried out to get an insight of the behaviour of reinforced slopes and soil nails.

4.1 Comparison of LE and FE method

The LEM is typically preferred by the majority of engineers. It enables to calculate the FOS without any knowledge of the initial state conditions and is thus often used to evaluate stability analysis. To solve the FOS, estimations on internal force distributions (e.g. pull-out capacity) need to be made. In contrast to LE approaches, finite element methods consider a stress-strain relation. The FOS is gained by the strength reduction method, including following benefits:

- critical failure surface is detected automatically
- no assumptions on distribution of inter-slice forces
- employable for complex conditions

A main disadvantage can be the time consuming computation. However, using a high performance computer, the computation time can be noticeably reduced. The selection of a suitable constitutive model and boundary conditions are of course necessary. Several researches verified that LE and FE give similar FOS, when considering simple geometries with homogeneous soil slopes (Cheng, Lansivaara, & Wei, 2006).

In this thesis, a comparison of reinforced slopes is performed, to show the difference to FOS for LE and FE calculations.

4.2 Description and implementations of Plaxis 2D

PLAXIS version 2015.02 is a two-dimensional finite element tool for commercial applications to perform deformation and stability analysis for a variety of geotechnical problems. For the following calculations, a plane strain modelling is employed. Besides the plane strain condition also an axisymmetric model is available (Brinkgreve & et al., PLAXIS 2D 2015 - User Manual, 2015).

For slope-stability problems the FOS is obtained by means of a φ-c reduction routine. As illustrated in the PLAXIS manual (Brinkgreve & et al., 2015), the strength reduction method is conducted with mobilised strengths for the friction angle φ' and the cohesion c'. An incremental decrease of $tan\varphi'$ and cohesion c' is performed assuming a Mohr-Coulomb failure criterion. In the FE code, the strength criterion is reduced until equilibrium can no longer be sustained and the structure fails. The FOS is governed by the following equation:

$$FOS_{FE} = \frac{tan\varphi'}{tan\varphi'_{mob.}} = \frac{c'}{c'_{mob.}} \tag{4.1}$$

4.2.1 Mesh configuration and density

To model soil layers or other clusters two types of elements are available in PLAXIS 2D, namely 6-node or 15-node triangular elements (Fig. 28). The element type influences the memory consumption, speed and accuracy of the calculation. To ensure a high accuracy, the 15-node elements are selected for the following 2D-studies.

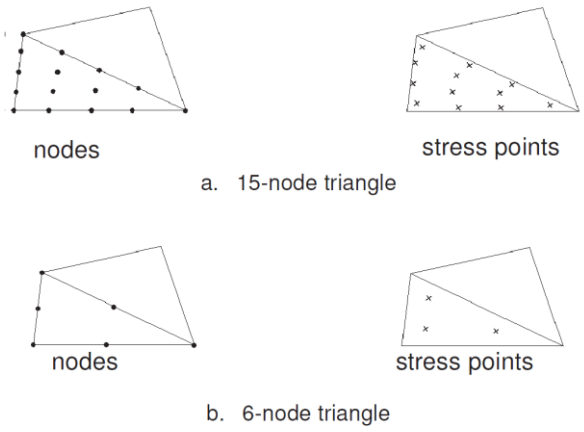

Fig. 28 FE elements in PLAXIS (Brinkgreve & et al., PLAXIS 2D 2015 - User Manual, 2015)

In PLAXIS, the mesh is generated automatically with the possibility of global and local refinements. The mesh density is varied to achieve an appropriate accuracy and computation time.

4.2.2 Soil constitutive model

For the prediction of stress-strain behaviour of soils, various material models have been developed. PLAXIS provides several models which differ in complexity and number of required parameters. With an increase in complexity of the used models, the number of parameters for the definition and the amount of required knowledge increase.

For the numerical simulations done in this thesis, the use of the Mohr-Coulomb model is sufficient. This simple linear-elastic and perfectly-plastic model also satisfies a comparison with LE-results. Compared to other soil constitutive models, a small number of input parameters is necessary. Elastic parameters (E, ν) and plastic parameters (c', φ', ψ) are utilised in the program. More information about the MC-model is visualised in chapter 3.2.1.3 and provided in the respective references (e.g. Schweiger, 2014). In-depth explanation, concerning the specified constitutive models in PLAXIS, is illustrated in Brinkgreve et al. (2015).

4.2.3 Support types concerning soil nail modelling in PLAXIS 2D

Although nails are real 3D objects (considered as bars, beams or columns), plane strain (2D) models are very important for practical geotechnical engineering. For the definition of soil nails, PLAXIS 2D provides the following feasible elements:

- geogrids (+interfaces)
- plates (+interfaces)
- volume elements (+interfaces)
- embedded beam row (EBR)

Until new embedded beam row facility was implemented in PLAXIS, 2D modelling of a nail was done mainly by means of plate or geogrid elements. The embedded beam rows are able to consider a 3D behaviour of bars. The different support types are evaluated and compared with several case studies in this work. Subsequently, a brief description of support types used in PLAXIS 2D is given. The explanations are mainly based on Brinkgreve et al. (2015).

4.2.3.1 *Interface elements*

Interface elements are used to model relative deformations between soil and structures. PLAXIS employs interface formulations with a virtual thickness. If a 15-noded soil element is used, the interface consists of five pairs of nodes and the shape

functions are compatible with the soil elements. For an evaluation of stresses at the interface elements, a Newton Cotes integration scheme is implemented. A schematic visualisation of interface elements is given in Fig. 29. Detailed information to the definition and theories of interface elements is illustrated in the dissertation of Tschuchnigg (2013).

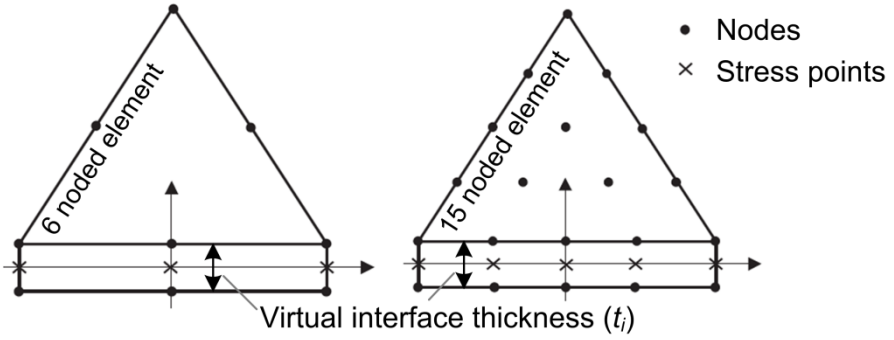

Fig. 29 Interfaces used in PLAXIS 2D (Tschuchnigg F. , 2013)

4.2.3.2 *Geogrid elements*

Geogrid elements represent a line element with axial stiffness but without bending stiffness. Hence, neither compression nor bending moments can be sustained; it can only receive traction. Since nails act primarily in tension, geogrid elements can be used for nails. To model an appropriate interaction between reinforcement and soil, geogrid elements have to be defined with interface elements. There is a single input parameter, which is the *axial stiffness* (*EA*). Hence, the focus is on an equivalent conversion of the nail diameter to determine the correct *EA*.

The required material set for geogrids:

- Input axial stiffness *EA*
- Selection of isotropic/anisotropic stiffness pattern
- Selection of elastic/elastoplastic behaviour.
- Maximum axial tension force N_p (in case of elastoplastic behaviour)

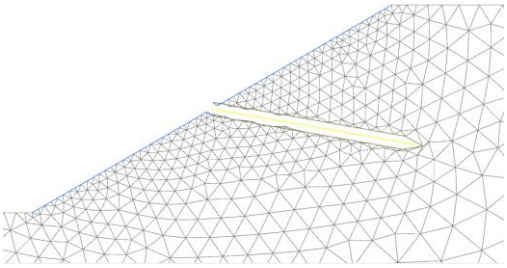

Fig. 30 Geogrid in combination with interfaces, plotted from PLAXIS 2D

If elastoplastic material behaviour of the structure type is selected, the input of a maximal bearing tension capacity (N_p) has to be entered. The stresses are redistributed to the adjacent soil if the maximal traction is exceeded.

4.2.3.3 *Plate elements*

Plates have similar properties as the above characterised geogrids. They are also a line element, additionally providing a bending stiffness input (*EI*). Similar to geogrids, modelling soil nails have to be combined with using interfaces to take nail-soil interaction into account. Soil cannot flow through the plates because of a 2D plane strain representation of the problem.

A new feature is the end bearing option, which allows a tip resistance at the end of a plate. This feature is useful for modelling piles or diaphragm walls but is inappropriate for modelling soil nails, since they do in general not act in compression. Note that a parameter study concerning the end bearing option is provided in appendix 8.1.

The required material set for plate elements:

- bending stiffness *EI*
- axial stiffness *EA*
- selection of isotropic/anisotropic stiffness pattern
- selection of elastic/elastoplastic behaviour
- end bearing option (neglected for modelling tension members)
- max. axial tension force N_p and max. bending moment M_p (in case of elastoplastic behaviour)

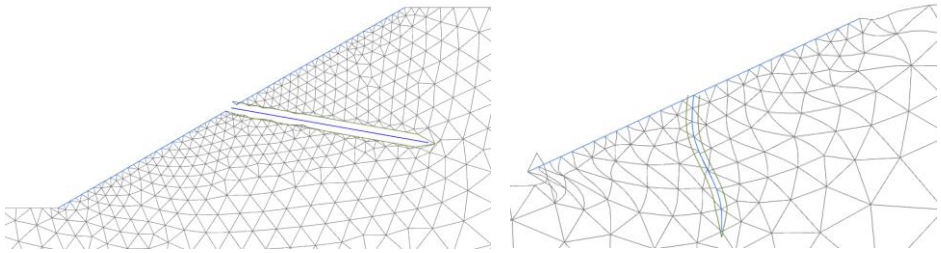

Fig. 31 Plate in combination with interfaces, plotted from PLAXIS 2D

If elastoplastic material behaviour for plates is chosen, the axial force is limited by N_p and the maximum bending moment is limited by M_p. The stresses are redistributed to the adjacent soil if the limits are reached (Brinkgreve & et al., PLAXIS 2D 2015 - User Manual, 2015).

4.2.3.4 *Embedded beam rows (EBR)*

This new function within PLAXIS is implemented to simulate a row of bars with an out-of-plane distance perpendicular to the model area. Due to that, embedded beams are schematised as a row of structural elements in 2D. Fig. 33 illustrates the principles of the 2D embedded beam row.

The EBR is able to sustain axial forces and bending. Because of the usage of special line-to-line interfaces, the elements are not directly coupled to the mesh. The line-to-line interfaces consist of spring elements and sliders (Fig. 34), which enable a continuous mesh (soil can flow through the EBR) and the consideration of skin resistance. The image on the right for Fig. 32 (deformed mesh plot) shows that nail and soil can move independently.

With a point-to-line interface a base resistance can be simulated (negligible for soil nails). The bearing capacity in axial direction of the beam is provided by the skin (T_{skin}) and tip resistance (F_{max}). Elastic, as well as elastoplastic behaviour can be defined for this element type. With the introduction of new features in PLAXIS 2D v2015, it is possible to manipulate the lateral skin resistance of the EBR. With the manipulation of the lateral and axial skin resistances it is possible to enable a consideration of 3D effects.

The required material set for EBRs:

- Young's modulus E
- unit weight γ
- diameter D of the beam

- selection of a beam type (e.g. circular or squared)
- selection of elastic/elastoplastic behaviour.
- out-of-plane spacing L_s
- max. axial tension force N_p and max. bending moment M_p (in case of elastoplastic behaviour)
- axial skin resistance T_{skin}
- lateral skin resistance T_{lat}
- base resistance F_{max}

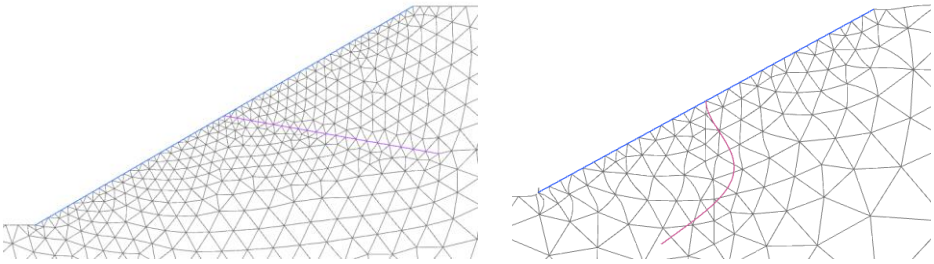

Fig. 32 EBR implemented in PLAXIS 2D, and deformed mesh

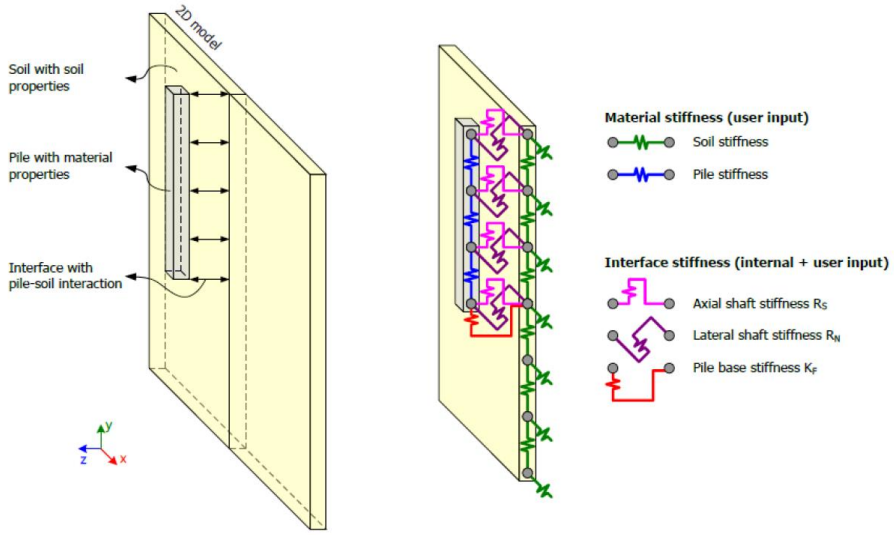

Fig. 33 2D principle of embedded beam interaction with soil (Sluis, 2012)

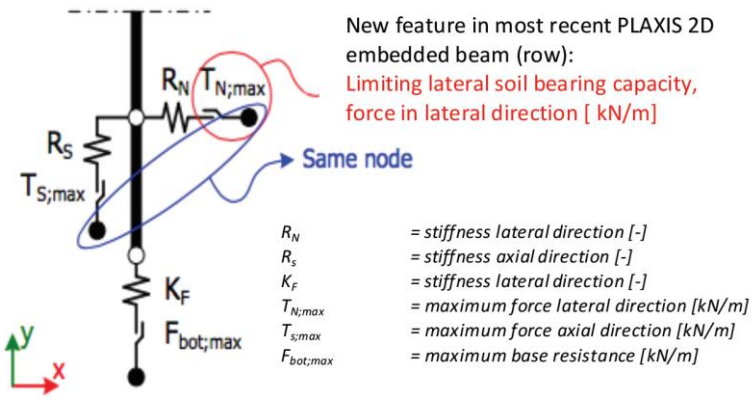

Fig. 34 Principle of interfaces (Sluis, 2012)

The derivation of the interface stiffness and resistant forces can be found in Sluis (2012). The original 3D formulation of an embedded pile is described in the dissertation of Tschuchnigg F. (2013).

4.2.4 Calculations phases

The calculation phases for the safety analysis in PLAXIS 2D can be found in Tab. 8. Four phases are computed for the case studies. Since the initial state is simulated with a K_0-procedure and a non-horizontal geometry is entered, a nil-step is added. In the second phase, the nails and other support types are activated. The numerical determination of the FOS in PLAXIS 2D is performed by φ/c-reduction.

Tab. 8 Calculation phases for FOS_{FE} in PLAXIS 2D

Phase nr.	Phase ID	Calculation type	Loading type
Phase 0	Initial phase	K_0-procedure	Staged construction
Phase 1	0-step	Plastic	Staged construction
Phase 2	Installation support	Plastic	Staged construction
Phase 3	Safety	φ/c-reduction	Incremental multipliers

4.3 Validation of support types in PLAXIS 2D

In these case studies, the behaviour of different support types (specified in PLAXIS 2D) is investigated. Furthermore, a comparison of FOS for LE and FE outcomes is applied. The results of the 'associated case studies' are compared with limit equilibrium calculations (computed with SLIDE). In the present study, both a non-associated flow rule (dilation angle = 0) and an associated flow rule (dilation angle = friction angle) are defined. The focus lies on the FOS results, the location of critical failure surface, and the maximum shear strain increment. The numerical determination of the FOS in

PLAXIS 2D is done by φ/c-reduction. In SLIDE, the FOS is done by means of the GLE/Morgenstern-Price method.

The first two examples represent a simple homogeneous reinforced slope. The geometry and soil parameters are related to Tschuchnigg, et al. (2015). A parameter study on the mesh discretisation and the cohesion was done in advance. The results of these calculations can be found in appendix 8.2.

4.3.1 Description of the model

The first model (depicted in Fig. 35) has a slope height (h) of 2 m and a slope inclination (α_s) of 30°. As support, a rigid facing and a single nail are installed (case 1). For case 2 (Fig. 36), a slope height of 10 m and the installation of 6 nails have been chosen. A constant spacing of 1.25 m in vertical direction of the nails is defined. The nail length is 2 m for case 1 and 5 m for case 2. For both cases the nail inclination equals to -10° and their out-of-space distance is 1 m. Due to non-cohesive ground, the installation of a rigid facing is required to prevent a slope-failure close to the surface (see Fig. 37). Note that a parametric study on rigid facing definitions can be found in appendix 8.1.

The FEM models are plane strain models consisting of 948, and 2479 15-noded elements. A fine mesh is applied in both cases with a refinement (coarseness factor = 0.25) along the slope and the nails.

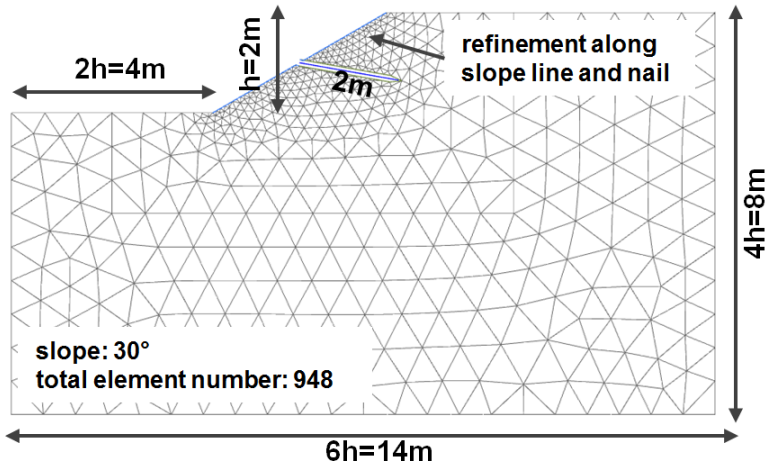

Fig. 35 Geometry and FEM mesh for case 1

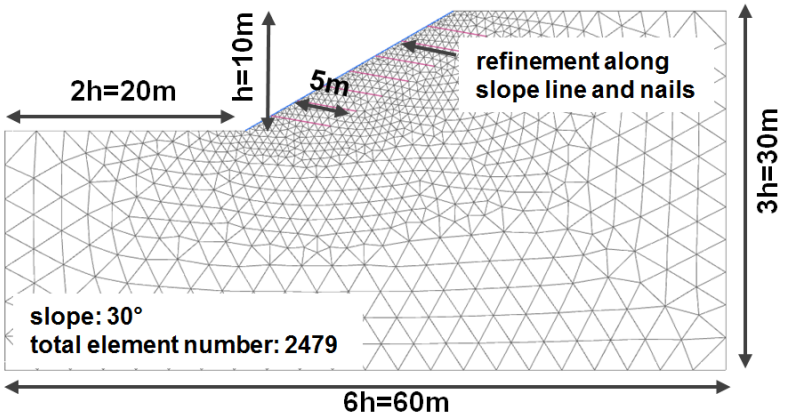

Fig. 36 Geometry and FEM mesh for case 2

4.3.2 Input parameters

One material set is investigated for both cases. The only variation concerns the geometry and the number of nails. Material properties for the calculation in SLIDE are given in Tab. 9.

Tab. 10 displays the soil parameters for the case studies in PLAXIS. To avoid numerical problems a small cohesion of 0.1 kN/m² is used. No water conditions are considered and drained conditions are applied in the analysis (unsaturated unit weight is equal to the saturated unit weight). Soil nails and the rigid facing are considered to have an elastic behaviour and an isotropic distribution of the stiffness. The plate element for the rigid facing is defined with zero weight to avoid any influence on the FOS. A tensile capacity of 100 kN and a diameter of 0.1 m is assumed for the grout body in SLIDE. For PLAXIS a Young's modulus of 2.1E7 kN/m² (concrete) is chosen for the support types. The plate and geogrid elements (nail) require a conversion into the appropriate equivalence in PLAXIS 2D. This is done via an equivalent thickness *d,* received from a conversion of cross section areas (circular area of the nail equals to the rectangular area of the plate).

For embedded beam rows, the influence of the skin friction parameters is eliminated by either setting high or unlimited values.

Tab. 9 Material parameters for LE analysis in SLIDE

Soil	**Symbol**	**Unit**	**Mat. Set**
Strength model	-	-	MC
Friction angle	φ'	°	35
Cohesion	c'	kN/m²	0.1
Unit weight	γ_{unsat}	kN/m³	17
Soil nail	**Symbol**	**Unit**	**Mat. Set**
Bond strength	T_m	kN/m	50
Tensile capacity	R_T	kN	100
Plate capacity	R_P	kN	100

Tab. 10 Material parameters for FE analysis in PLAXIS 2D (case 1 and 2)

Soil	**Symbol**	**Unit**	**Mat. Set**	
			associated	**non-associated**
Strength model	-	-	MC	MC
Stiffness	E'	kN/m²	40 000	40 000
Poisson ratio	ν'	-	0.3	0.3
Cohesion	c'	kN/m²	0.1	0.1
Unit weight	$\gamma_{unsat}/\gamma_{sat}$	kN/m³	17	17
Friction angle	φ'	°	35	35
Dilatancy angle	ψ'	°	35	0
Rigid facing (plate element)	**Symbol**	**Unit**	**Mat. Set**	
Axial stiffness	EA	kN/m	2 100 000	
Bending stiffness	EI	kN m²/m	1750	
weight	w	kN/m/m	0	
Nail (geogrid)	**Symbol**	**Unit**	**Mat. Set**	
Axial stiffness	EA	kN/m	165 000	
Nail (plate)	**Symbol**	**Unit**	**Mat. Set**	
Axial stiffness	EA	kN/m	165 000	
Bending stiffness	EI	kN m²/m	0.85	
Nail (EBR)	**Symbol**	**Unit**	**Mat. Set**	
Young's modulus	E	kN/m²	2.1*E7	
Unit weight	γ	kN/m³	25	
Diameter	D	m	0.1	
Out-of-plane spacing	L_s	m	1.0	
Axial skin resistance	T_{skin}	kN/m	500	
Lateral skin resistance	T_{lat}	kN/m	unlimited	
Base resistance	F_{max}	kN	0	

4.3.3 Results

The rigid face is designed with a plate element and is installed to avoid failure near the slope surface (Fig. 37). A failure near the slope was also excluded for LE analysis by setting external boundaries. The objective is to obtain a failure mechanism behind the soil nails. This is possible due to linear elastic behaviour of the structural elements.

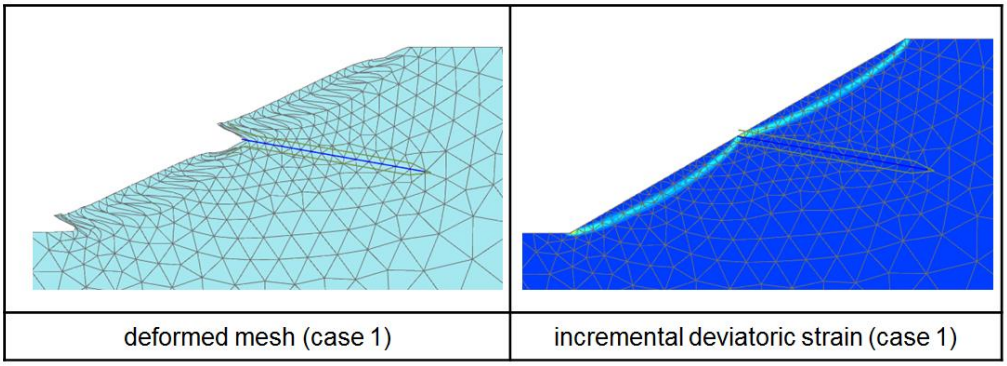

Fig. 37 Failure mechanism (case 1) without rigid facing

The difference in the FOS between the various support types is illustrated below. For the comparison of LE and FE ($\psi=\varphi$), roughly the same results are gained, except for geogrids in case 1 (see Tab. 11). This is due to a different failure mechanism (Fig. 39) and is most probably caused by the lack of a bending stiffness. In case 2, all results of FOS correspond and give similar values of FOS. Tab. 12 compares the same conditions with a non-associated flow rule ($\psi=0$). By neglecting the influence of the skin resistance (set to high values for EBR), embedded beam rows and plates exhibit a similar behaviour. A parameter study on the skin resistance is shown in chapter 4.6. The FOS for associated and non-associated flow rule differs within 4%– 7%. It can be seen in appendix 8.2, a higher cohesion leads to less difference between the flow rules. The flow rule may have significant influence on the results when having a high friction angle. In-depth information concerning the influence of a non-associated flow rule can be found in Tschuchnigg, et al. (2015).

Tab. 11 LE and FE (associated) results for factor of safety

case	SLIDE		PLAXIS 2D (associated)			
	No support	nail	No support	geogrid	plate	EBR
Case 1	1.32	2.00	1.32	1.83	1.96	1.96
Case 2	1.25	1.68	1.22	1.62	1.64	1.64

Tab. 12 FE (non-associated) results for factor of safety

case	PLAXIS 2D (non-associated)			
	No support	geogrid	plate	EBR
Case 1	1.22	1.74	1.88	1.88
Case 2	1.14	1.49	1.50	1.52

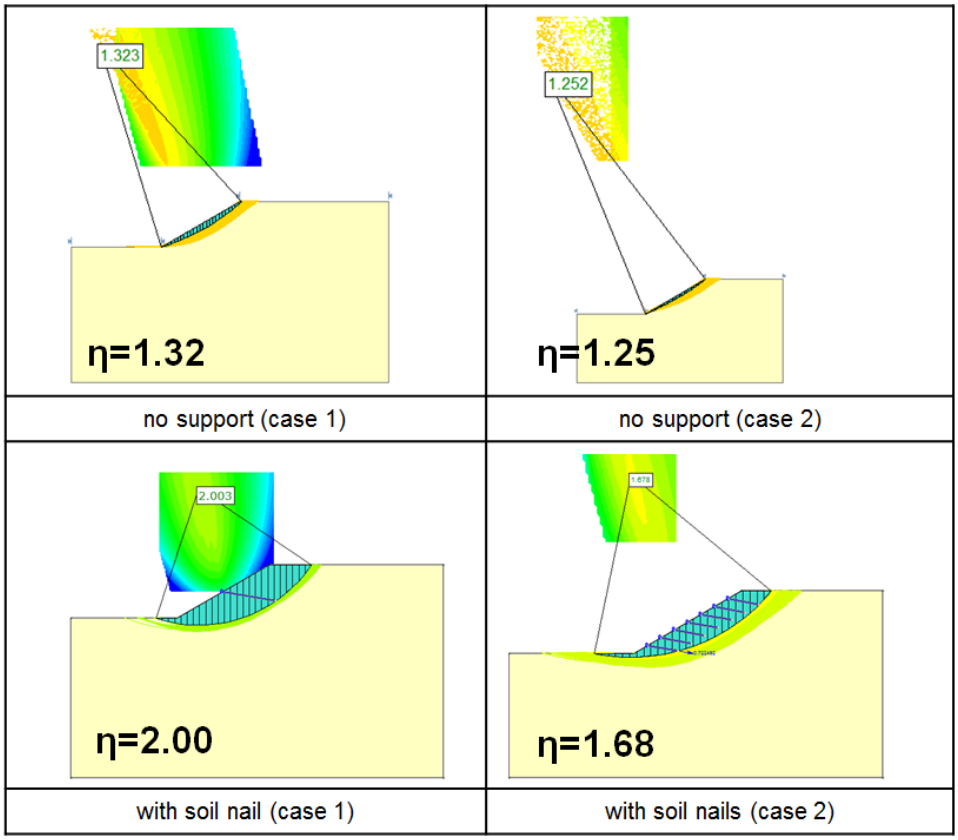

Fig. 38 FOS detection with SLIDE (GLE-Morgenstern/Price)

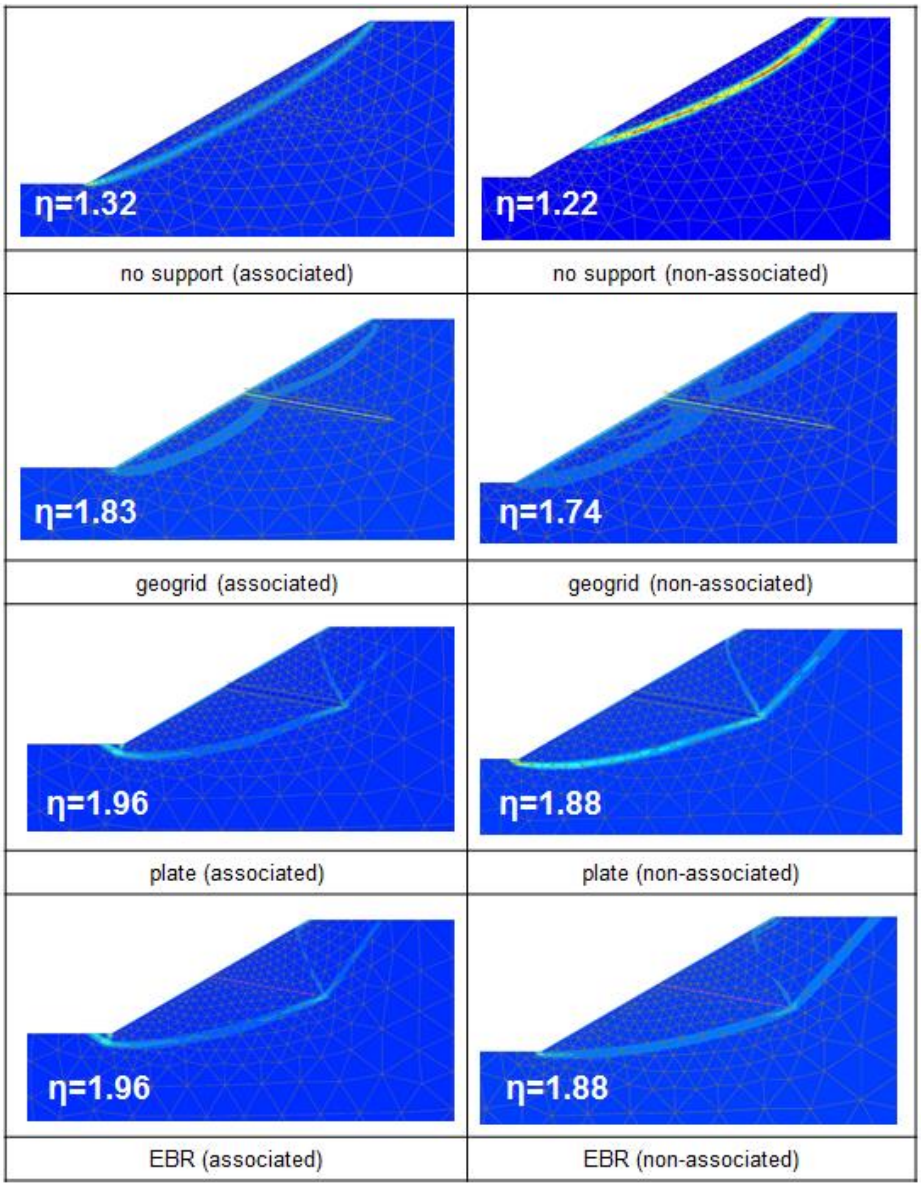

Fig. 39 Failure mechanisms for case 1 (incremental deviatoric strains)

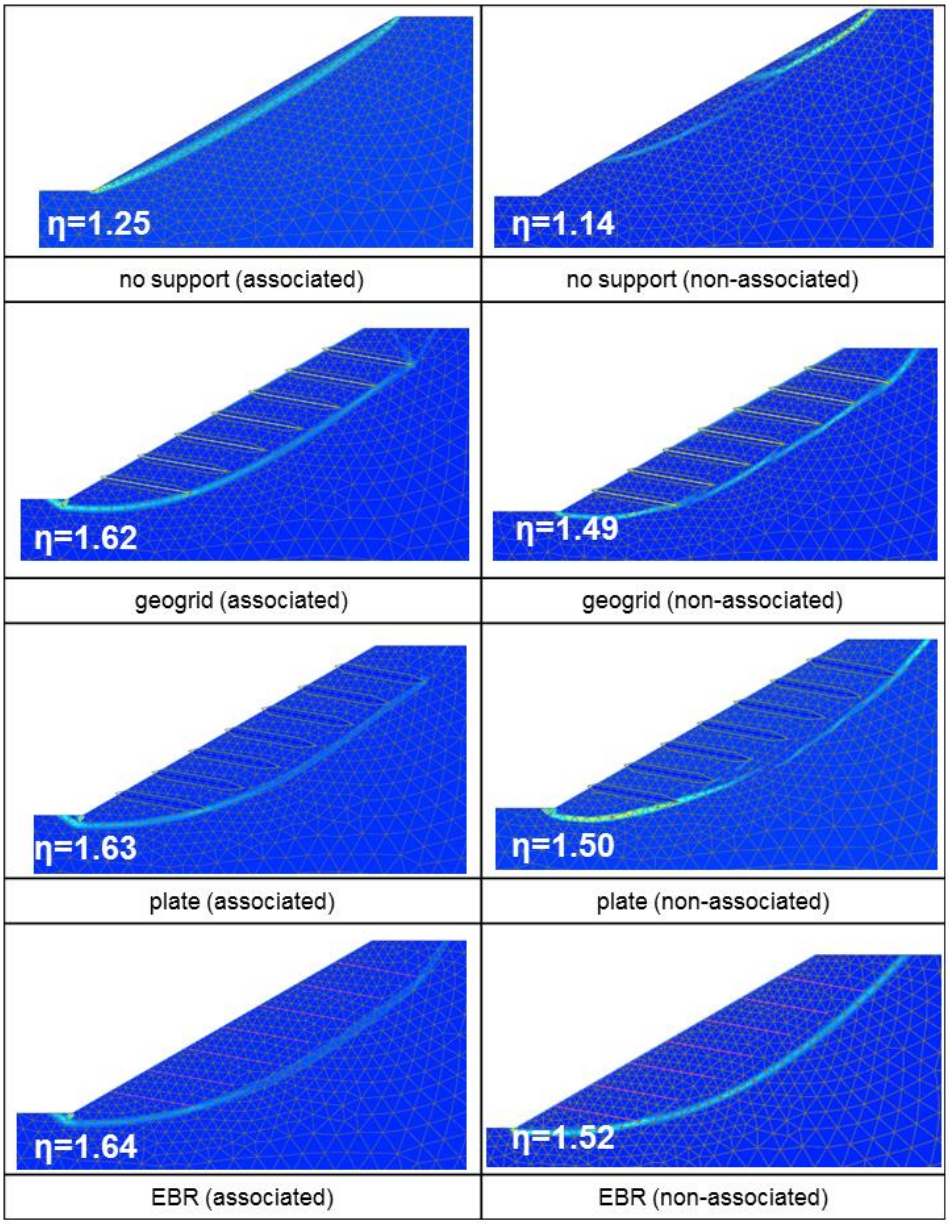

Fig. 40 Failure mechanisms for case 2 (incremental deviatoric strains)

Fig. 41 and Fig. 42 show FOS_{FE} versus the total displacements. An irregular oscillation of the FOS_{FE}-curve is obtained in the non-associated calculations especially for case 2 (mean values are taken). A detailed explanation to this phenomenon can be found in the paper Tschuchnigg, et al. (2015).

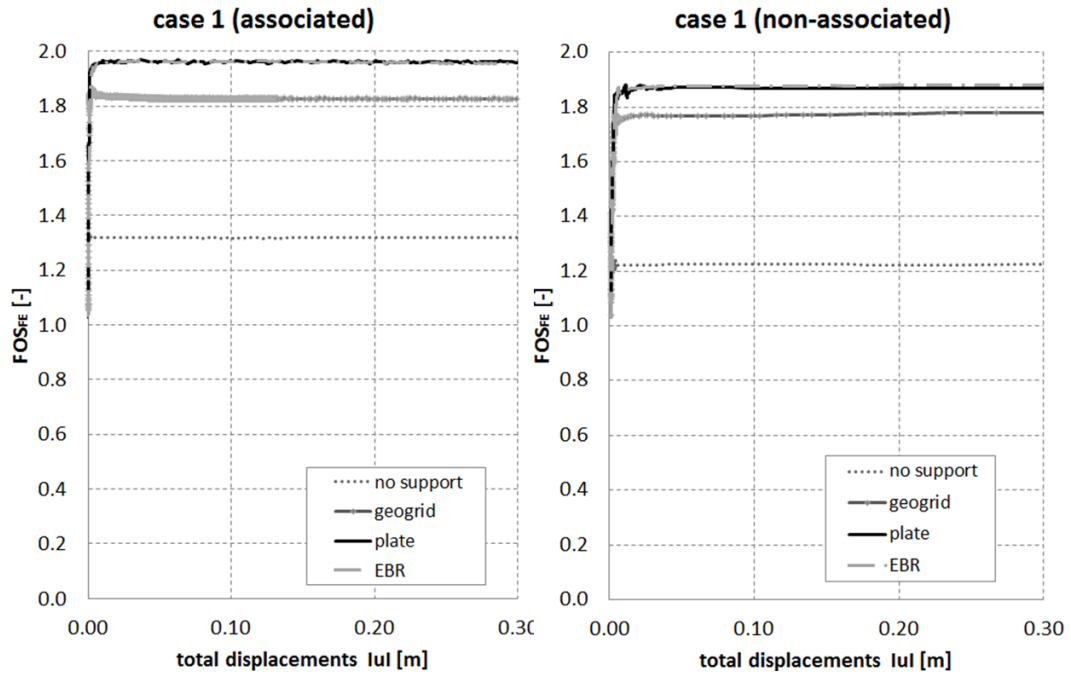

Fig. 41 FOS_{FE}-progression of different support types (case1)

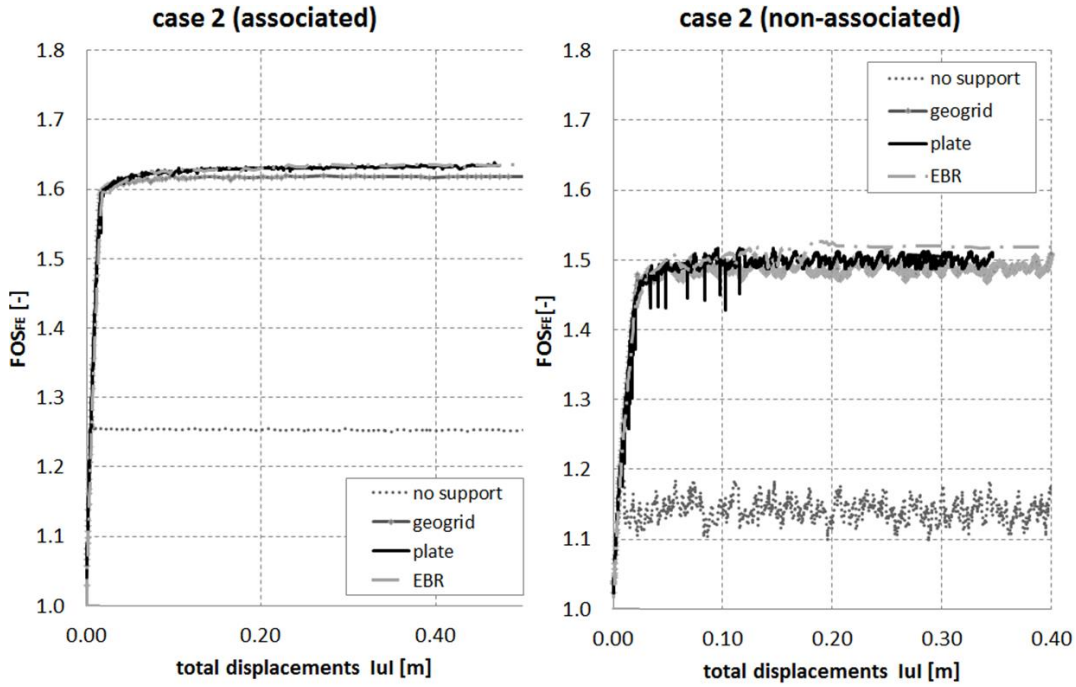

Fig. 42 FOS_{FE}-progression of different support types (case2)

4.4 Validation of elastoplastic material behaviour

The purpose of the following numerical simulations is the investigation of an elastoplastic material behaviour for different support types in PLAXIS 2D. The study is applied for case 1, described in chapter 4.3, with an associated ($\psi=\varphi$) and non-associated ($\psi=0$) flow rule. The objective is to reach the elastoplastic bearing capacity

and receive a failure surface inside the reinforced body mass. To achieve such a failure, the maximum axial force N_p and the bending moment M_p are set to values smaller than the values gained from the study utilising elastic material behaviour. Since the main part of the load occurs in axial direction of the nail (for case 1), the elastoplastic behaviour primarily depends on the limitation of the N_p. Note that the entered elastoplastic limits do not correspond with real material behaviour.

4.4.1 Description of the model

Fig. 35 represents the geometry for the numerical simulation. As support, a rigid facing and a single nail (ε = -10°) are defined (case 1). The detailed description of the model can be found in chapter 4.3.1.

4.4.2 Input parameters

The soil properties remain the same as in case 1 (chapter 4.3.2, Tab. 9). In addition to the previous soil nail features, elastoplastic material parameters are added. The calculation phases for the safety analysis can be found in the Tab. 8.

Tab. 13 Material parameters for soil nail structures

Nail (geogrid)	**Symbol**	**Unit**	**Mat. Set**
Axial stiffness	EA	kN/m	165 000
Max. axial force	N_p	kN/m	variable
Nail (plate)	**Symbol**	**Unit**	**Mat. Set**
Axial stiffness	EA	kN/m	165 000
Bending stiffness	EI	kN m²/m	0.85
Max. axial force	N_p	kN/m	100/3/1/0.1
Max bending moment	M_p	kNm/m	100/0.01
Nail (EBR)	**Symbol**	**Unit**	**Mat. Set**
Young's modulus	E	kN/m²	2.1*E7
Unit weight	γ	kN/m³	25
Diameter	D	m	0.1
Out-of-plane spacing	L_s	m	1.0
Axial skin resistance	T_{skin}	kN/m	500
Max. axial force	N_p	kN/m	100/3/1/0.1
Max bending moment	M_p	kNm/m	100/0.01
Lateral skin resistance	T_{lat}	kN/m	unlimited
Base resistance	F_{max}	kN	0

4.4.3 Evaluation of nail forces with elastic material behaviour

To set limits for N_p and M_p, a determination of the nail forces for elastic material behaviour is performed. Achieving a reasonable comparison between the different support types is difficult, since the FOS-development varies among them. Fig. 43 illustrates the evaluation results of the forces for case 1 with an associated flow rule. As shown in the figures below, the force distributions are obtained right before the bend of the FOS_{FE}-curves (FOS_{FE}=1.92 for plate and EBR, FOS_{FE}=1.82 for geogrid).

Tab. 14 Evaluation of nail forces for case 1 (elastic material behaviour)

	Case 1 (associated)			Case 1 (non-associated)		
	Geogrid	**Plate**	**EBR**	**Geogrid**	**Plate**	**EBR**
N [kN/m]	3.6	4.3	4.6	4.5	4.3	4.3
Q [kN/m]	-	-0.8	-1.5	-	-0.6	-1.0
M [kNm/m]	-	0.1	0.3	-	0.12	-0.3

For the definition of elastoplastic material behaviour of the support, the parameters N_p and M_p are set to values below the ones in Tab. 14.

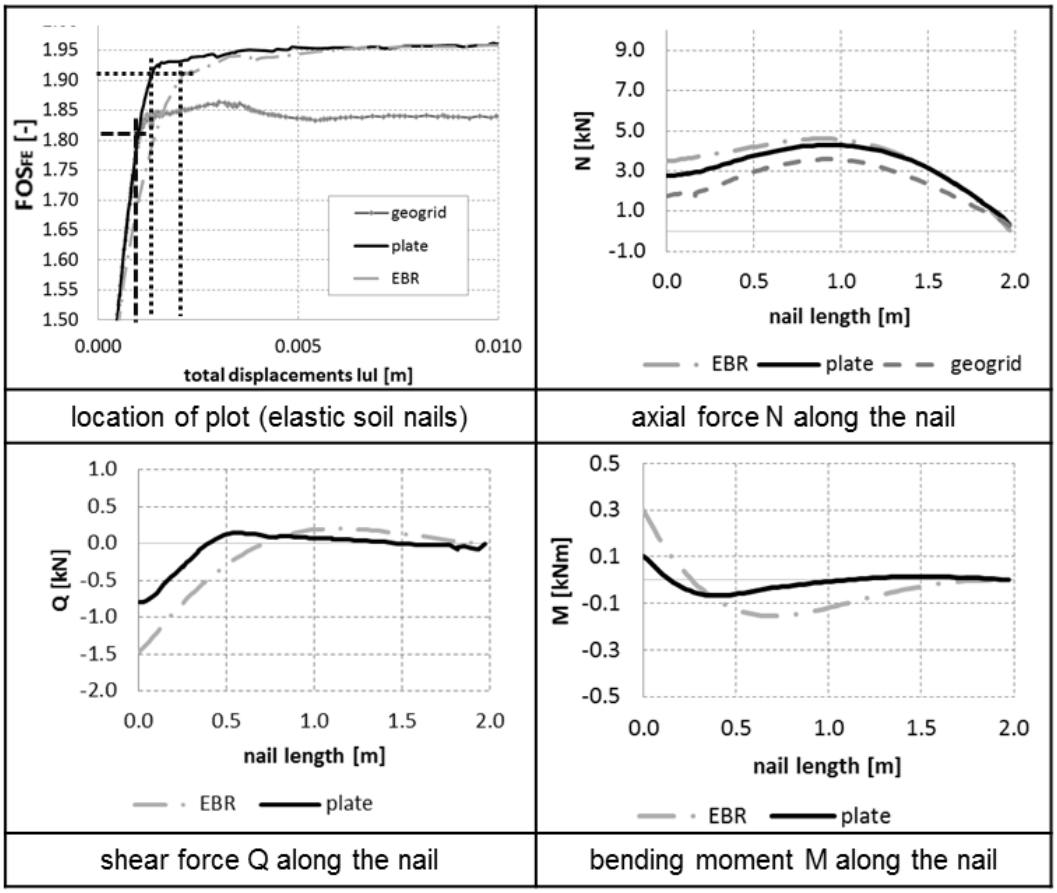

Fig. 43 Evaluation of nail forces for case 1 (associated)

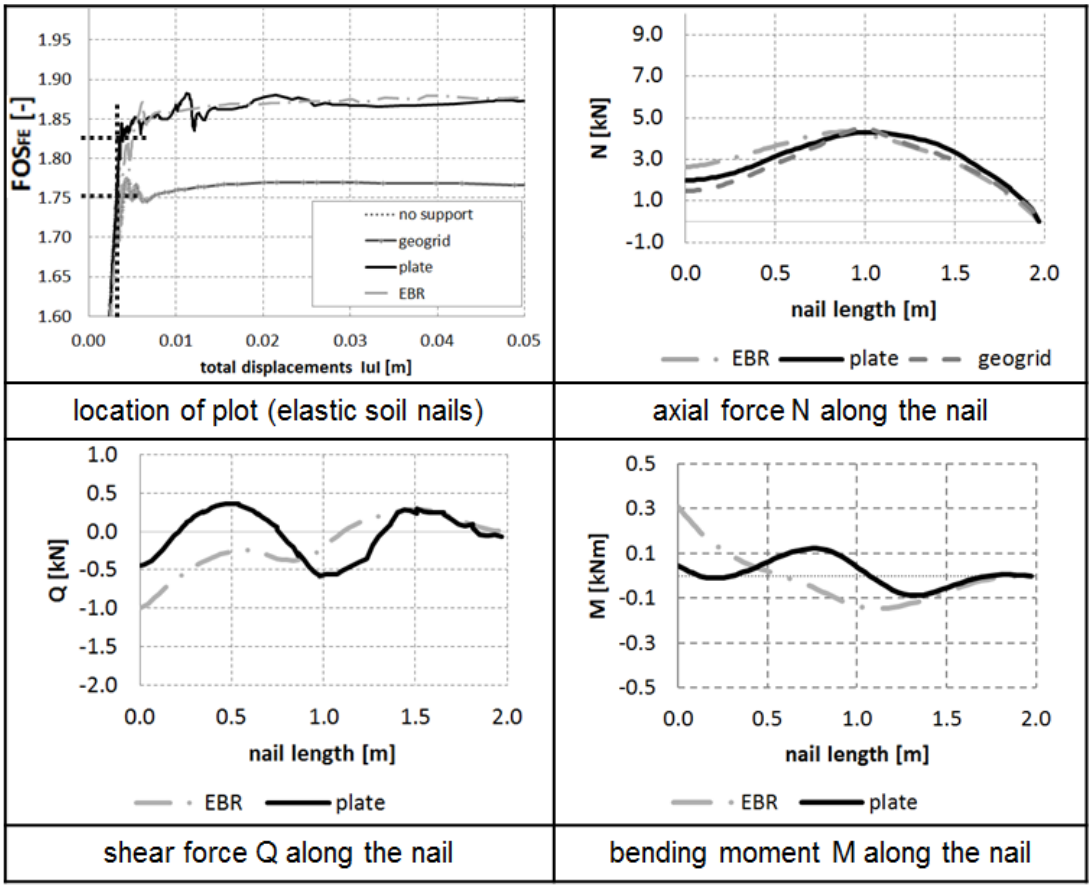

Fig. 44 Evaluation of nail forces for case 1 (non-associated)

Note that the development of shear forces and bending moments is changing for the different flow rules.

4.4.4 Results

To have an impact on the outcomes of the factor of safety, the maximum axial force N_p is defined with a value lower than 3.6 kN. The maximum bending moment M_p is 0.01 kNm/m. To observe individual influences, one of the two parameters is set to a very high value. Tab. 15 summarises the results for FOS of the simulation. The results show, that the bending moment has a low impact on the overall stability, especially when the axial force is restricted to a low value. A graphical representation of the failure mechanism and force distribution (input N_p=3kN/m, M_p=0.01kNm/m) is provided in Fig. 45 (for an associated study). An example for non-associated analysis is illustrated in Fig. 46. The main focus lies on the axial force distribution for the different support elements. As soon as the bearing capacity of the soil nail is reached, the failure surface shifts into the reinforced soil body.

Tab. 15 Results for FOS_{FE} - elastoplastic material validation

N_p [kN/m]	M_p [kNm/m]	Case 3 (associated)			Case 3 (non-associated)		
		Geogrid	Plate	EBR	Geogrid	Plate	EBR
>	**>**	1.86	1.96	1.96	1.74	1.88	1.88
3	**>**	-	1.81	1.82	-	1.71	1.71
1	**>**	-	1.52	1.51	-	1.40	1.40
0.1	**>**	-	1.41	1.41	-	1.29	1.29
>	**0.01**	1.86	1.93	1.93	1.74	1.83	1.83
3	**0.01**	1.80	1.80	1.80	1.70	1.70	1.70
1	**0.01**	1.52	1.52	1.52	1.39	1.40	1.40
0	**0**	1.32	1.32	1.32	1.22	1.22	1.22

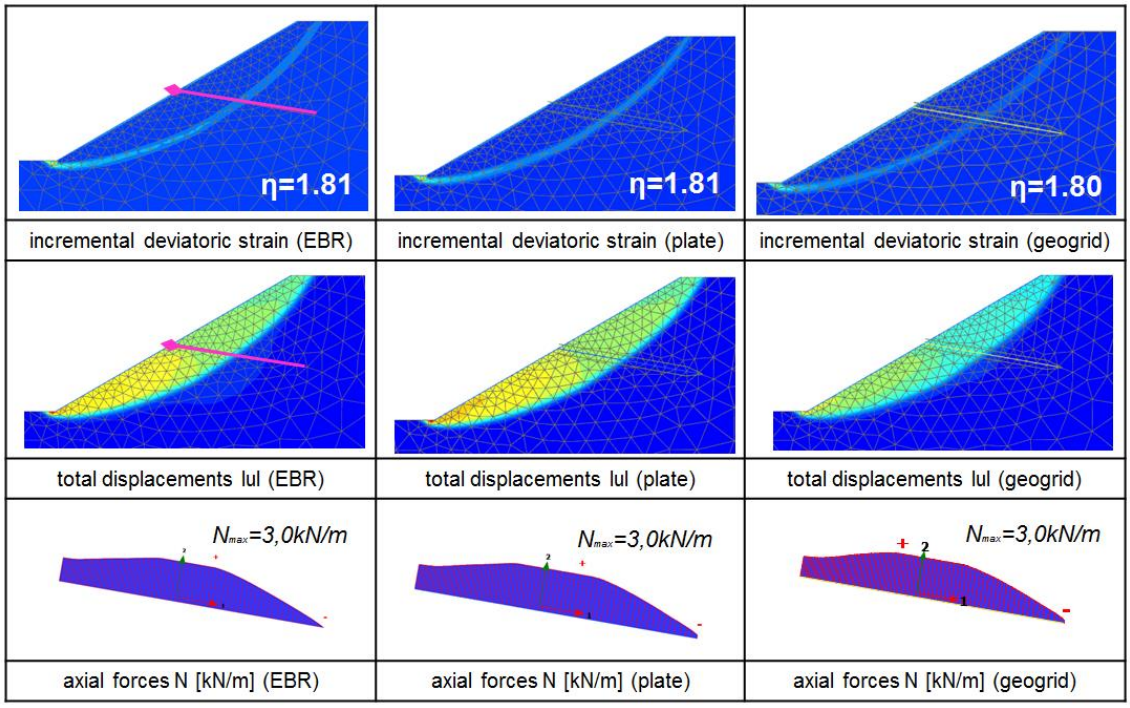

Fig. 45 Failure mechanism analysis - case 1 - associated flow rule (N_p = 3 kN/m, M_p = 0.01 kNm/m)

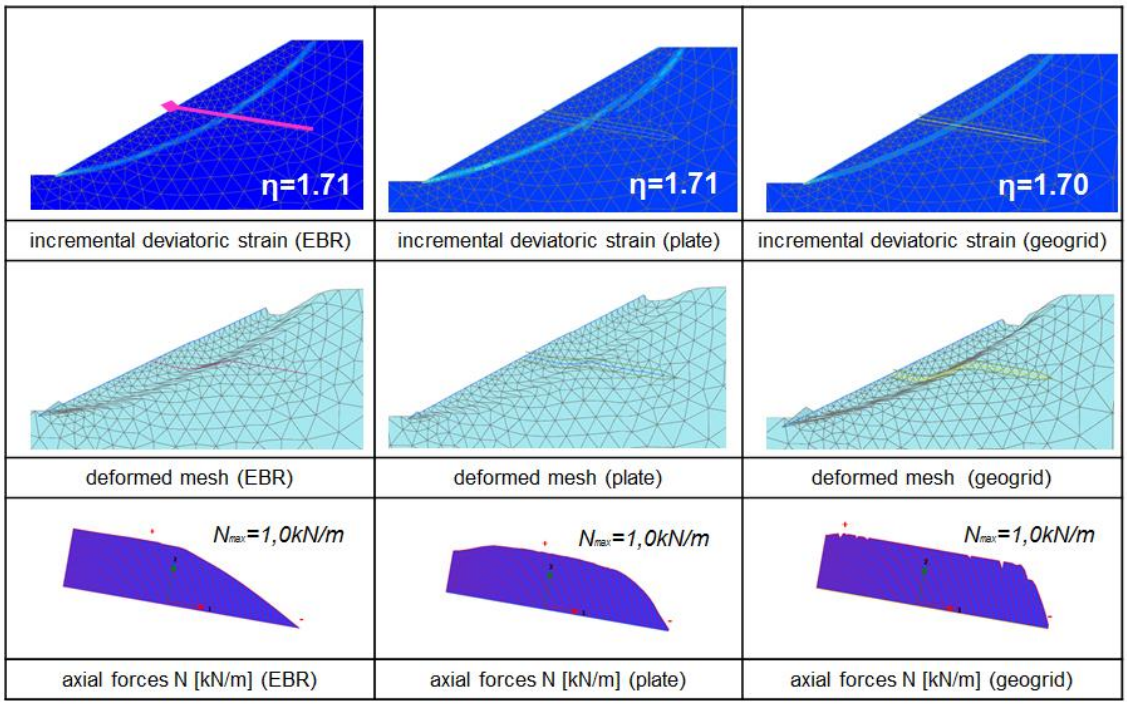

Fig. 46 Failure mechanism analysis - case 1 - non-associated flow rule (N_p=1kN/m, M_p=0.01kNm/m)

4.5 Validation of nail orientation

In this analysis (case 3), four different nail inclinations ε with three nail-rows are investigated with PLAXIS 2D. The effect of nail inclinations, which either exceed or deceed the horizontal, is evaluated. Geogrids, plates and embedded beam rows are used to model soil nails and are finally compared in this case study. The slope stability and the force distribution along soil nails are examined. Both, a non-associated flow rule ($\psi = 0$) and an associated flow rule ($\varphi = \psi$) are used. The geometry and soil parameters are adapted from the paper Tschuchnigg, et al. (2015).

4.5.1 Description of the model

The geometry model (Fig. 47) with a slope height of 10 m and a slope inclination (α_s) of 45°, is reinforced with 3 rows of nails (horizontal spacing is 1 m). The vertical distance of the nails is 2.5 m. The lengths of the support elements are 8 m. A variation of the nail orientation is modelled with different nail inclinations:

$$\varepsilon = 10°/0°/\text{-}10°/\text{-}20°$$

The installation of a facing is due to cohesive soil not necessary (no failure mechanism close to the slope surface). The FEM used in this study consists of a plane strain model

with 1494 15-noded elements. A fine mesh is applied to the computation with a refinement (coarseness factor = 0.25) along the slope line and soil nails.

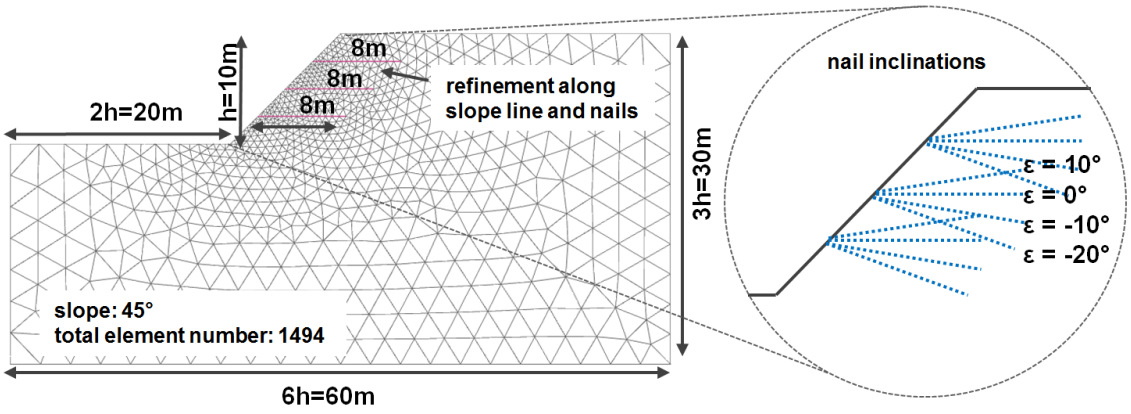

Fig. 47 Geometry and FEM mesh for case 3

The left figure above represents one example with a horizontal nail installation ($\varepsilon = 0°$) and the mesh discretisation.

4.5.2 Input parameters

The material set for case 3 is illustrated in Tab. 16. The table shows material parameters for a homogeneous soil and all used support types. A cohesive soil (c' = 20 kN/m²) with a friction angle of 25° is chosen. The only variation concerns the support orientation - the material parameters remain the same for this numerical computation. The soil nails are defined with an elastic behaviour and isotropic stiffness. A Young's modulus of 2.1E7 kN/m² is used for the support types. For embedded beam rows, the influence of lateral and axial skin resistance is eliminated by setting high or unlimited values. The plate elements (nail) require a conversion of the cross section area to achieve an appropriate equivalence.

Tab. 16 Material parameters for case 3 (PLAXIS 2D)

Soil	Symbol	Unit	Mat. Set	
			associated	non-associated
strength model	-	-	MC	MC
stiffness	E'	kN/m²	20 000	20 000
Poisson ratio	ν'	-	0.3	0.3
Cohesion	c'	kN/m²	20	20
Unit weight	$\gamma_{unsat}/\gamma_{sat}$	kN/m³	19	19
Friction angle	φ'	°	25	25
Dilatancy angle	ψ'	°	25	0
Nail (geogrid)	**Symbol**	**Unit**	**Mat. Set**	
Axial stiffness	EA	kN/m	165 000	
Nail (plate)	**Symbol**	**Unit**	**Mat. Set**	
Axial stiffness	EA	kN/m	165 000	
Bending stiffness	EI	kN m²/m	0.85	
Nail (EBR)	**Symbol**	**Unit**	**Mat. Set**	
Young's modulus	E	kN/m²	2.1*E7	
Unit weight	γ	kN/m³	25	
Diameter	D	m	0.1	
Out-of-plane spacing	L_s	m	1.0	
Axial skin resistance	T_{skin}	kN/m	500	
Lateral skin resistance	T_{lat}	kN/m	unlimited	
Base resistance	F_{max}	kN	0	

4.5.3 Results

A summary of the FOS_{FE} outcomes for non-associated and associated flow-rule definitions is given in Tab. 17. The corresponding FOS_{FE}-curves (development of FOS_{FE} vs. lul), plotted for EBR-elements, can be found in Fig. 48. The safety without reinforcements is 1.44 for the associated and 1.38 for the non-associated analysis. An evaluation of the impact on the axial force distribution is shown in the figures below. A comparison of all used support elements for the associated case with a nail orientation of ε = 10° is shown in Fig. 51. The effect of the nail inclinations on the axial nail-force-distribution for the associated case and a slope, reinforced with embedded beam rows, is shown in Fig. 52.

Tab. 17 FOS_{FE}-results of different nail inclinations

	Case 3 (associated)			Case 3 (non-associated)		
	Geogrid	Plate	EBR	Geogrid	Plate	EBR
No nails	1.44			1.38		
ε = 10°	1.51	1.51	1.51	1.47	1.47	1.48
ε = 0°	1.60	1.60	1.60	1.56	1.56	1.56
ε = -10°	1.73	1.73	1.73	1.69	1.69	1.70
ε = -20°	1.84	1.84	1.84	1.80	1.81	1.82

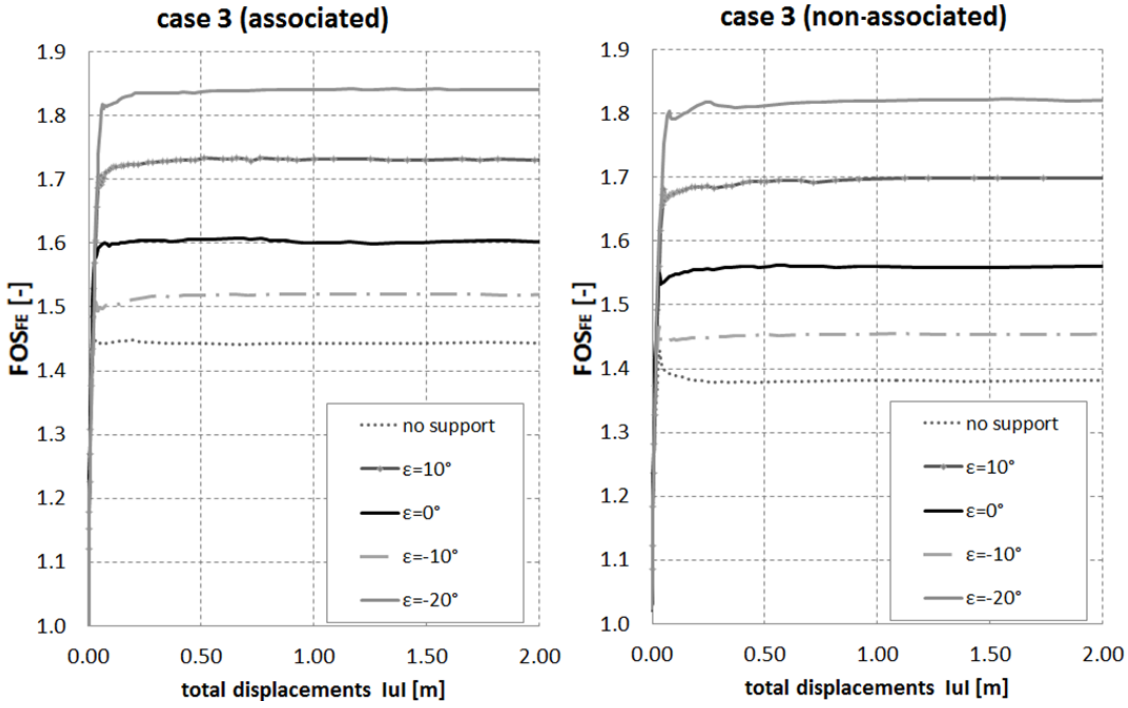

Fig. 48 FOS_{FE}-curves of EBR for different nail inclinations

Considering the different support elements, there is a small difference among the results of the FOS_{FE}. Even though geogrids are not equipped with a bending resistance, the results of the FOS_{FE} are slightly lower or even equal compared to the other support types. Due to elastic material behaviour, a failure of the nails does not occur, which means that the influence of the bending stiffness cannot be evaluated. As shown in Fig. 49, failure mechanisms only appear behind the reinforced soil mass. Applying elastic support shows that the results of the FOS_{FE} depend on geometrical conditions. A nail inclination which exceeds the horizontal (e.g., $\varepsilon = 10°$) leads to the most disadvantageous failure surface among the present cases (see Fig. 49). The highest slope stability is achieved with a nail inclination of $\varepsilon = -20°$. Fig. 50 summarises the results of FOS_{FE} depending on the nail inclination.

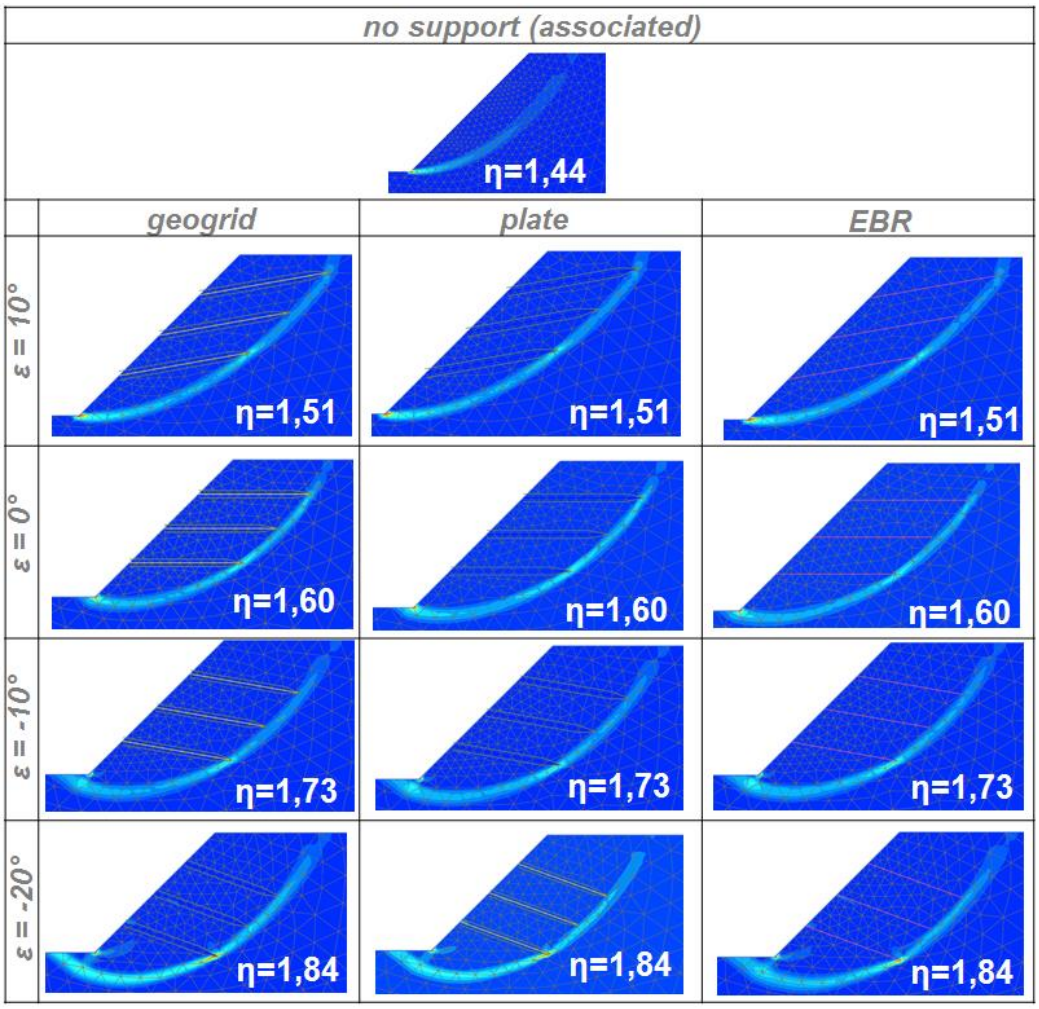

Fig. 49 Failure mechanisms for case 3 (incremental deviatoric strains) – associated flow rule

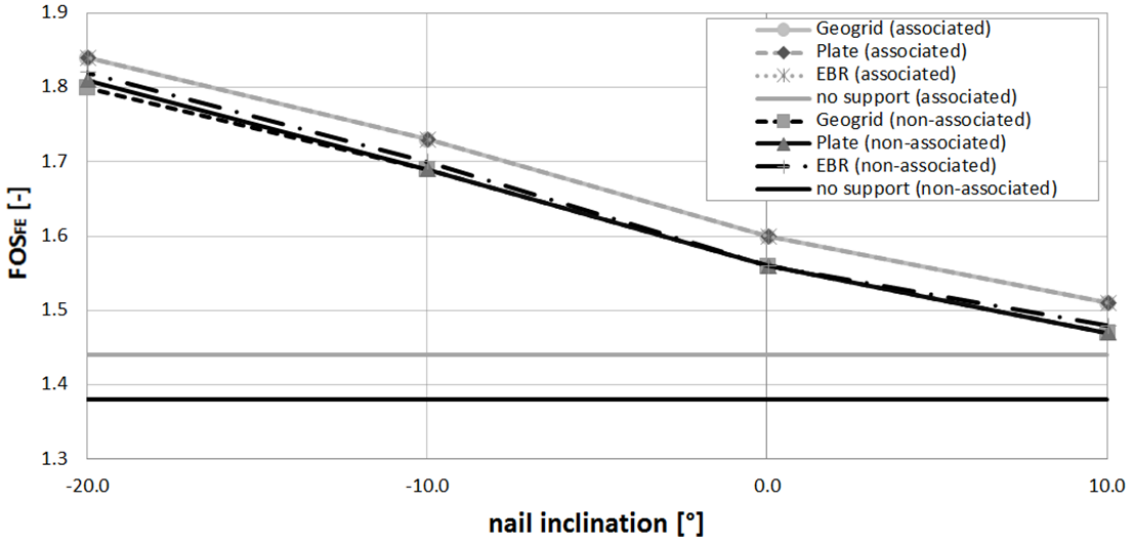

Fig. 50 FOS_{FE}-distribution of case 3 (associated and non-associated)

The behaviour of the FOS_{FE}-distribution (Fig. 50 - FOS_{FE} vs. nail inclination) is similar for all support types. As shown in Fig. 51 (FOS_{FE} vs. |u|), the force distributions are obtained just before the bend of the FOS_{FE}-curves (FOS_{FE}=1.58 for geogrid/plate/EBR). The distribution of axial nail forces slightly differs for the various support types, due to inaccuracies of readings or the conversion of the cross section area for the support types.

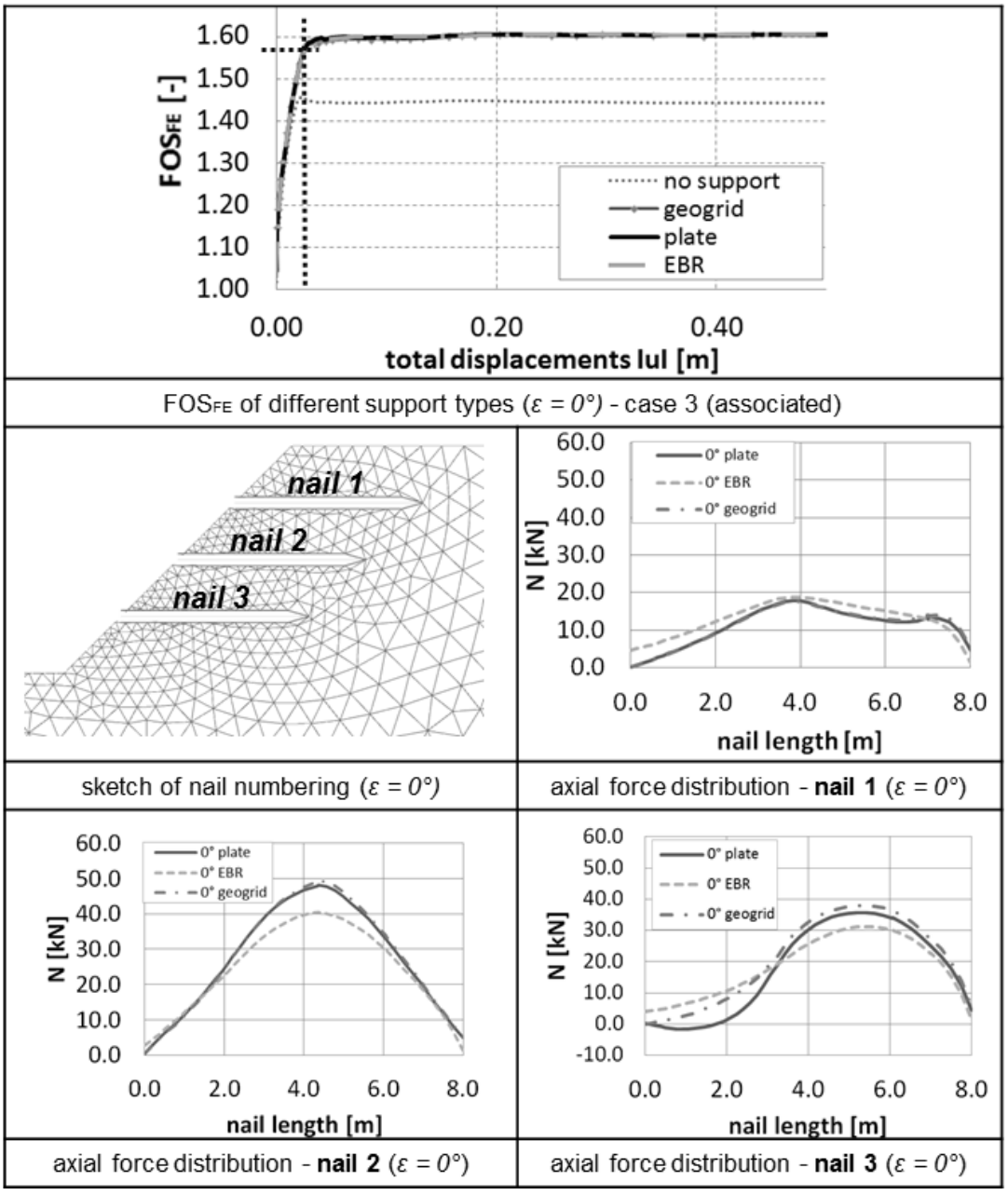

Fig. 51 Axial force distribution of different support types - ε = 10° (associated)

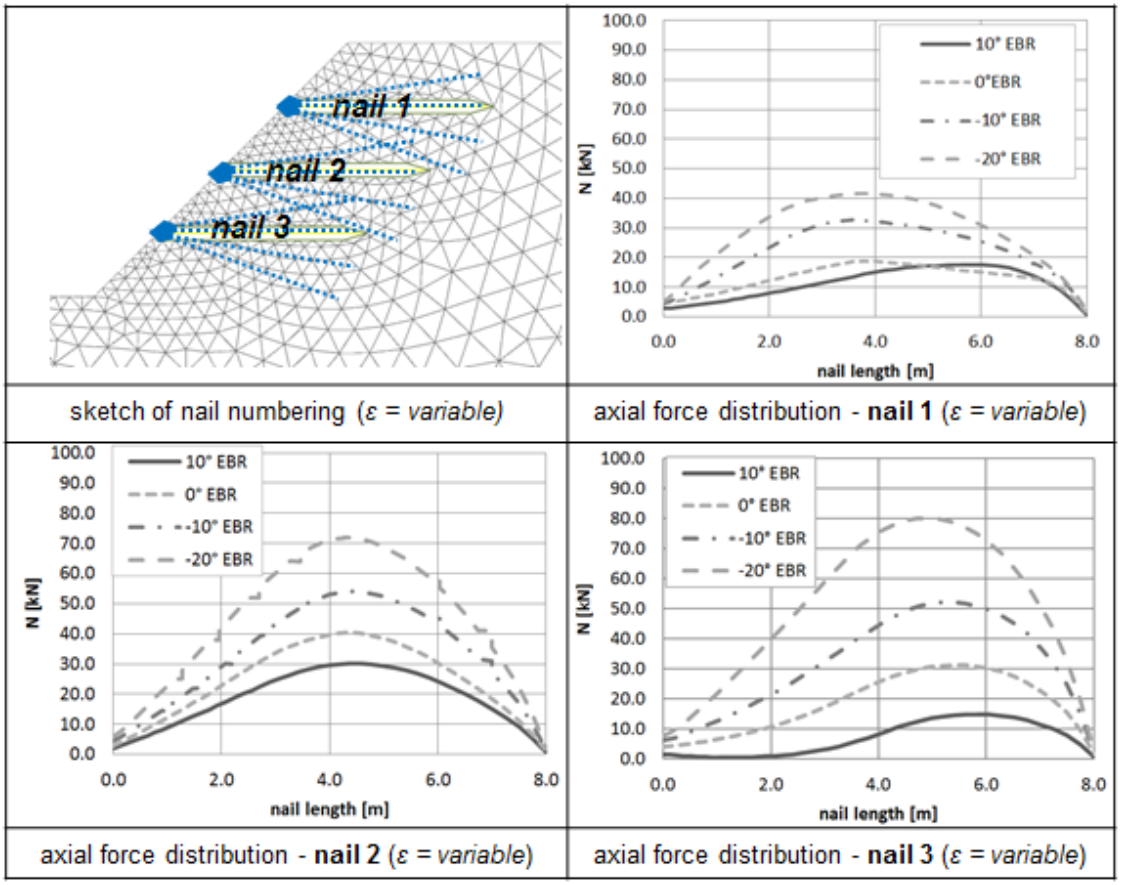

Fig. 52 Axial force distribution of different nail inclinations - ε = variable (associated)

As shown in the picture above (only EBRs are evaluated), soil nails inclined with -20° receive the highest axial forces. Nails with an inclination exceeding the horizontal (+10°), receive the lowest traction.

4.6 Validation of out-of-plane spacing

This study is performed to investigate the impact of out-of-plane distance (L_s) on the FOS and the failure mechanism. In reality, a nail is surrounded by ground (3D problem) which is difficult to model with a 2D approach. Recently, plates and geogrids are being used to model nail rows. As described in chapter 4.2.3, plate and geogrid elements are coupled to the mesh and soil cannot flow through them (behaviour can be compared to a wall). For a real 'bar-behaviour', soil should be able to flow between beam rows. The recently introduced embedded beam row facility allows the consideration of 3D characteristics. The beam is separated from the mesh, which enables the soil to flow through the nail rows (Fig. 53, right). The interaction between nail and soil is considered by special interface elements.

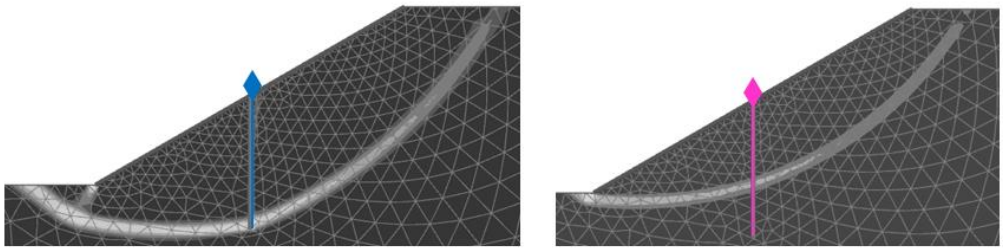

Fig. 53 Failure surface under and between nail rows

To analyse the above mentioned behaviour, only one vertical nail is modelled in the following FE analysis.

First, an elastic material behaviour is evaluated without the manipulation of the (axial and lateral) skin resistance regarding EBRs (only a variation of L_s is employed). Under these conditions, the failure surface occurs below the reinforcements, independent of alteration variation of L_s.

Secondly, an evaluation of the lateral skin resistance is done (again with elastic support behaviour). Since the nail is installed vertically, it obtains primary shear stresses (like a dowel). From that follows that the axial skin resistance has a negligible influence.

4.6.1 Description of the model

The geometry for the present case 4 has the same dimensions as case 1. A slope height of 2 m and a slope inclination of 30° are used. A vertical nail with a length of 1.5 m is considered. The dowel is placed in the middle of the slope with a variable out-of-plane distance (L_s). The parameter study is conducted with and without a rigid facing. The plane strain FE model consists of 1398 15-noded elements. A fine mesh with a refinement (coarseness factor = 0.25) along the slope line/facing and the nail, is used.

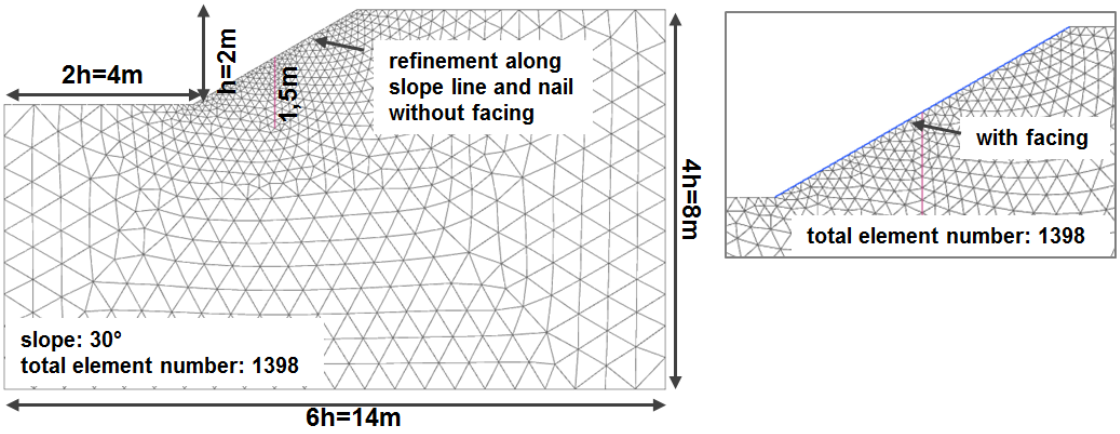

Fig. 54 Geometry and FEM mesh for case 4 – with and without facing

4.6.2 Input parameters

The soil parameters correspond to case 1, except for the change of effective cohesion (2.0 kN/m²) and the effective friction angle (30°). The entire material set for case 4 is summarised in Tab. 18. For the following analysis, the material parameters remain the same. To take a change of L_s into account, the thickness *d* (plate elements) requires a conversion to the appropriate equivalence in PLAXIS 2D. Note that the program calculates *d* automatically. This means, the input of the equivalent thickness needs to be defined via axial stiffness and bending stiffness. This analysis only considers an elastic material behaviour of the support type. For embedded beam rows, the influence of lateral and axial skin resistance is eliminated in the first step (by setting high values). However, for the second step the influence is taken into account.

Tab. 18 Material parameters for case 4 (PLAXIS 2D)

Soil	**Symbol**	**Unit**	**Mat. Set**	
			associated	**non-associated**
Strength model	-	-	MC	MC
Stiffness	E'	kN/m²	40 000	40 000
Poisson ratio	ν'	-	0.3	0.3
Cohesion	c'	kN/m²	2	2
Unit weight	$\gamma_{unsat}/\gamma_{sat}$	kN/m³	17	17
Friction angle	φ'	°	30	30
Dilatancy angle	ψ'	°	30	0
Rigid facing (plate element)	**Symbol**	**Unit**	**Mat. Set**	
Axial stiffness	*EA*	kN/m	2 100 000	
Bending stiffness	*EI*	kN m²/m	1750	
weight	*w*	kN/m/m	0	
Nail (plate)	**Symbol**	**Unit**	**Mat. Set**	
Axial stiffness	*EA*	kN/m	2.1*E7*A_i	
Bending stiffness	*EI*	kN m²/m	2.1*E7*I_i	
Nail (EBR)	**Symbol**	**Unit**	**Mat. Set**	
Young's modulus	*E*	kN/m²	2.1*E7	
Unit weight	γ	kN/m³	25	
Diameter	D	m	0.1	
Base resistance	F_{max}	kN	0	
Axial skin resistance	T_{skin}	kN/m	500	

4.6.3 Comparison of plates and embedded beam row

As already mentioned above, elastic support behaviour is applied in the first step of the study without any modifications of skin resistances (related to EBR). Considering an out-of-plane distance of 0.1 m, an overlap of the beams is achieved. In this case, the EBR should behave like a plate-element.

The used L_s values and the corresponding values for plates are provided in Tab. 19 (*EA* and *EI* depend on *d*). The numerical simulation is done with and without rigid facing. The results of the FOS_{FE} for the associated and non-associated case study are listed in Tab. 20. The rigid facing is defined to avoid the development of an unfavourable failure mechanism at the slope surface (showed in Fig. 59 and Fig. 60). The installation of a plate-element along the slope leads to a failure mechanism below the dowel. Concerning an unreinforced slope, the rigid facing element has no influence on the FOS_{FE} ($FOS_{\text{no nail, no facing}} = FOS_{\text{no nail, with facing}}$). Hence, a more expressive comparison of plates and EBRs can be made.

The usage of plates for modelling nail rows is limited to a specified out-of-plane distance. In case the out-of-plane distance L_s is 10 m, low stiffness values lead to numerical problems. Fig. 55 shows the characterisation of these issues using plate elements. Note that a deformation of the elastic plate elements occurs (see Fig. 55 – deformed mesh).

Tab. 19 Consideration of out-of-plane distance for plates and EBRs

Nail (plate)	**Symbol**	**Unit**	**Mat. Set**
Axial stiffness	*EA*	kN/m	1.65*E6/1.65*E5/1.65*E4
Bending stiffness	*EI*	kN m²/m	850/0.85/0.00085
Equivalent thickness	*d*	m	0.078/0.0078/0.00078
Nail (EBR)	**Symbol**	**Unit**	**Mat. Set**
Out-of-plane spacing	L_s	m	0.1/1.0/10

The cross section area *A* of the plate element results from the equivalent thickness multiplied with L_s. The moment of inertia is calculated with $\frac{d_i^3 * L_{s,i}}{12}$.

Tab. 20 FOS_{FE} results for case 4 with and without facing

		Case 4 (associated)		Case 4 (non-associated)	
		Plate	EBR	Plate	EBR
No support	***No facing***	1.78		1.71	
L_s = 0.1 m	***No facing***	1.91	1.91	1.87	1.87
L_s = 1.0 m	***No facing***	1.91	1.91	1.87	1.87
L_s = 10.0 m	***No facing***	no solution	1.90	no solution	1.87
L_s = 100.0 m	***No facing***	no solution	1.90	no solution	no. solution
No support	***With facing***	1.78		1.71	
L_s = 0.1 m	***With facing***	2.17	2.20	2.11	2.15
L_s = 1.0 m	***With facing***	2.17	2.17	2.11	2.11
L_s = 10.0 m	***With facing***	no solution	2.17	no solution	2.11
L_s = 100.0 m	***With facing***	no solution	2.17	no solution	2.11

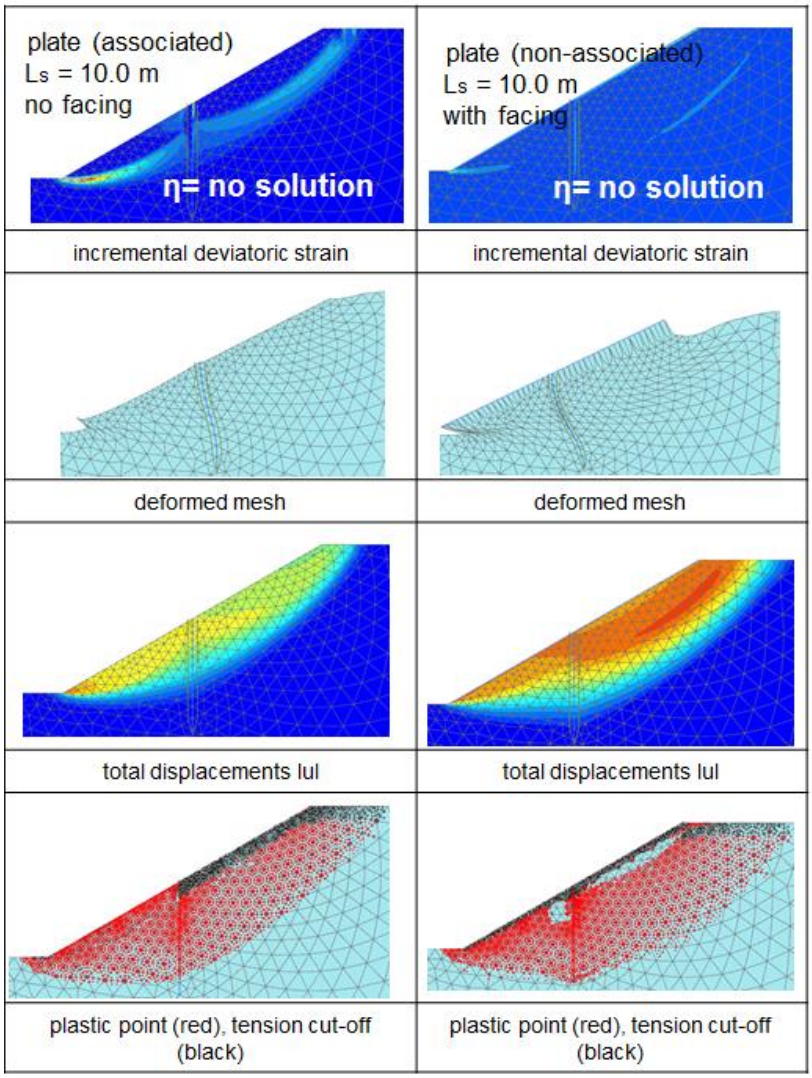

Fig. 55 Examples of failure mechanisms using plates (L_s = 10 m)

The studies described below were done with embedded beam rows. The results concerning plate-elements are illustrated in appendix 8.3.

4.6.3.1 *Evaluation of case 4 - without facing*

The FOS_{FE}-development for EBRs (Fig. 56) shows numerical oscillations during non-associated calculations (L_s = 10 m). A trial run with an out-of-plane spacing of 100 m was performed, leading also to numerical problems for an associated computation. The results are depicted in Fig. 57. During the simulation, the failure surface jumps between different mechanisms.

Fig. 59 (associated) and Fig. 60 (non-associated) show an evaluation of the failure mechanisms depending on the out-of-plane distance. Without the rigid facing a distinctive failure mechanism cannot be detected. The results of the total displacements *|ul|* show a movement above the ending of the nail. In case incremental deviatoric strains are inspected, no precise failure mechanism can be detected. The deformed mesh (Ls = 10 m - associated) indicates stability problems at the nail-head.

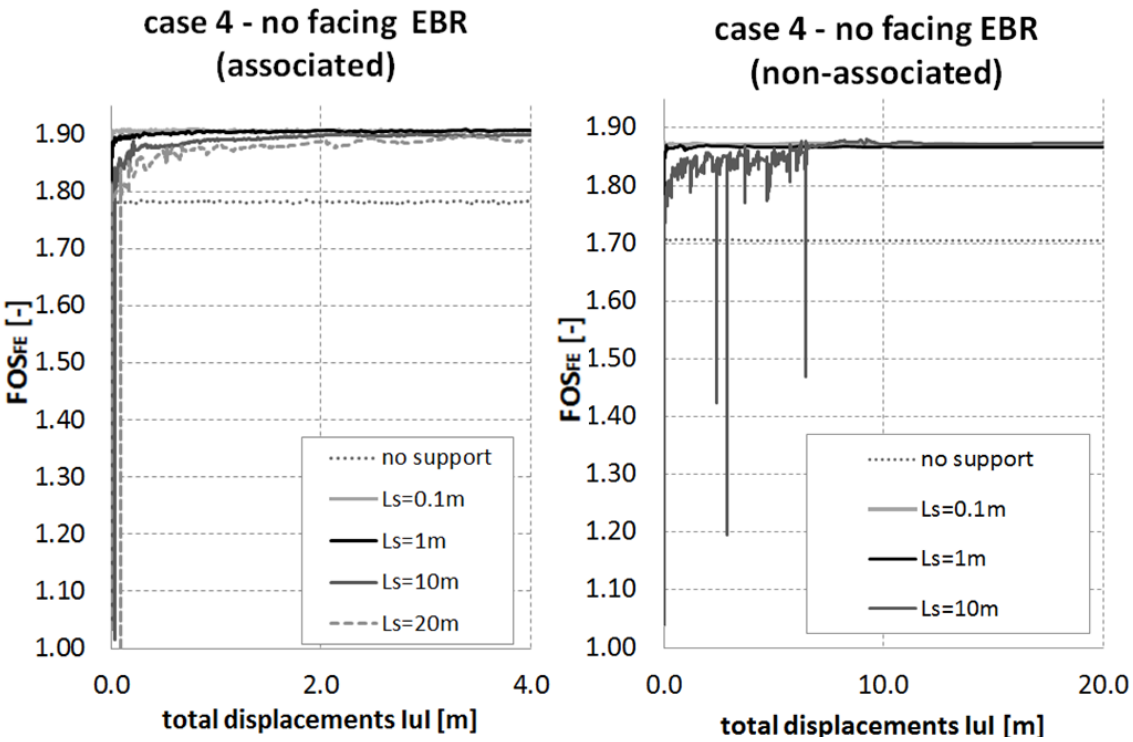

Fig. 56 FOS-development without facing – EBR (associated/non-associated)

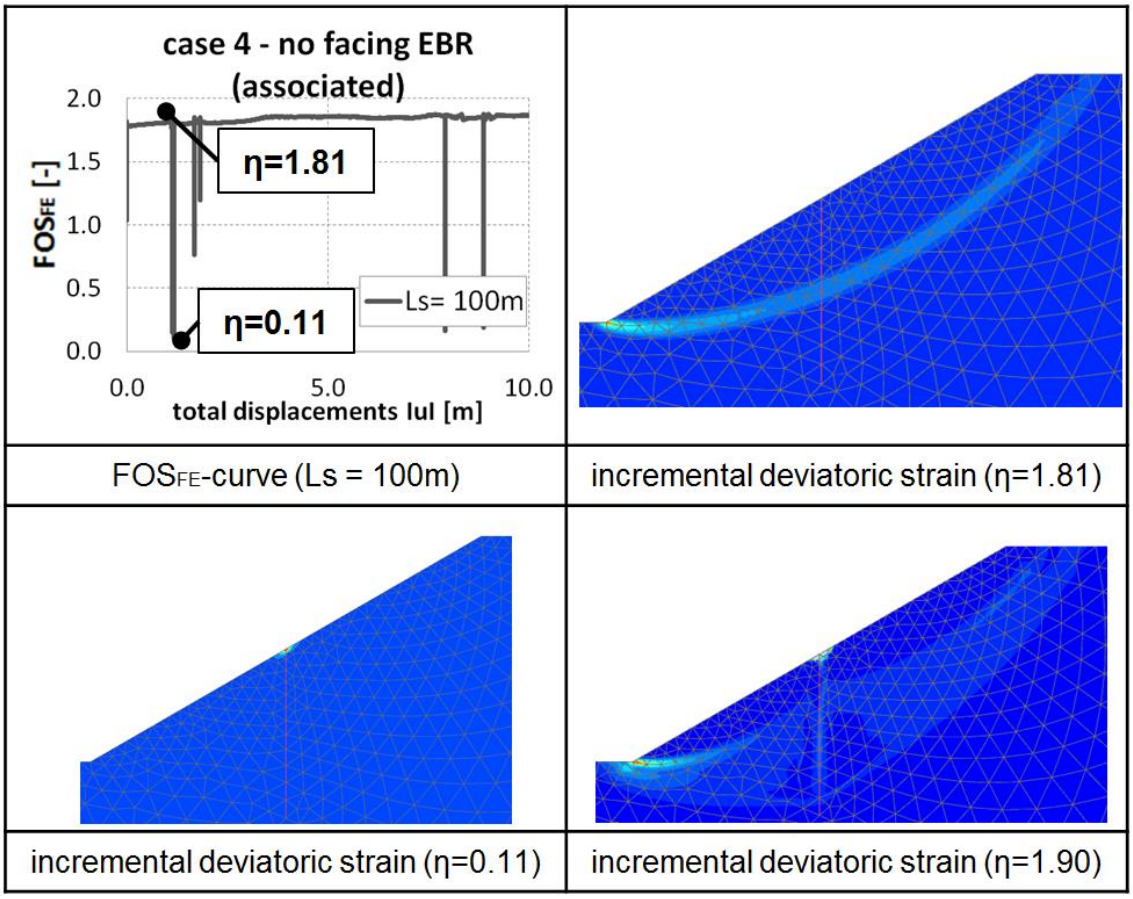

Fig. 57 Evaluation of unstable FOS-curve – EBR (associated), L_s = 100 m, no facing

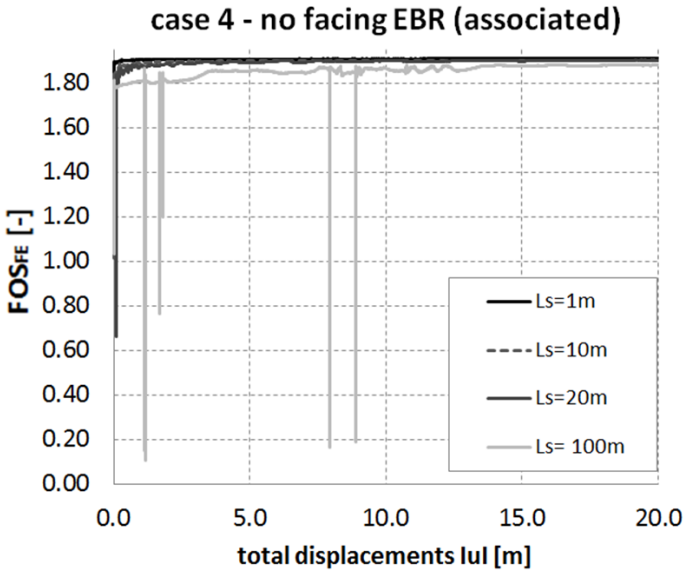

Fig. 58 FOS_{FE}-development without facing – EBR (associated), including L_s = 100 m

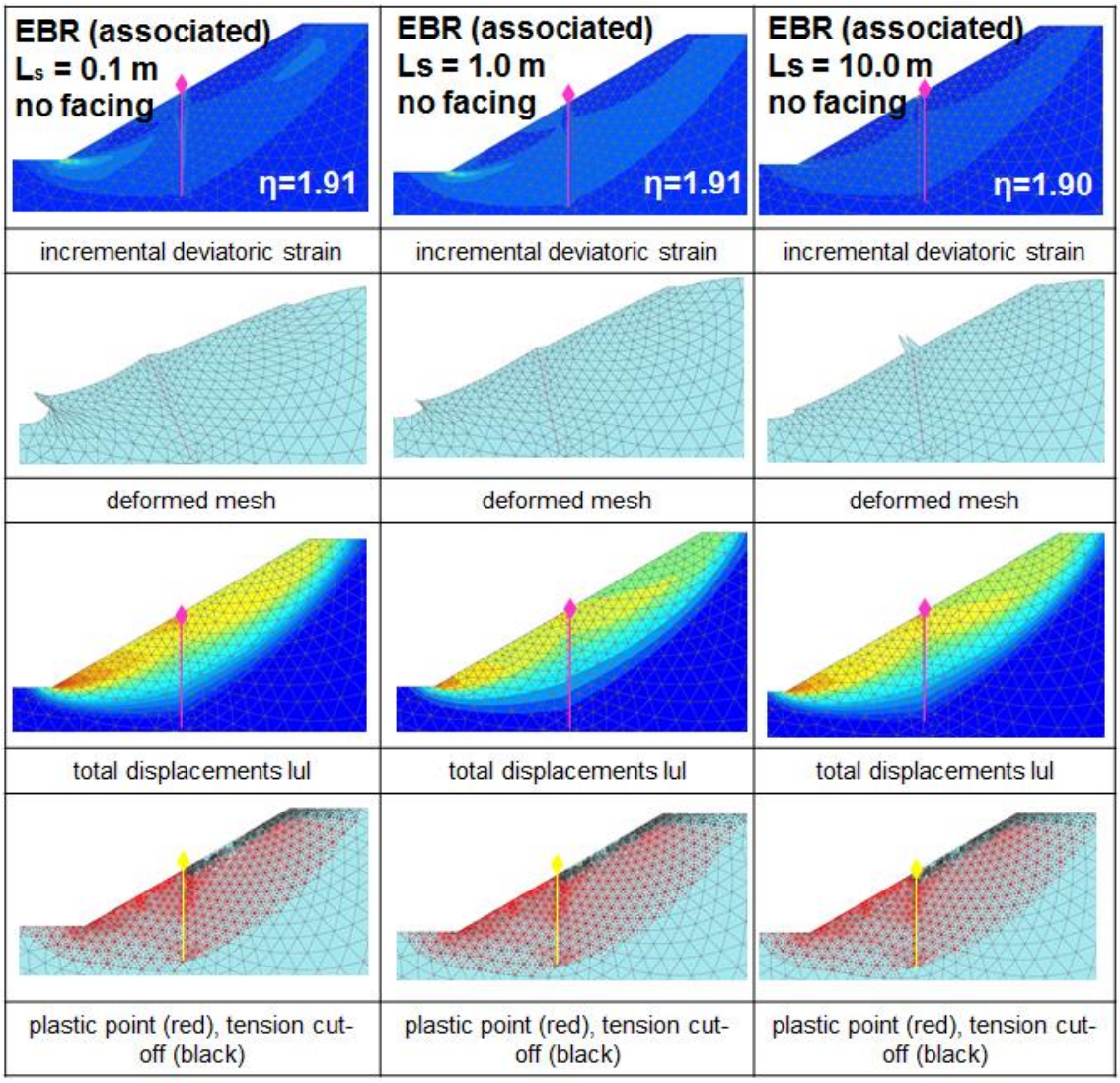

Fig. 59 Evaluation of failure mechanism without facing - EBR (associated)

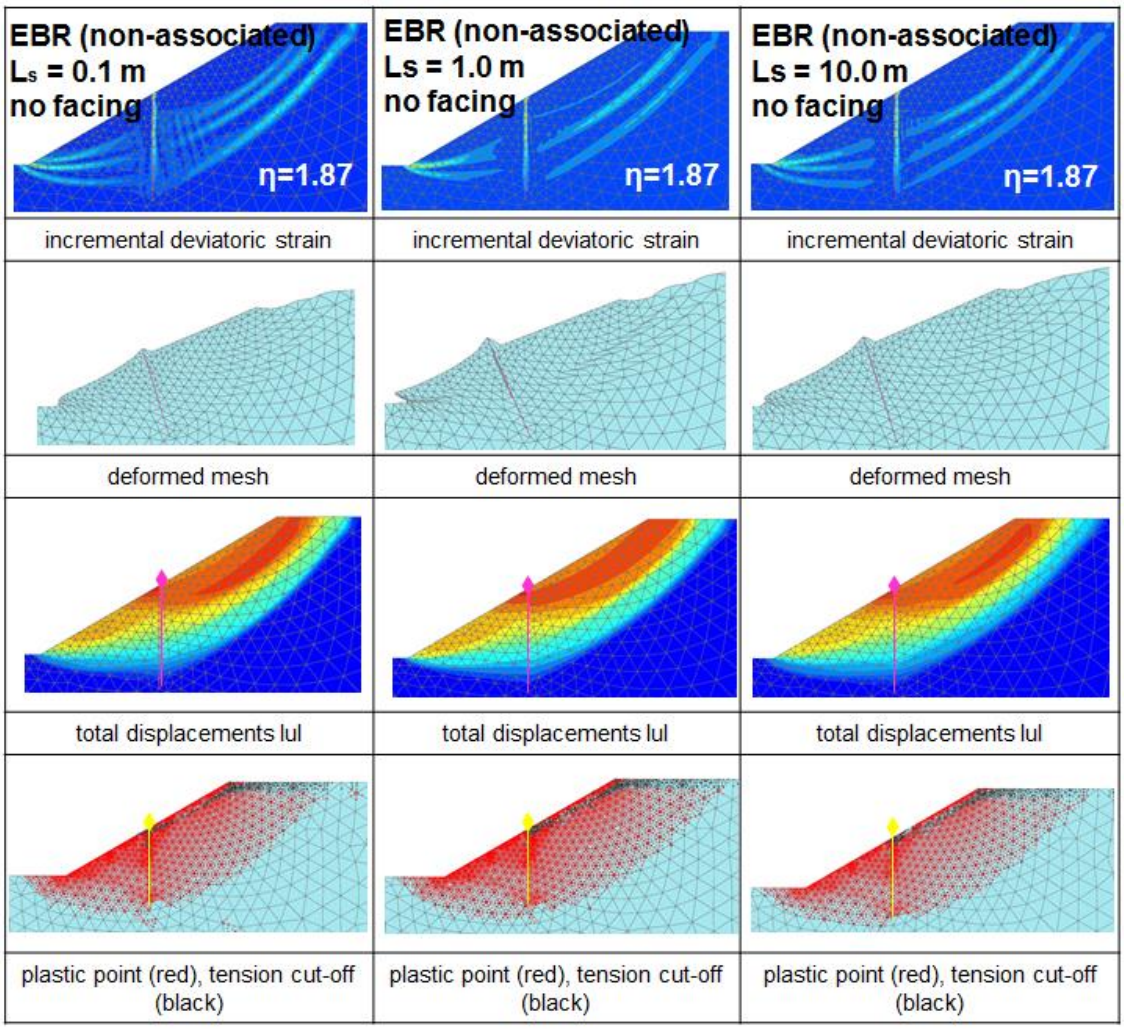

Fig. 60 Evaluation of failure mechanism without facing - EBR (non-associated)

4.6.3.2 *Evaluation of case 4 – with facing*

The rigid facing is added to enforce a failure mechanism below the soil nails. The outcomes of FOS_{FE} do not really change (shown in Fig. 61). The previously described numerical problems disappear and a computation with an out-of-plane distance of 100 m leads to similar results of the FOS_{FE} (for EBR). Fig. 62 (associated) and Fig. 63 (non-associated) show the evaluation of the failure mechanisms depending on the out-of-plane distance. The images of total displacements *lul* demonstrate a movement below the ending of the nail. By looking at the incremental deviatoric strains, a precise failure mechanism is detected. But the failure surface is not located between the beam rows. Without the manipulation of the skin resistant parameters, EBRs do not correspond to real 3D characteristics.

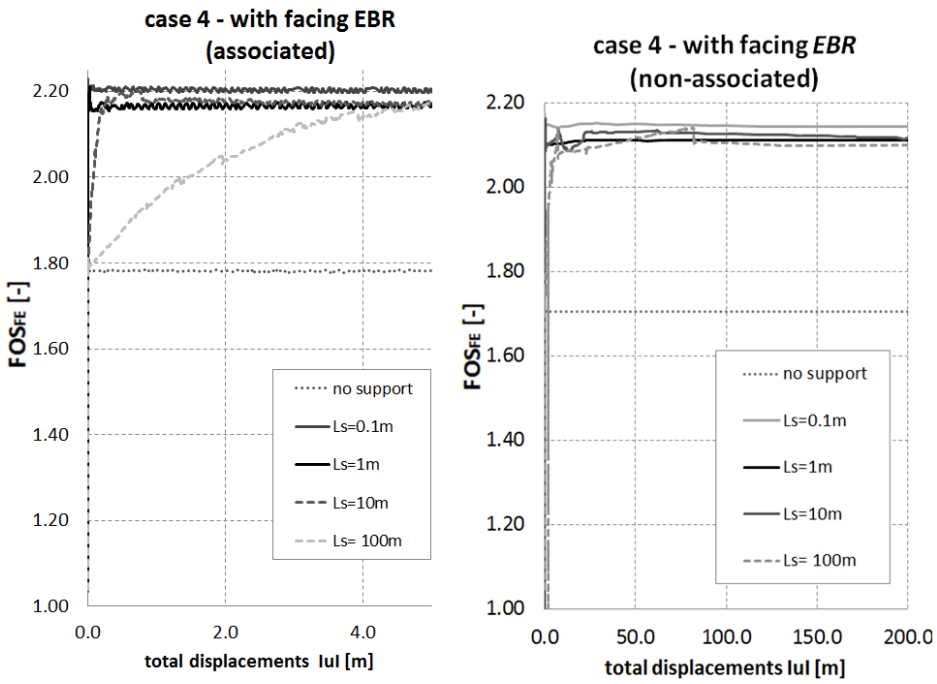

Fig. 61 FOS-development with facing – EBR (associated/non-associated)

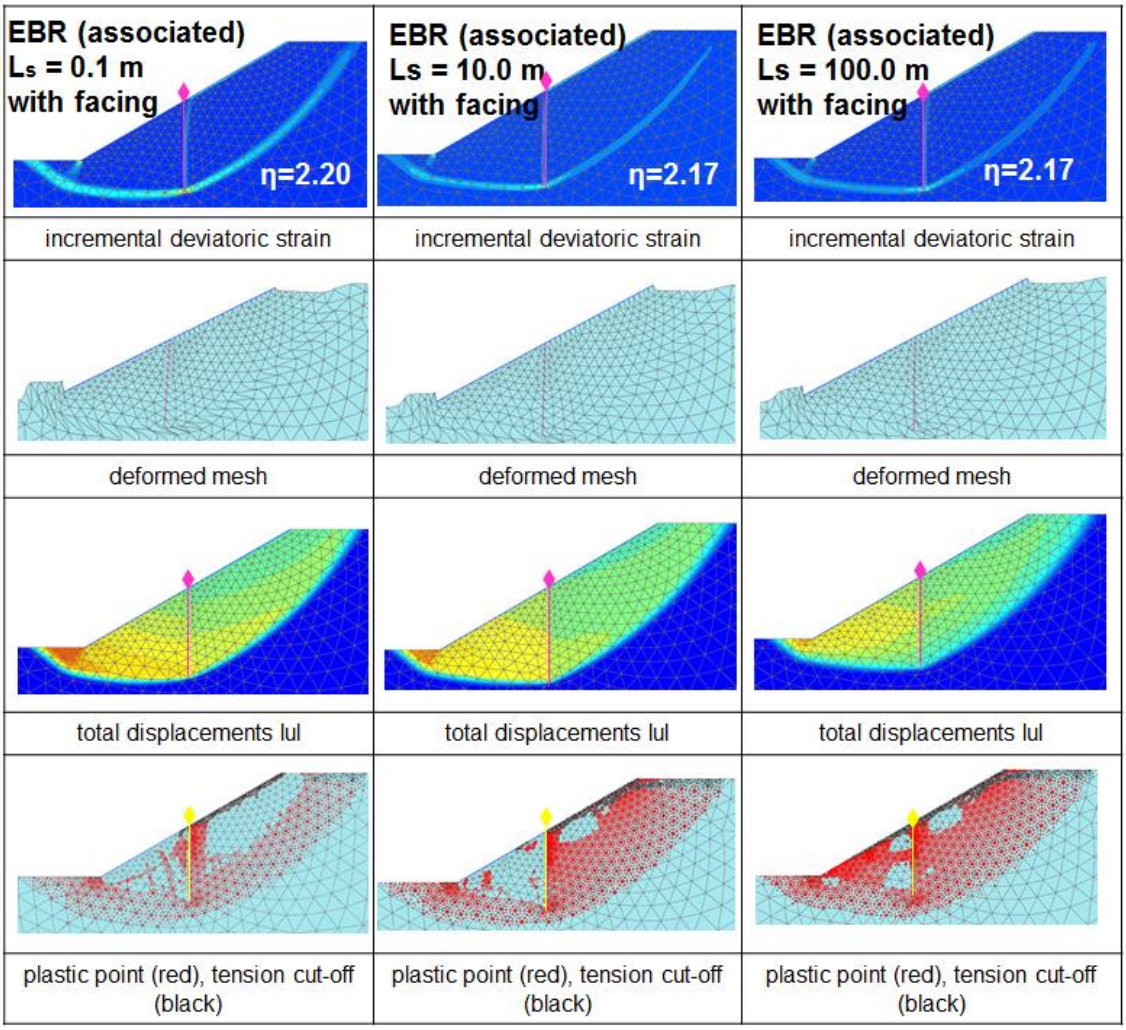

Fig. 62 Evaluation of failure mechanism wit facing - EBR (associated)

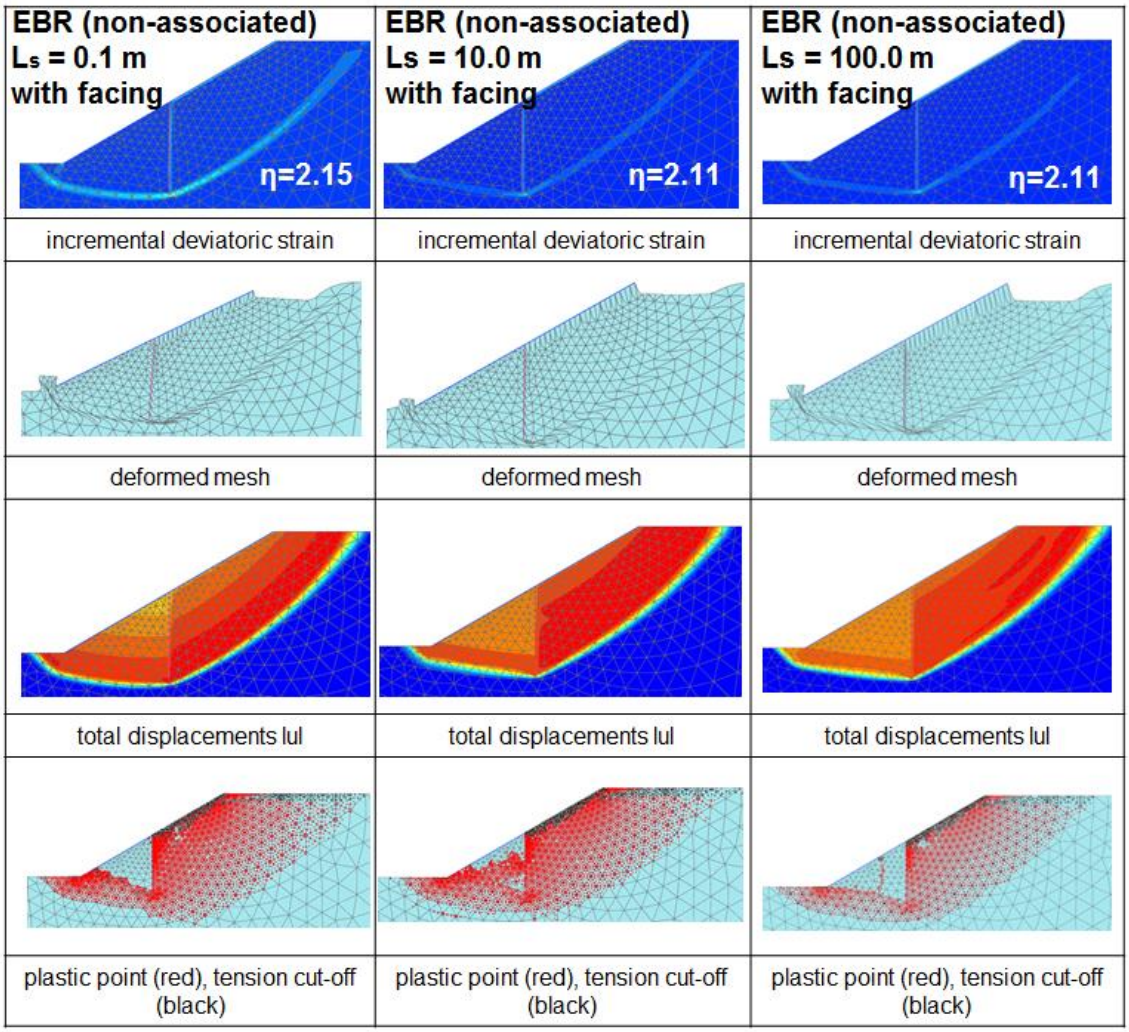

Fig. 63 Evaluation of failure mechanism with facing - EBR (non-associated)

4.6.4 Parameter study on lateral skin resistance T_{lat} (EBR)

For the second simulation of case 4, only the behaviour of embedded beam rows is investigated. To obtain a realistic failure mechanism, a rigid facing is implemented. The outcome of the first study showed, that the failure surface is located below the reinforcement and that the soil does not flow between the beams. In the following a variation of the lateral skin resistance and the out-of-plane spacing is provided (Tab. 21. The results of the safety factors for an associated and non-associated approach can be found in Tab. 22. The corresponding FOS_{FE}-curves are shown in the figures below.

This parameter study proves a realistic 3D-related behaviour of the EBR-elements. By increasing the out-of-plane distance, the FOS_{FE} value approaches the initial state (without support). The failure mechanism varies and soil ‘flows’ through bar rows. An

example for T_{lat} = 1.0kN/m is visualised in Fig. 65. A distribution of the FOS_{FE} depending on L_s is provided in Fig. 66 for an associated flow rule. Fig. 67 depicts the FOS_{FE}-distribution for non-associated conditions.

Tab. 21 Input values for parameter study on T_{lat}

Nail (EBR)	Symbol	Unit	Mat. Set
Out-of-plane spacing	L_s	m	0.1/0.5/1.0/3.0/6.0/10.0/15.0/20.0
Axial skin resistance	T_{lat}	kN/m	0.1/1.0/2.0/5.0

Tab. 22 FOS results for parameter study on T_{lat} (associated/non-associated)

	T_{lat} [kN/m] (associated)					T_{lat} [kN/m] (non-associated)				
	0.1	**1.0**	**2.0**	**5.0**	**500**	**0.1**	**1.0**	**2.0**	**5.0**	**500**
No support	1.79					1.71				
L_s = 0.1 m	1.88	2.17	2.19	2.21	2.21	1.79	2.12	2.14	2.15	2.15
L_s = 0.5 m	1.81	1.96	2.06	2.13	2.17	1.73	1.85	1.97	2.10	2.11
L_s = 1.0 m	1.80	1.88	1.95	2.08	2.17	1.72	1.79	1.87	2.05	2.11
L_s = 3.0 m	1.79	1.84	1.85	1.94	2.17	1.71	1.74	1.77	1.86	2.11
L_s = 6.0 m	1.79	1.82	1.82	1.87	2.17	1.71	1.73	1.75	1.80	2.11
L_s = 10.0 m	1.79	1.80	1.81	1.84	2.17	1.71	1.73	1.73	1.78	2.11
L_s = 15.0 m	1.79	1.80	1.80	1.82	2.17	1.71	1.72	1.73	1.75	2.11
L_s = 20.0 m	1.79	1.79	1.80	1.81	2.17	1.71	1.72	1.72	1.74	2.11

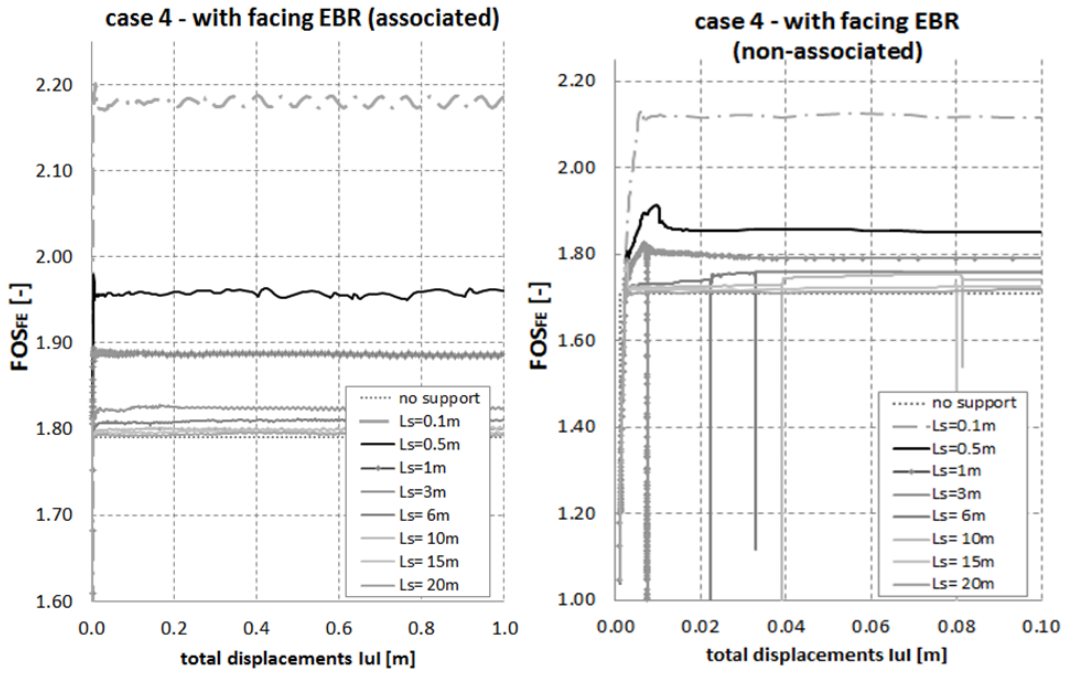

Fig. 64 FOS-curves for parameter study on T_{lat} (associated/non-associated)

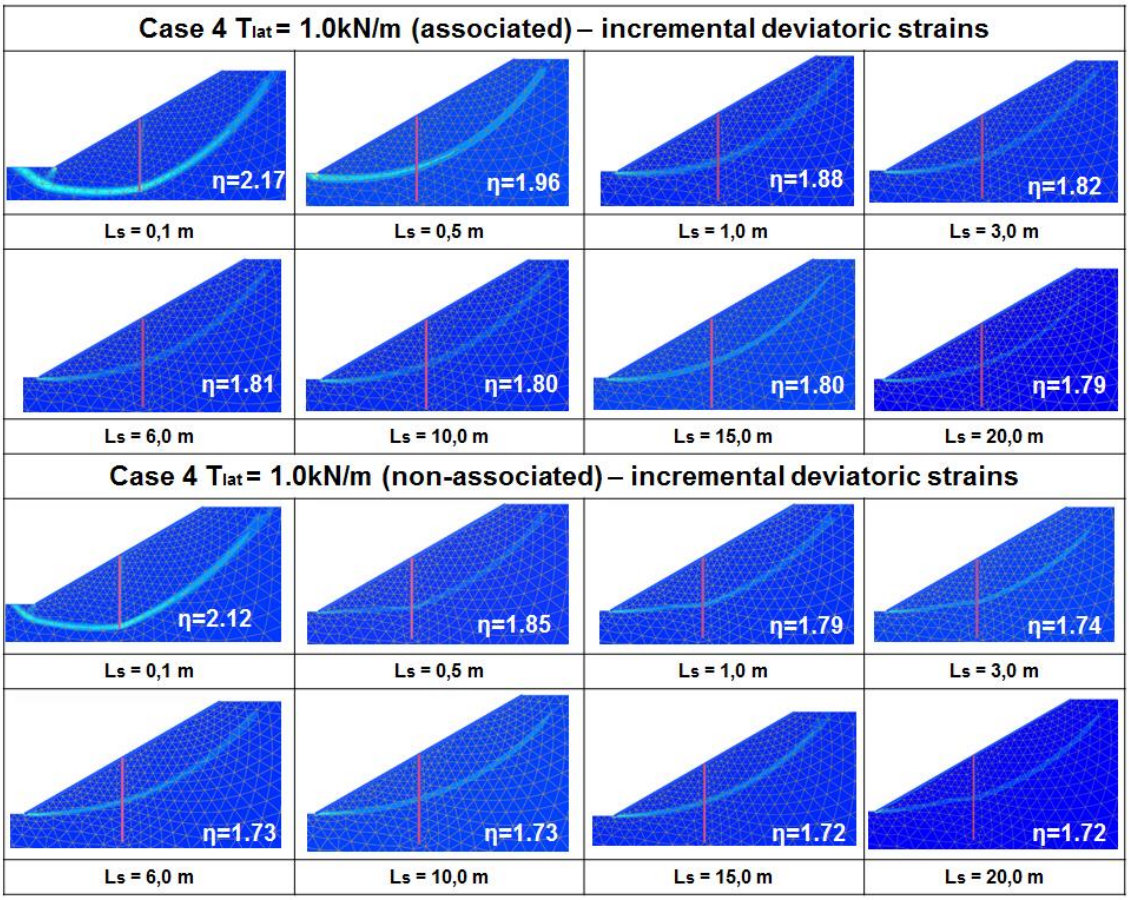

Fig. 65 Development of failure mechanisms depending on L_s – T_{lat} = 1.0 kN/m (associated)

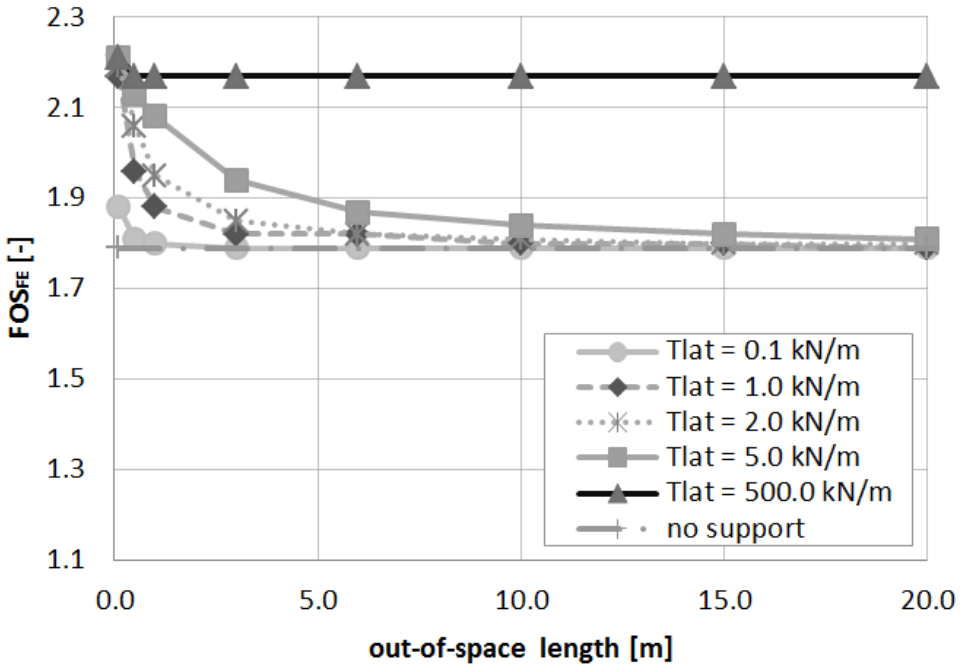

Fig. 66 FOS_{FE}-distribution - parameter study on T_{lat} (associated)

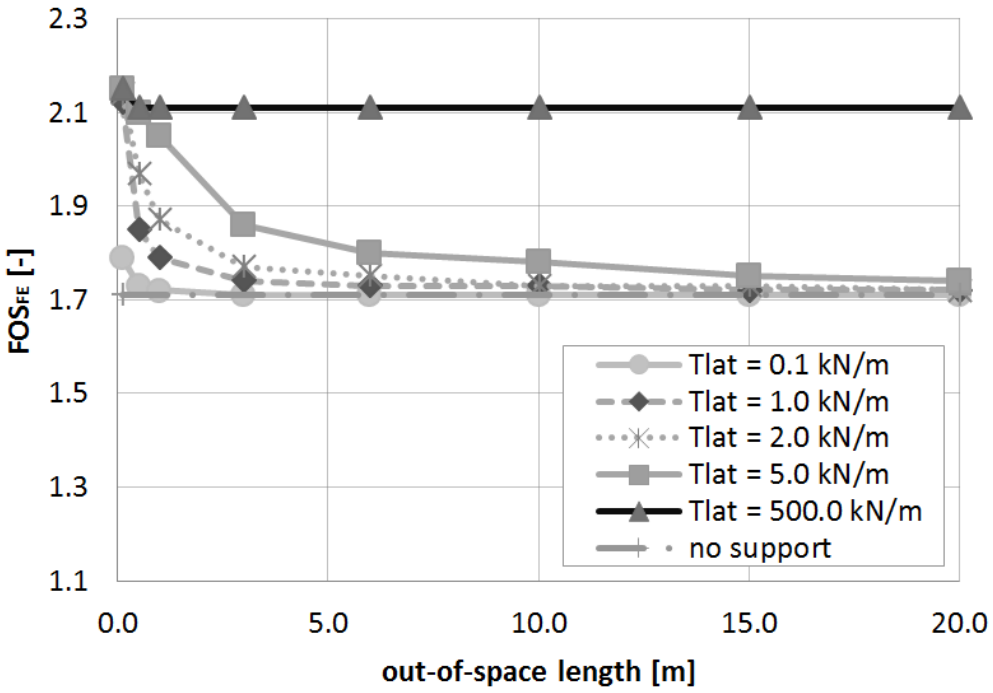

Fig. 67 FOS_{FE}-distribution - parameter study on T_{lat} (non-associated)

5 Finite element analysis using PLAXIS 3D

In this chapter results of three-dimensional finite element analysis of reinforced slope structures are presented. Since 2D plane strain FE analyses have certain limitations in modelling the ground-nail interaction, 3D FE analysis are required for validation purposes.

For the numerical simulations, the three-dimensional FE program PLAXIS 3D (Brinkgreve & et al., PLAXIS 3D - Reference Manual, 2015) is used. The objective of these simulations is the verification of the previously performed two-dimensional FE calculations. The main focus is drawn to the results of the safety factors and the developed failure mechanisms.

5.1 Plaxis 2D versus 3D

In order to use a 2D model instead of a 3D model, several changes and simplifications concerning the geometry have to be made (see Fig. 68). A plane strain model can be reasonable, e.g. in a case where one dimension is very large compared to the other two dimensions (like strip footings). But for more complex structures, a 3D finite element analysis has to be performed. The main disadvantage of 3D models is the time-consuming input and calculation procedure.

The issue of modelling columnar structures like nails in 2D is the modification of either the dimensions or the stiffness of the pile elements. When modelling piles or nails with plate elements in 2D, the calculations may deliver a realistic axial load-displacement behaviour but an unrealistic lateral load-displacement behaviour. With the embedded beam row element (2D) the required stiffness properties are determined automatically and show a more realistic behaviour (Tschuchnigg F. , 2013).

In this thesis, comparisons of 2D plane strain models with full 3D calculations are provided.

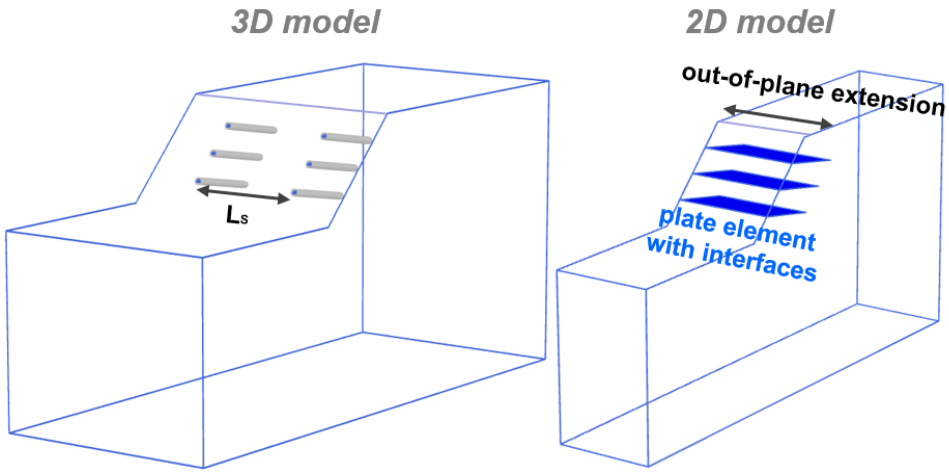

Fig. 68 3D model versus 2D model

5.2 Description of FE models

PLAXIS 3D version AE.01 is a three-dimensional finite element code for commercial applications, able to perform deformation and stability analyses for various geotechnical problems.

This chapter describes the modelling approaches in PLAXIS 3D as well as the structural elements used.

5.2.1 Mesh configuration and constitutive model

To model soil layers or other volume clusters, two types of mesh elements are provided in PLAXIS 2D, namely 6-node or 15-node triangular elements. In PLAXIS 3DF (3D foundations), 15-noded wedge elements are additionally available. For the models used in this thesis (PLAXIS 3D), 10-noded tetrahedral elements are used (Fig. 69).

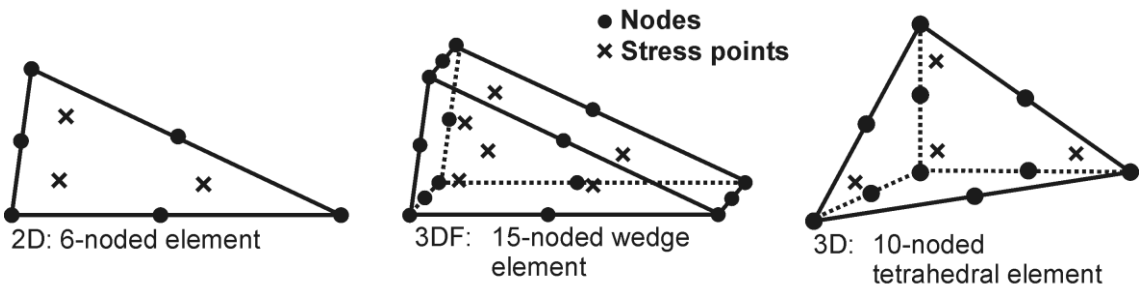

Fig. 69 Finite elements in PLAXIS 2D (left) PLAXIS 3DF (middle) and PLAXIS 3D (right)

(Tschuchnigg F. , 2013)

In PLAXIS 3D, the mesh is generated automatically with the opportunity of global and local refinement.

As constitutive model, the Mohr-Coulomb criterion is used. More information about the MC-model can be found in chapter 3.2.1.3 or in the respective references (e.g. Schweiger, 2014).

5.2.2 Support types for modelling soil nails in PLAXIS 3D

For the definition of soil nails, PLAXIS 3D provides the following feasible elements:

- geogrids (+interfaces)
- plates (+interfaces)
- volume elements (+interfaces)
- embedded beams (EB)

Realistic modelling of piles or nails can be achieved by employing embedded beams or volume elements, both approaches are elaborated in the next sections. A description of plate, geogrid and interface elements can be found in chapter 4.2.3 and in the reference manual provided by PLAXIS 3D (Brinkgreve & et al., 2015).

5.2.2.1 *Volume elements*

In the standard 3D finite element approach, columnar structures are modelled with volume elements. Additionally interface elements (Fig. 70), which consider the interaction of the nail with the surrounding soil, must be modelled. The interface reduction factor R_{inter} defines the strength along interaction between soil and structure (by means of soil strength reduction). If a large number of nails is modelled, this modelling technique leads to several problems, such as highly time consuming calculations or exceedance of computing capacities. Therefore, this approach is not very popular in practical engineering.

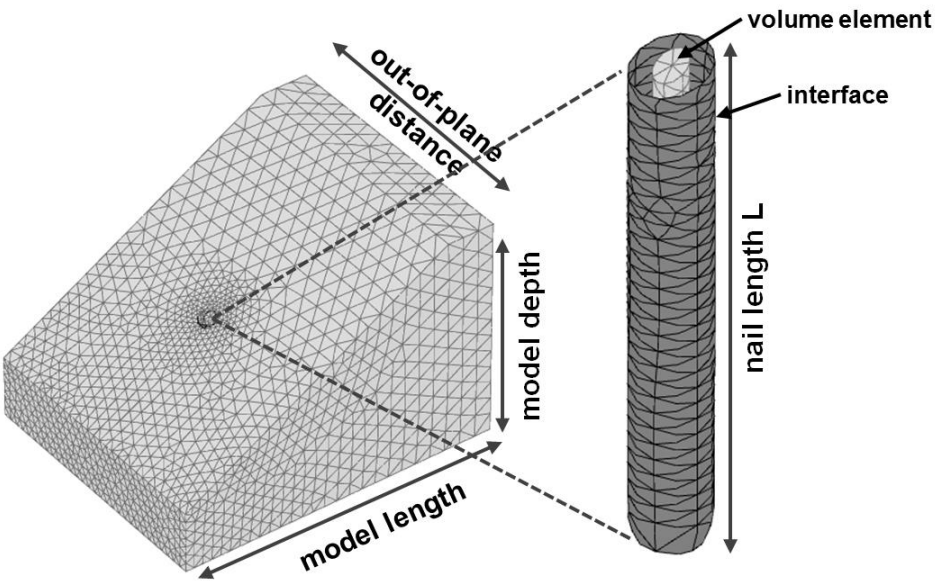

Fig. 70 Standard finite element approach in PLAXIS 3D

5.2.2.2 *Embedded beams*

An alternative to volume elements are embedded beams (EB). The complexity of finite element definition is reduced and the calculation time is decreased.

Embedded beams consist of beam structures and special interface-elements to model the soil/nail interaction. The embedded beam does not significantly affect the finite element mesh (see Fig. 71). The load transfer occurs via skin resistance and base resistance. As EBs are line elements, they do not occupy a real volume. However, EBs depend on the specified beam-diameter which generates a zone where elastoplastic soil-behaviour is excluded. The formulation of embedded beams is given in the dissertation of Tschuchnigg (2013).

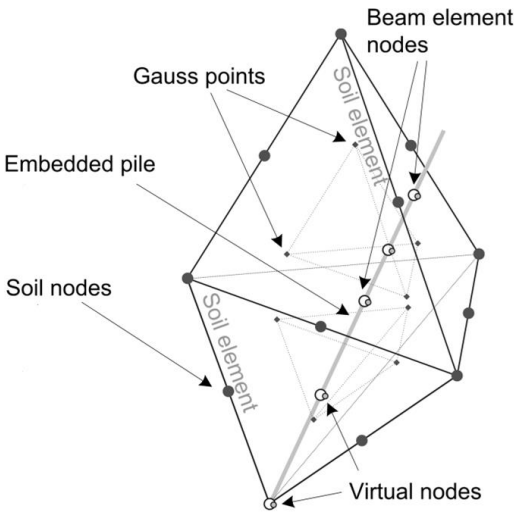

Fig. 71 Embedded beam with a 10-noded tetrahedral element (Tschuchnigg F. , 2013)

5.3 Validation of nail orientation in 3D

The purpose of this numerical simulation is the verification of the outcomes of case 3 (PLAXIS 2D, chapter 4.5) by means of a 3D approach. Four nail inclinations *(ε)* are evaluated, using different support types (plate, geogrid, embedded beam and volume element).

In addition a parameter study on the out-of-plane distance (L_s) is provided with a comparison of 2D and 3D analyses. For this comparison, a nail inclination of -10° is investigated. For both analyses, a non-associated flow rule ($\psi = 0$) and an associated flow rule ($\varphi = \psi$) is applied. The evaluation of the results focuses on the obtained safety factors and failure mechanisms.

5.3.1 Description of FE model

The slope is reinforced with 3 nails and no rigid facing is used. The vertical distance of the nails is 2.5 m. A variation of the nail orientation is implemented by:

$$\varepsilon = 10°/0°/\text{-}10°/\text{-}20°$$

In the first part of the study, the geometry (Fig. 72) has a slope height of 10 m, a slope inclination (α_s) of 45° and a width of 1m.

The FE model consists of approximately 145 000 10-noded tetrahedral elements with a quadratic shape function. A very fine mesh is used with refinements around the slope (coarseness factor: 0.4/0.2) and along the soil nails (coarseness factor: 0.1).

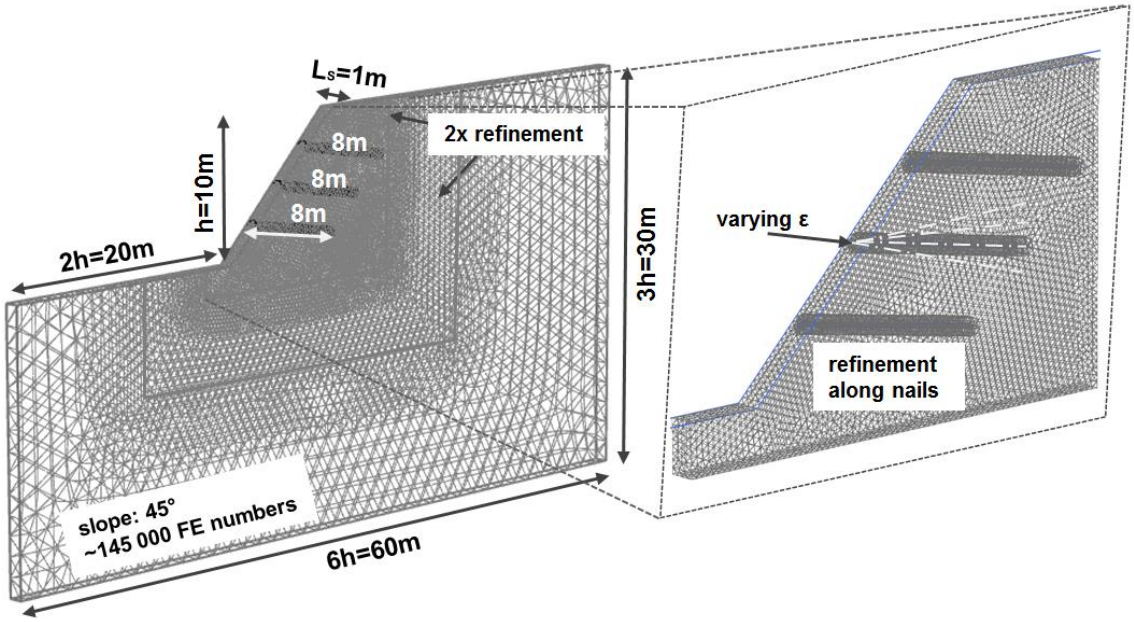

Fig. 72 Geometry and FEM mesh for inclination study (L_s = 1 m)

In the second part, a variation of the out-of-plane distance is performed. Three additional PLAXIS models (Fig. 73) are prepared with widths of 0.5 m, 3.0 m, and 12.0 m. A nail inclination of -10° is used. The number of FE elements varies depending on the support type and model width.

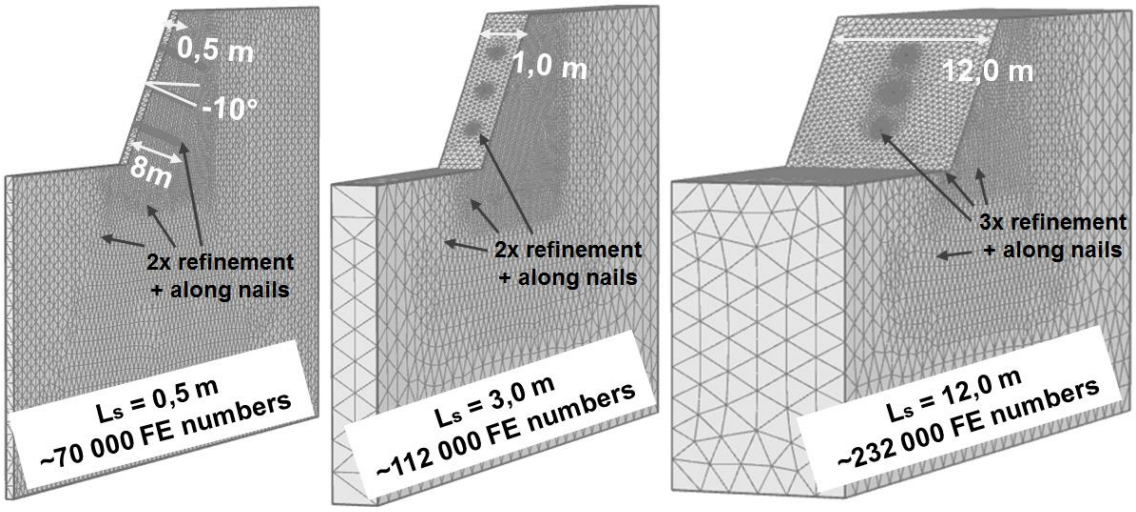

Fig. 73 Geometry and FEM mesh for out-of-plane study

5.3.2 Input parameters

The material parameters shown in Tab. 23 are used for homogeneous soil and the different support type. The soil nails are elastic with an isotropic stiffness. A Young's modulus of 2.1E7 kN/m² is defined for the support types. Regarding the EBs, the influence of axial skin resistance is eliminated by setting a high value. Note that the equivalent thickness *d* of plate elements is changing for the out-of-plane study. To take a change of L_s into account, *d* requires a conversion to the appropriate equivalence (defined via an equation of nail cross section areas).

For the volume elements used in PLAXIS 3D a non-porous drainage type is selected with a linear elastic material model.

Tab. 23 Material parameters for case 3 (PLAXIS 3D)

Soil	**Symbol**	**Unit**	**Mat. Set**
strength model	-	-	MC
stiffness	E'	kN/m²	20 000
Poisson ratio	ν'	-	0.3
Cohesion	c'	kN/m²	20
Unit weight	$\gamma_{unsat}/\gamma_{sat}$	kN/m³	19
Friction angle	φ'	°	25
Dilatancy angle	ψ'	°	0/25
Nail (geogrid)	**Symbol**	**Unit**	**Mat. Set**
Axial stiffness	EA	kN/m	165 000
Nail (plate)	**Symbol**	**Unit**	**Mat. Set**
Equivalent thickness	d	m	0.078/0.0078/0.00078
Unit weight	γ	kN/m³	25
Young's modulus	E	kN/m²	2.1*E7
Poisson ratio	ν'	-	0.2
Nail (EB)	**Symbol**	**Unit**	**Mat. Set**
Young's modulus	E	kN/m²	2.1*E7
Unit weight	γ	kN/m³	25
Diameter	D	m	0.1
Axial skin resistance	T_{skin}	kN/m	500
Base resistance	F_{max}	kN	0
Nail (soil – volume element)	**Symbol**	**Unit**	**Mat. Set**
strength model	-	-	Linear elastic
stiffness	E'	kN/m²	2.1*E7
Poisson ratio	ν'	-	0.2
Unit weight	$\gamma_{unsat}/\gamma_{sat}$	kN/m³	25
Interface reduction factor	R_{inter}	-	1.0

5.3.3 Results of inclination study

As stated above, the outcomes of the 2D-study (case 3) are verified by means of a 3D approach. This analysis is performed with an L_s equal to 1 m. The FOS_{FE} results (2D and 3D analysis) are summarised in Tab. 24 for an associated flow rule. The corresponding $FOS_{FE,3D}$ curves can be found in Fig. 74, plotted for EB and volume elements. Additionally, Fig. 74 shows the $FOS_{FE,3D}$ curves of the 'no support' cases (no nails are installed).

A visualisation of the failure surfaces for EB and volume elements is provided in Fig. 75. The incremental shear strains result in a failure behind the reinforced soil mass, like in the 2D approach.

Tab. 24 FOS_{FE}-results of different nail inclinations for Ls = 1 m (associated)

	Case 3 2D (associated)			Case 3 3D (associated)			
	Geogrid	Plate	EBR	Geogrid	Plate	EB	Volume element
No nails	1.44			1.44			
ε = 10°	1.51	1.51	1.51	1.50	1.48	1.51	1.50
ε = 0°	1.60	1.60	1.60	1.59	1.58	1.60	1.59
ε = -10°	1.73	1.73	1.73	1.70	1.71	1.71	1.70
ε = -20°	1.84	1.84	1.84	1.81	1.80	1.81	1.80

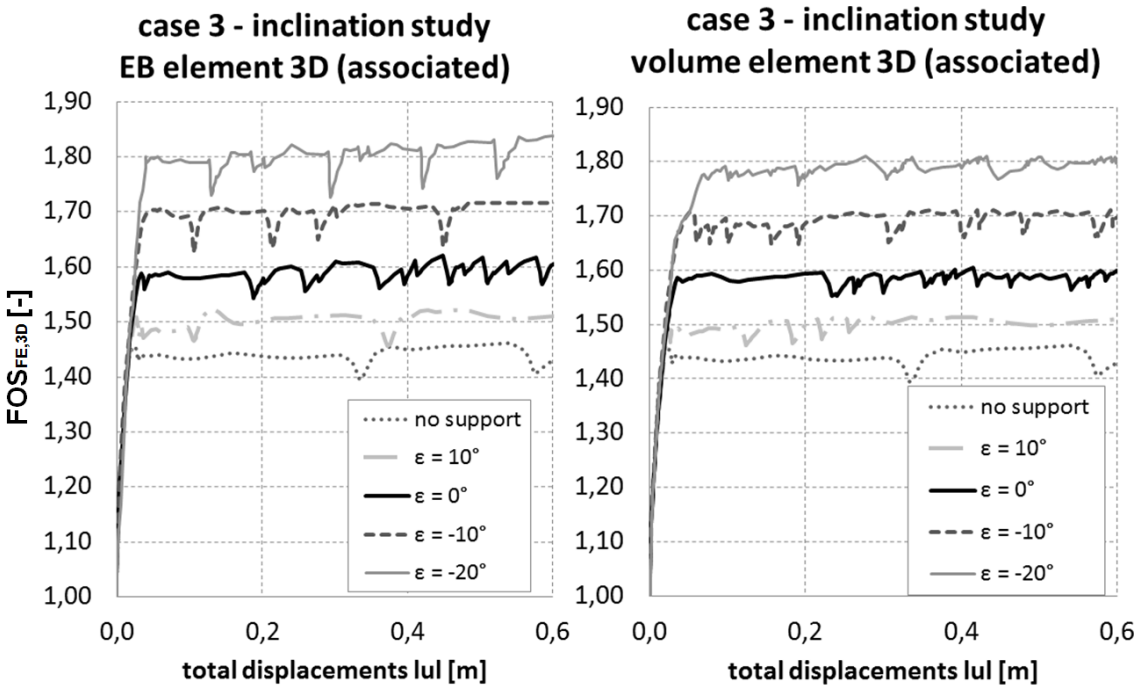

Fig. 74 FOS-development – EB and volume elements (associated)

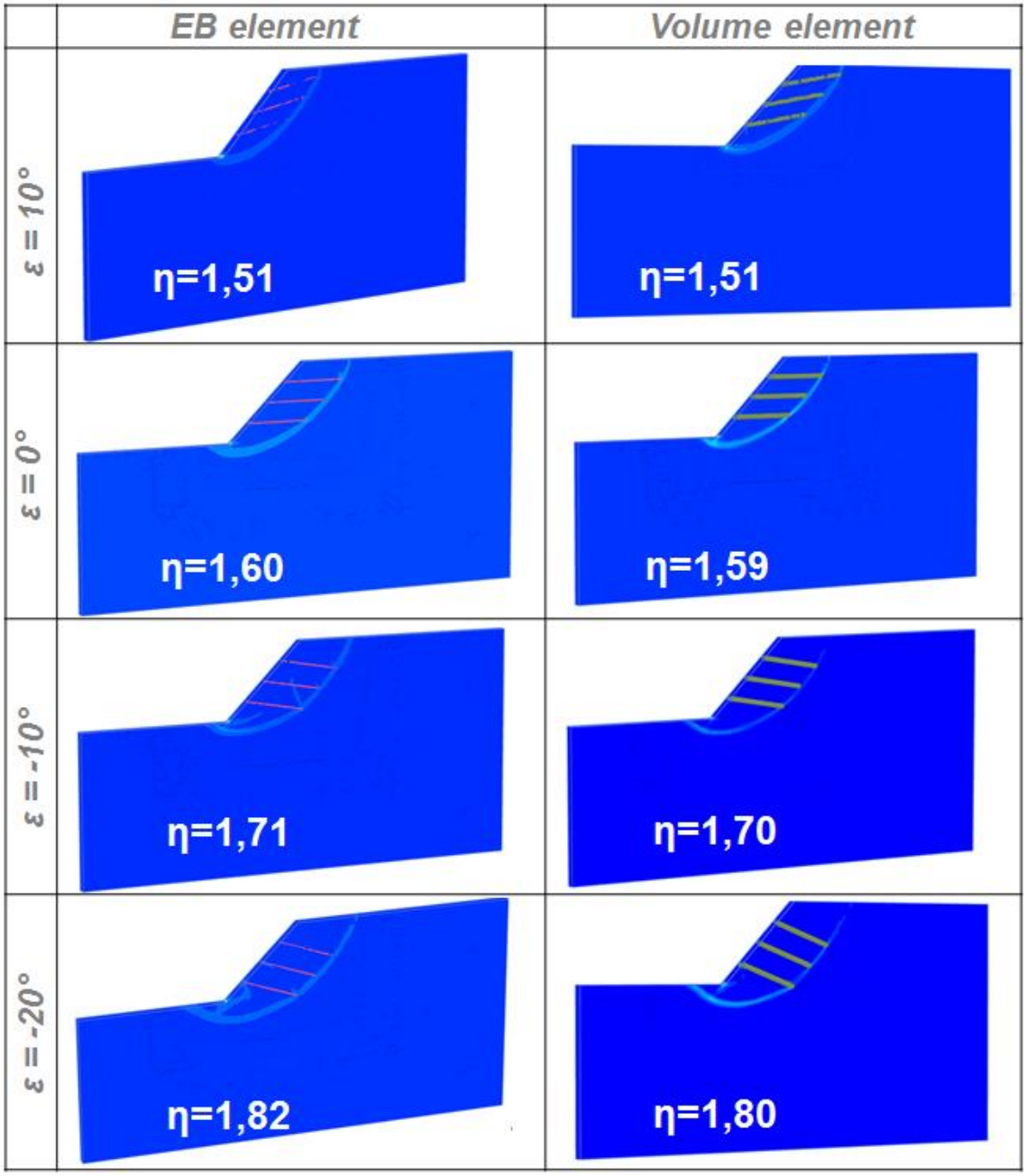

Fig. 75 Incremental shear strains - inclination study (case 3 - 3D) – associated

When comparing 2D and 3D calculation, corresponding results are obtained for inclinations of 10 and 0°. A difference of about 2% is obtained for inclination of -10° and -20°. All in all a good correspondence between 2D and 3D FOS_{FE} results is achieved.

The FOS_{FE} results for non-associated conditions can be found in appendix 8.4.

5.3.4 Results of out-of-plane study

The parameter study on the out-of-plane distance (L_S) is performed with a nail inclination of -10°. The 3D calculations are performed with plates, EBs and volume elements. For the 2D approach, embedded beam rows are used as support types. To achieve 3D effects, the (axial and lateral) skin resistance is manipulated. As shown in Tab. 25, the lateral skin resistance has a minimal influence on the FOS_{FE} results.

The corresponding $FOS_{FE,3D}$ developments for EBs and volume elements are shown in Fig. 75. The dotted lines in Fig. 75 represent the corresponding $FOS_{FE,3D}$ developments of 'no support' cases (no nails are installed) for all used models. A visualization of the failure surfaces is provided in Fig. 78 for EB and volume elements. The size of the failure surface decreases with increasing L_S.

Fig. 77 shows that the 2D and 3D results for EBs and volume elements correspond if T_{skin} is 20.0kN/m (T_{lat} = unlimited).

The FOS_{FE} results for non-associated conditions can be found in appendix 8.4.

Tab. 25 FOS_{FE}-results of out-of-plane study for ε = -10° (associated)

	2D - Case 3 (associated)				**3D -** Case 3 (associated)		
	EBR						
	T_{skin} = unlimited T_{lat} = **1.0** [kN/m]	T_{skin} = **1.0** [kN/m] T_{lat} = unlimited	T_{skin} = **5.0** [kN/m] T_{lat} = unlimited	T_{skin} = **20.0** [kN/m] T_{lat} = unlimited	**Plate**	**EB**	**Volume element**
No nails	1.44				1.44		
L_s = 0.5 m	1.72	1.60	1.69	1.72	1.72	1.72	1.71
L_s = 1.0 m	1.72	1.57	1.66	1.71	1.71	1.70	1.70
L_s = 3.0 m	1.72	1.55	1.60	1.67	1.71	1.67	1.67
L_s = 12.0 m	1.72	1.51	1.52	1.56	1.71	1.57	1.55

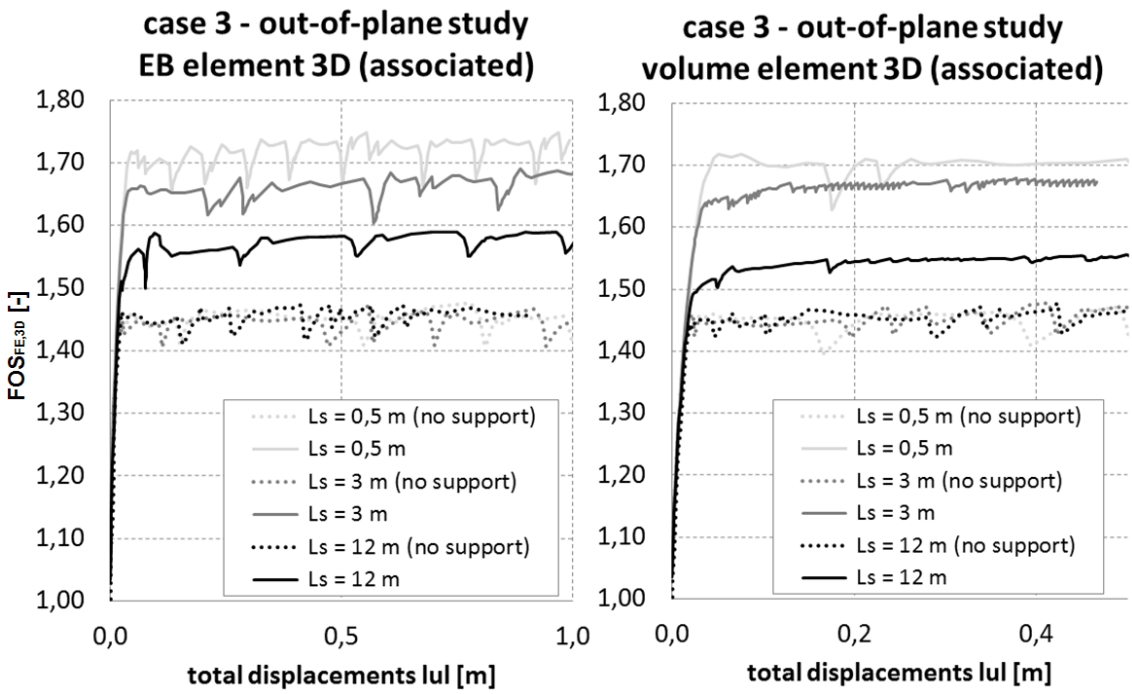

Fig. 76 FOS-development for out-of-plane study– EB and volume elements 3D (associated)

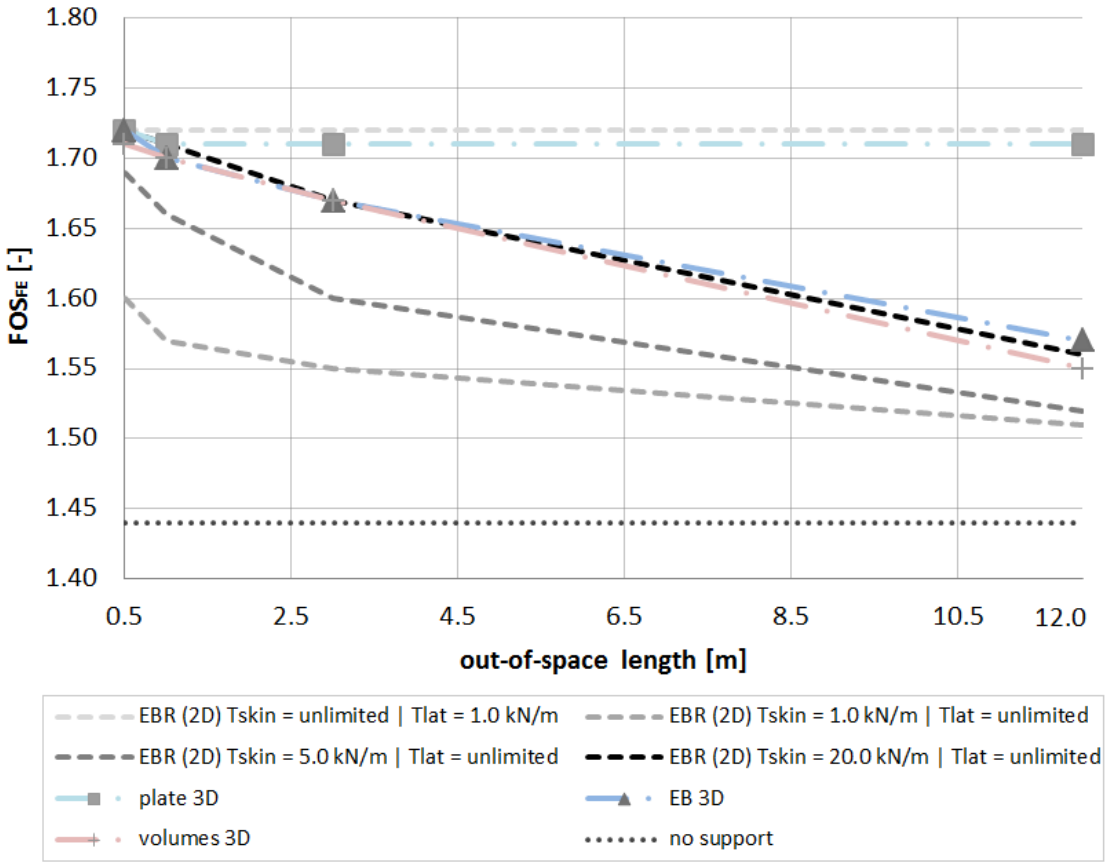

Fig. 77 FOS-distribution - out-of-plane study (case 3 – 2D/3D) - associated

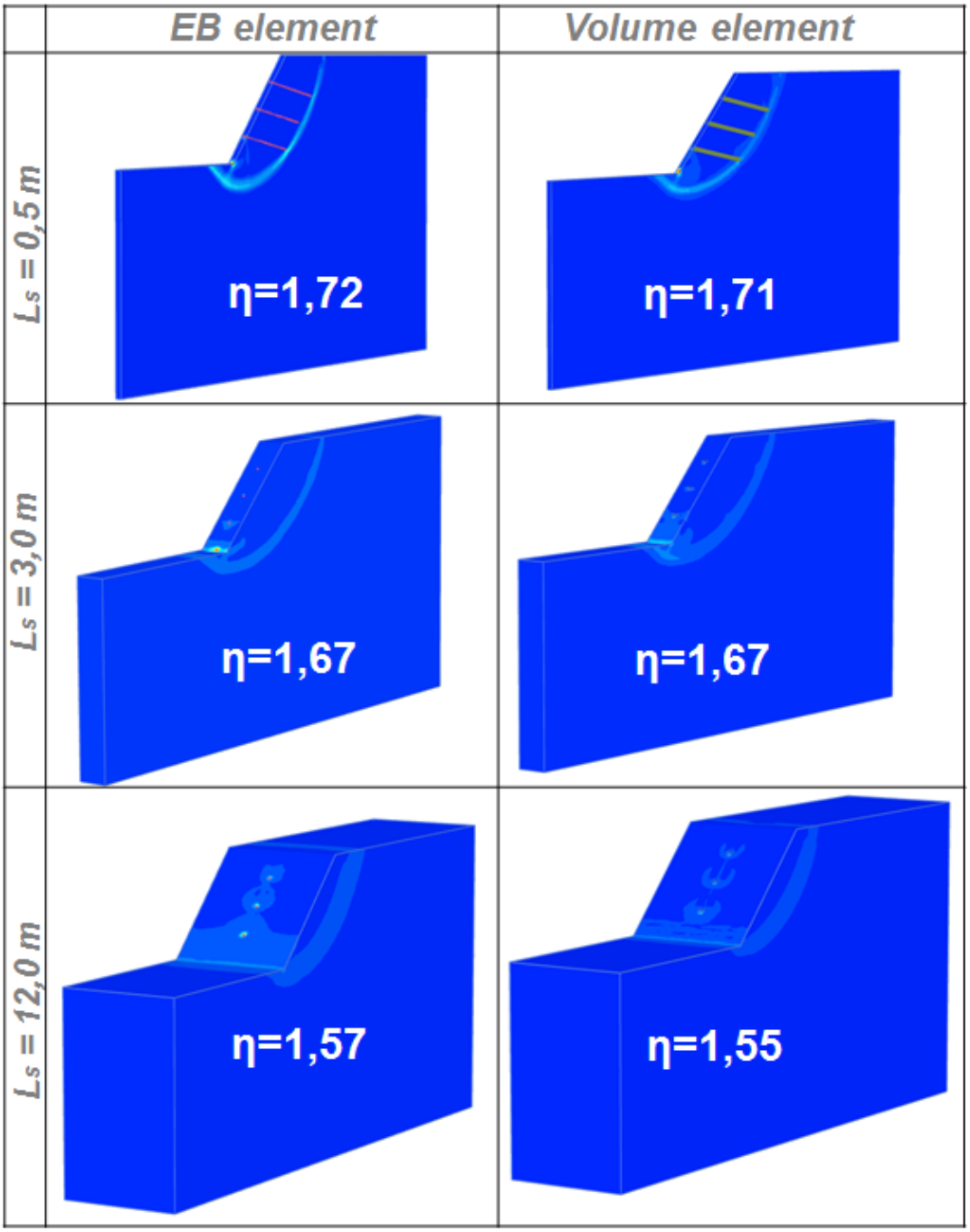

Fig. 78 Incremental shear strains – out-of-pane study (case 3 - 3D) – associated

5.4 Validation of out-of-plane spacing in 3D

This numerical study provides a verification of the results of 'case 4 – with facing' (PLAXIS 2D, chapter 4.6.3.2) by means of a 3D FE analysis. Four different out-of-plane spacings (L_s) are investigated in PLAXIS 3D, using embedded beams and volume elements as support types. An associated flow rule is applied to the calculated models.

The main focus lies on the comparison of FOS, obtained from 2D and 3D simulations. An evaluation of the 3D failure mechanism is additionally provided.

5.4.1 Description of the FE model

Fig. 79 illustrates a longitudinal cross section of the geometry including the FE mesh. A slope height of 2 m and a slope inclination of 30° are used. The vertically constructed support element is placed in the middle of the slope. From the gained experiences of the 2D simulations of case 4, a rigid facing is applied along the slope. To perform a variation of out-of-plane distances of nails, four PLAXIS models are used with widths of 0.5 m, 1.0 m, 3.0 m, and 12.0 m.

The FEM structures consist of a varying number of 10-noded elements. A very fine mesh is used with refinements around the slope (coarseness factor: 0.4/0.2) and along the soil nails (coarseness factor: 0.1).

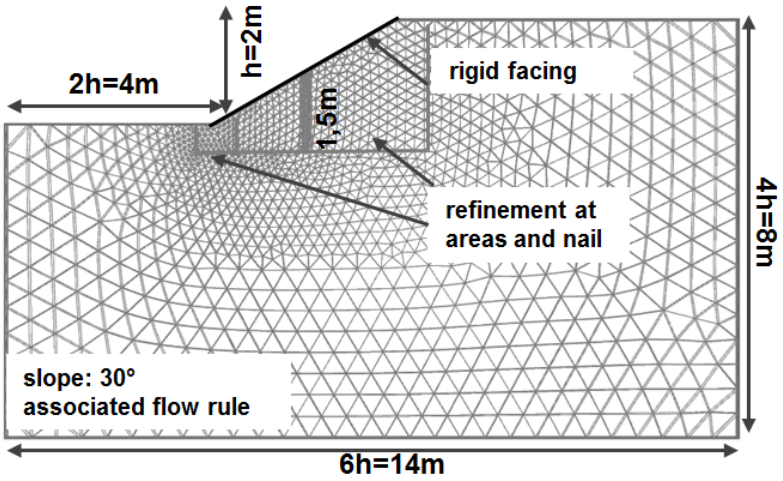

Fig. 79 Profile view and FEM mesh for case 4 3D – with facing

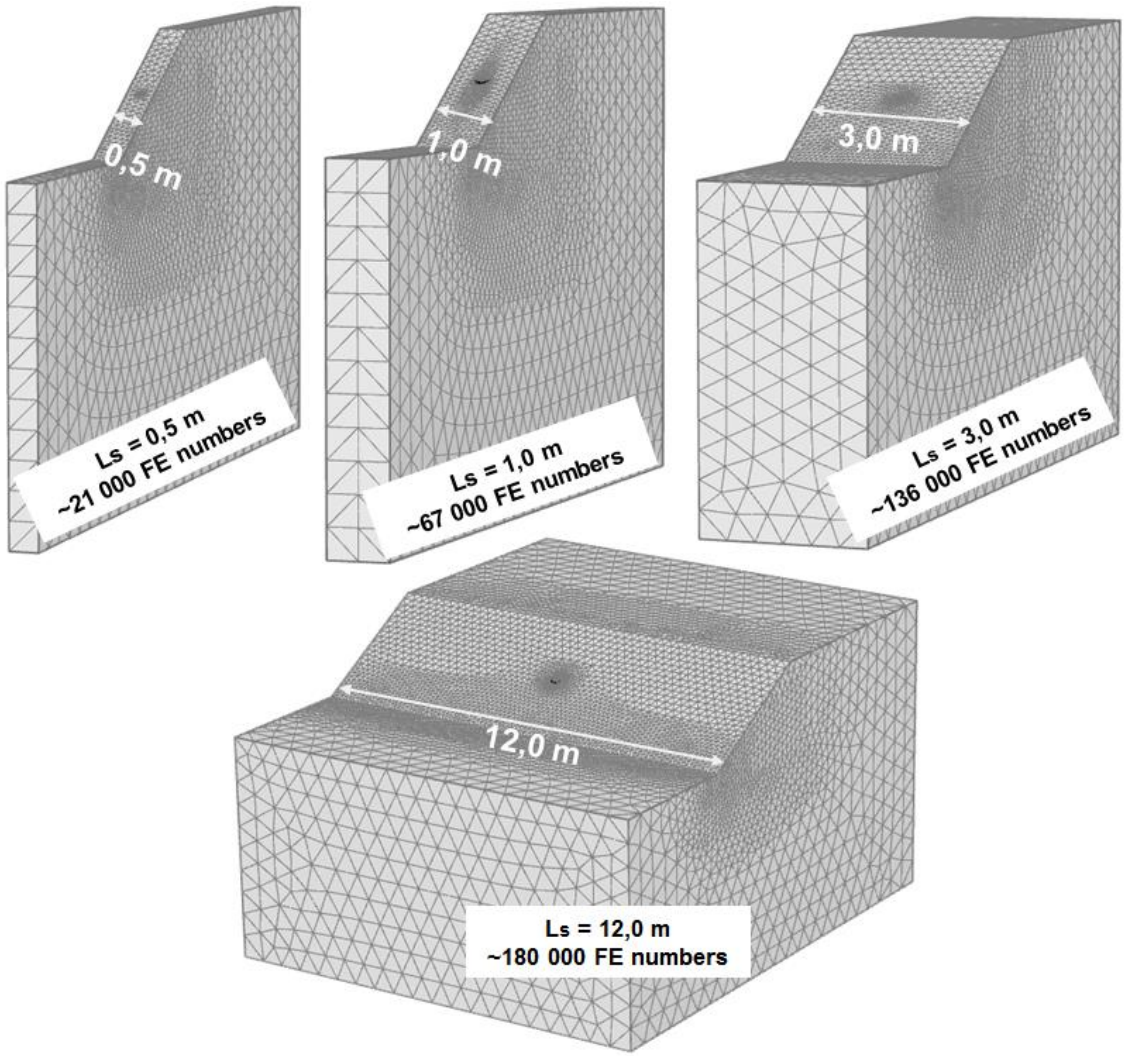

Fig. 80 Geometry and FEM mesh for the used out-of-plane distances

5.4.2 Input parameters

The material set for case 4 is summarised in Tab. 26. The 3D study is performed with EBs and volume elements. The influence of axial skin resistance of EBs is neglected by setting a high value. For the volume elements used in PLAXIS 3D a non-porous drainage type is selected with a linear elastic material model.

Embedded beam rows are used as support types for the 2D approach (chapter 4.6.2.).

Tab. 26 Material parameters for case 4 (PLAXIS 3D) – associated

Soil	**Symbol**	**Unit**	**Mat. Set**
strength model	-	-	MC
stiffness	E'	kN/m²	40 000
Poisson ratio	ν'	-	0.3
Cohesion	c'	kN/m²	2
Unit weight	$\gamma_{unsat}/\gamma_{sat}$	kN/m³	17
Friction angle	φ'	°	30
Dilatancy angle	ψ'	°	30
Rigid facing (plate)	**Symbol**	**Unit**	**Mat. Set**
Equivalent thickness	d	m	0.1
Unit weight	γ	kN/m³	0
Young's modulus	E	kN/m²	2.1*E7
Poisson ratio	ν'	-	0.2
Nail (EB)	**Symbol**	**Unit**	**Mat. Set**
Young's modulus	E	kN/m²	2.1*E7
Unit weight	γ	kN/m³	25
Diameter	D	m	0.1
Axial skin resistance	T_{skin}	kN/m	500
Base resistance	F_{max}	kN	0
Nail (soil – volume element)	**Symbol**	**Unit**	**Mat. Set**
strength model	-	-	Linear elastic
stiffness	E'	kN/m²	2.1*E7
Poisson ratio	ν'	-	0.2
Unit weight	$\gamma_{unsat}/\gamma_{sat}$	kN/m³	25
Interface reduction factor	R_{inter}	-	1.0

5.4.3 Results

The FOS_{FE} results (2D and 3D analysis) are summarised in Tab. 27 for associated conditions. The corresponding $FOS_{FE,3D}$ developments for EBs and volume elements are shown in Fig. 81. Fig. 82 represents a zoom of the $FOS_{FE,3D}$ developments of the 'no support' cases (no installation of rigid facing and nails) for every model. A visualisation of the failure mechanisms for EBs and volume elements is provided in Fig. 83 and Fig. 84.

Due to the orientation of the nail, the axial skin resistance has a minor influence on the FOS_{FE} values (see Tab. 27).

Fig. 85 compares FOS_{FE}-distribution of 2D-EBR analyses (T_{skin} = unlimited | T_{lat} = 15.0 kN/m) and the computations. This comparison indicates that EBRs are able to consider

3D effects with the manipulation of the skin resistances. The 2D and 3D results for EBs and volume elements correspond if T_{lat} is 5.0kN/m (T_{skin} = unlimited).

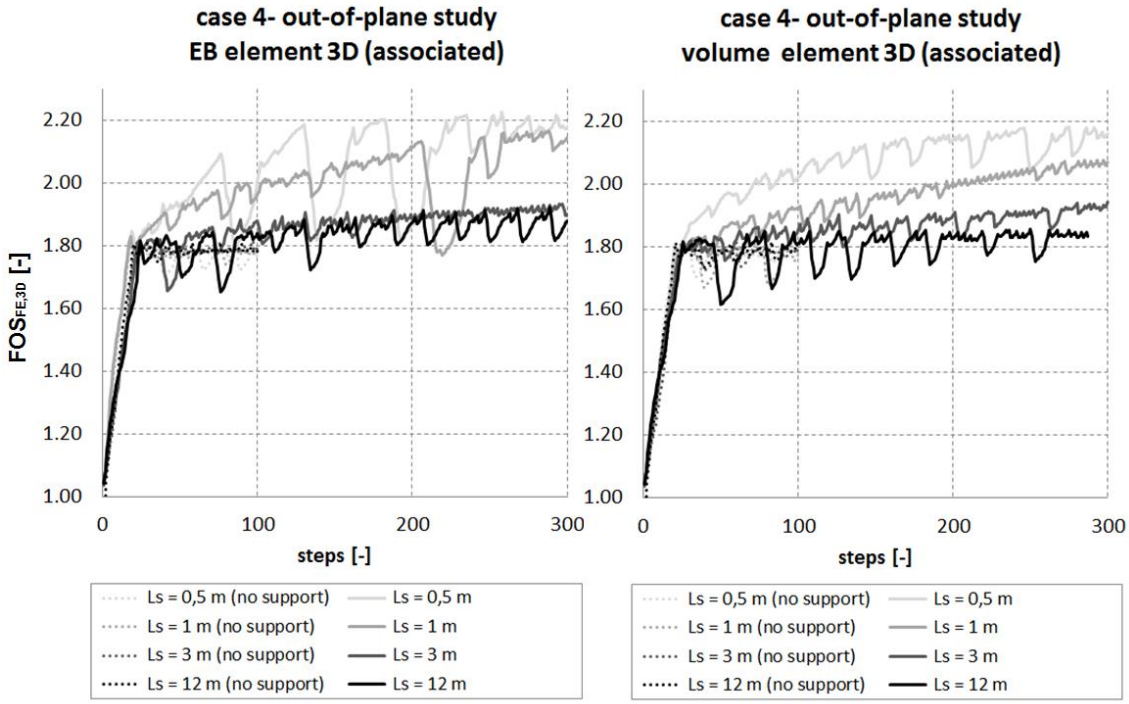

Fig. 81 FOS-development – case 4 with facing 3D – EB and volume elements (associated)

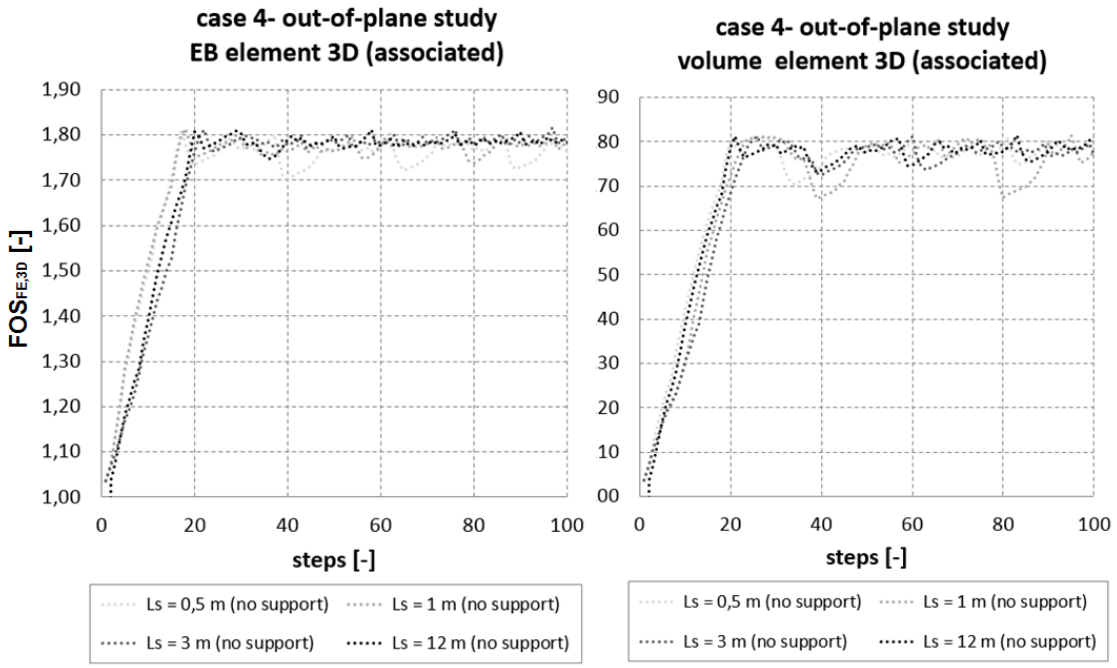

Fig. 82 FOS-development – case 4 no support 3D – EB and volume elements (associated)

Tab. 27 FOS_{FE}-results of out-of-plane study – case 4 with facing (2D/3D) associated

	2D - Case 4 –with facing (associated)				**3D -** Case 4 - with facing (associated)	
	EBR					
	T_{skin} = **1.0** [kN/m]	T_{skin} = unlimited	T_{skin} = unlimited	T_{skin} = unlimited	**EB**	**Volume element**
	T_{lat} = unlimited	T_{lat} = **5.0** [kN/m]	T_{lat} = **10.0** [kN/m]	T_{lat} = **15.0** [kN/m]		
No nails	1.78				1.78	
L_s = 0.5 m	2.17	2.14	2.16	2.17	2.20	2.16
L_s = 1.0 m	2.17	2.09	2.12	2.14	2.14	2.10
L_s = 3.0 m	2.17	1.94	2.03	2.09	1.92	1.94
L_s = 12.0 m	2.17	1.82	1.87	1.91	1.86	1.84

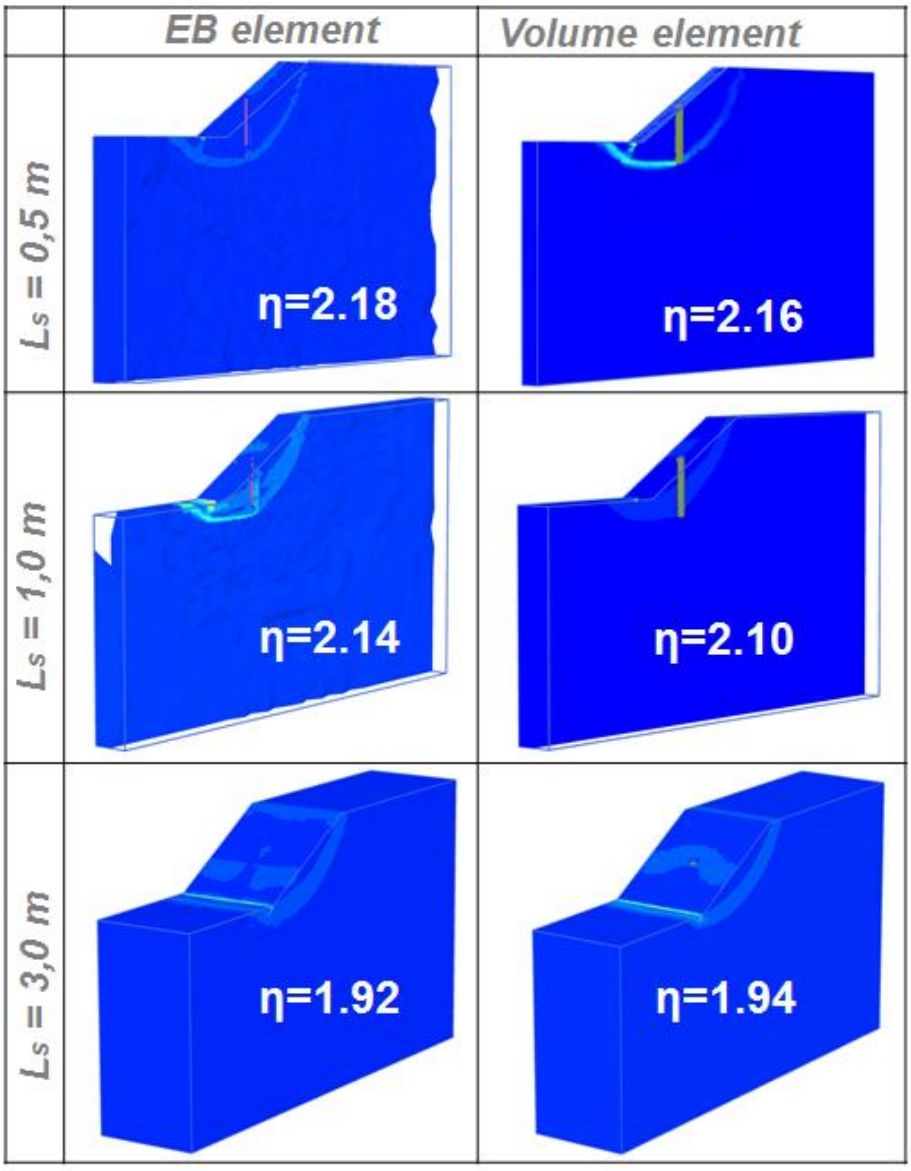

Fig. 83 Incremental shear strains – case 4 with facing 3D (associated) – L_s = 0.5/1.0/3.0 m

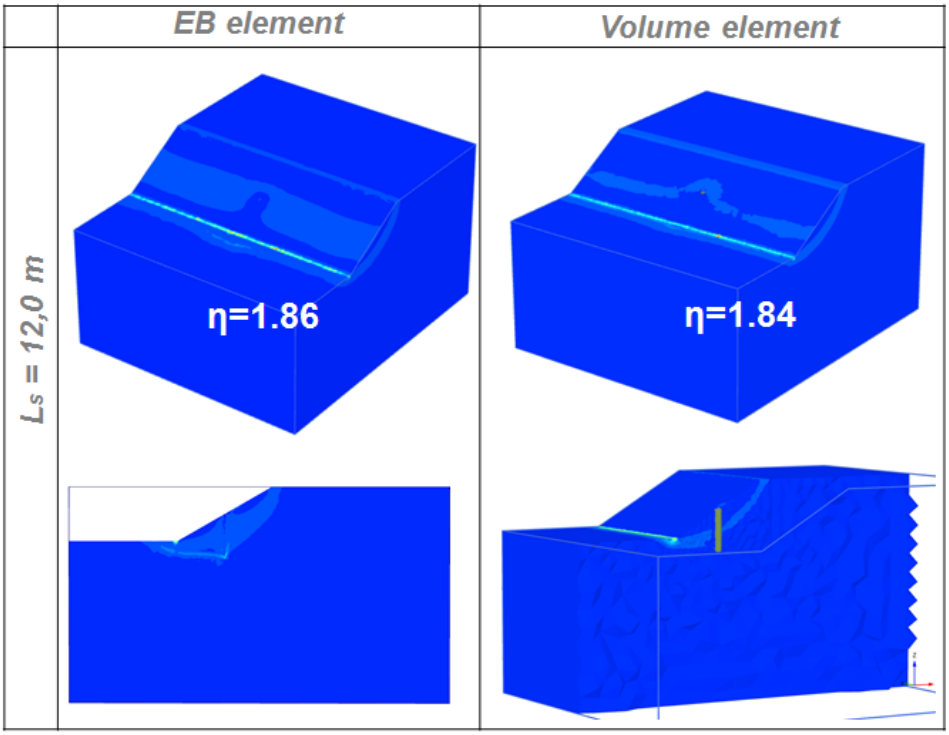

Fig. 84 Incremental shear strains – case 4 with facing 3D (associated) – L_s = 12.0 m

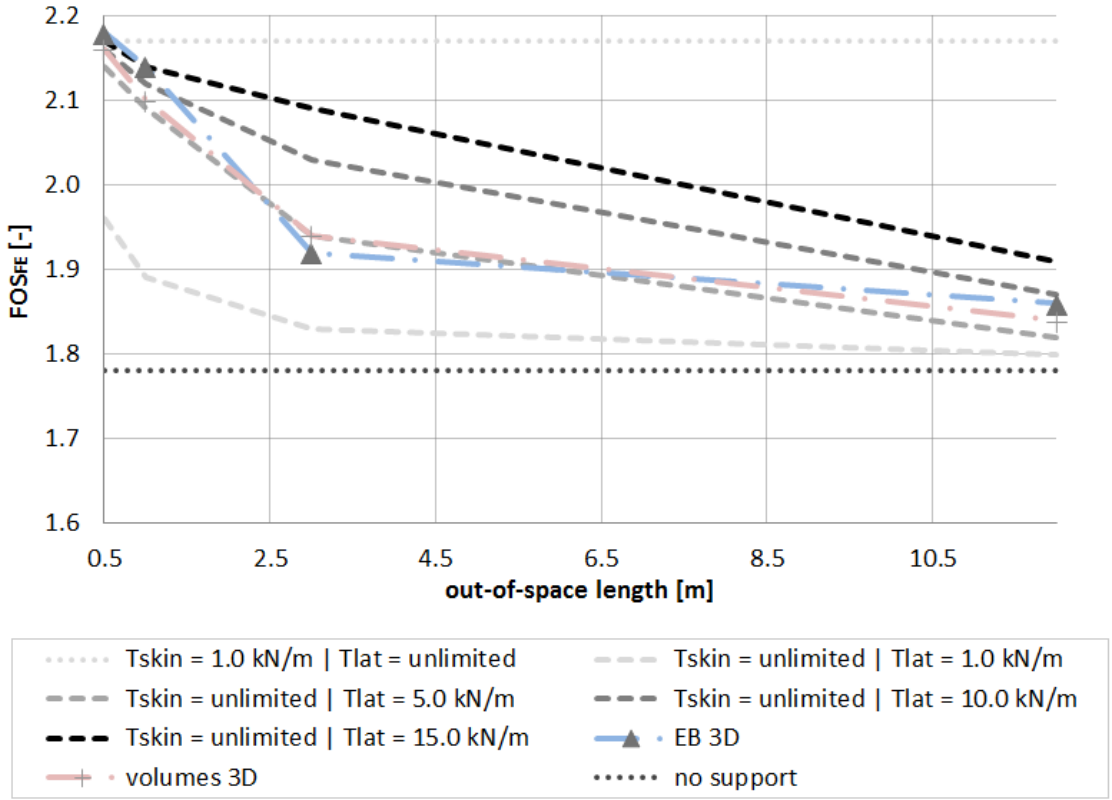

Fig. 85 FOS-distribution - case 4 with facing 2D/3D (associated)

6 Conclusion

This thesis deals with numerical studies on the behaviour of soil nails as well as a comprehensive review and comparison of current calculation methods. Additionally, the implementations of soil nails in analytical and numerical programs are investigated.

First, the theoretical background regarding load transfer concepts in soil-nailed structures was discussed. Chapter 2 covers nail tension distribution, bending stiffness and shear stress in nails as well as failure modes of soil nailed structures.

After discussing the theoretical background, the validation of the limit equilibrium (LE) programs SLIDE and GGU was done to reveal how soil nails are implemented in analytical programs. The comparative simulations showed that SLIDE and GGU use the same equations according to German standards (DIN 4084) to define the factor of safety. Renk's approach of defining the safety reduction on soil nails delivers a noticeable overestimation of the factor of safety.

Further, comparative studies on the LE method and FE method were done. Those studies gave a correspondence (between LE and FE analysis of FOS) when using a homogenous soil and an associated flow rule ($\psi=\varphi$). An associated and non-associated case study was elaborated as well. With an increasing friction angle φ, the influence of a non-associated flow rule on the FOS increases as well (Tschuchnigg & et al., 2015). Due to the lack of a bending stiffness, it is not recommended to use geogrids for modelling soil nails.

The investigation of the nail orientation using PLAXIS 2D showed, that upward inclined soil nails (with elastic behaviour) produced the most unfavourable failure surface among all analyses. Interpreting the evaluation of elastoplastic soil nail behaviour leads to the conclusion, that the bending stiffness has a low impact on the overall stability.

To compare simplified 2D plane strain models and 3D models, parametric studies on the out-of-plane distance were conducted in PLAXIS 2D. When using plate or geogrid elements to model soil nails, 3D characteristics are not considered. The 2D embedded beam row (EBR) enables a consideration of 3D effects with a 2D plane strain model. It was shown that the FOS decreases with an increasing distance between the nails. The results of the 2D analyses were verified with 3D simulations in PLAXIS 3D. Good agreement was achieved when optimising the axial and lateral skin resistance factors

of a 2D EBR. Nevertheless, the input of the lateral skin resistant values (T_{lat}) for EBRs is uncertain and requires more research.

This is why future works could include deeper parameter studies on the behaviour of embedded beam rows. Further work could also focus on the determination of force distributions along soil nails.

7 Literature

Bridle, R., & Barr, B. (1990). *the analysis and design of soil nails: Performance of reinforced soil structures.* British Geotechnical Society.

Brinkgreve, R., & et al. (2015). *PLAXIS 2D 2015 - User Manual.* Deltf, The Netherlands: Plaxis bv.

Brinkgreve, R., & et al. (2015). *PLAXIS 3D - Reference Manual.* Delft, The Netherlands: Plaxis bv.

Cheng, Y., Lansivaara, T., & Wei, W. (2006). *Two-dimensional slope stability analysis by limit equilibrium and strength reduction methods.* Hong Kong: Computers and Geotechnics 34 (2007) 137–150.

Clouterre. (1991). *Recommendation Clouterre 1991.* Paris: Presses de l' ENPC.

Esterhuizen, J., Filz, G., & Duncan, J. (2001). *Constitutive Behaviour of Geosynthetic Interfaces.* Journal of GeoTechnical and Geoenvironmental Engineering.

FHWA. (2003). *Geotechnical Engeneering Circular No.7 : Soil Nail Walls.* Columbia, Maryland: GeoSyntec Consults.

Gässler, G. (1987). *Vernagelte Geländesprünge - Tragverhalten und Standsicherheit.* Universität Fridericiana Karlsruhe: PhD thesis.

GGU. (2014). GGU-STABILITY, Version 10. In *Slope stability analysis and analysis of soil nailing and reinforced earth walls to DIN 4084 and EC 7.* Steinfeld: Civilserve GmbH.

Jewell, R., & Pedley, M. (1990). *Soil nailing design: the role of bending stiffness.* Ground Eng.

Jewell, R., & Pedley, M. (1992). *Analysis for soil reinforcement with bending stiffness.* J Geotech Eng ASCE.

Juran, I. (1990). *Kinematical limit analysis for design of soil.nailed structures.* Journal of the Geotechnical Engineering.

Juran, I., & Elias, V. (September 1990). *Behaviour and working stress design of soil nailed structures.* British Geotechnical Society.

Marte, R. (2014). *Anchorage: (grouted anchors, injection piles, soil nails) acc. to ÖNORM B 1997-1-1:2013.* Graz University of Technology: Institute for Soil Mechanics and Foundation Engineering.

Renk, D. (2011). *PhD thesis: Zur Statik der Bodenvernagelung.* Innsbruck: Berlin Logos. ISBN 978-3-8325-2947-5.

Schweiger, H. F. (2014). *Steifigkeit von Böden.* Graz University of Technology: Institute for Soil Mechanics and Foundation Engineering.

SLIDE. (2016). *Rocscience Inc., Canada*. Retrieved from Slide, User's Guide, Geomechanics Software Solution: www.rocscience.com

Sluis, J. (2012). *Validation of Embedded Pile Row in PLAXIS 2D.* Delft: Delft University of Technology.

Tschuchnigg, F. (2013). *3D Finite Element modelling of Deep Foundations Employing an Embedded Pile Formulation.* TU Graz: Gruppe Geotechnik Graz.

Tschuchnigg, F., & et al. (2015). *Comparison of finite-element limit analysis and strength reduction techniques.* Geotechnique 65, No. 4, 249–257.

8 Appendix

List of figures appendix

List of tables appendix

8.1 Appendix chapter 4.2 – rigid facing

Tab. A 1 Material parameters for case 1 – rigid facing analysis

Soil	**Symbol**	**Unit**	**Mat. Set**
Strength model	-	-	MC
Stiffness	E'	kN/m²	40 000
Poisson ratio	ν'	-	0.3
Cohesion	c'	kN/m²	0.1
Unit weight	$\gamma_{unsat}/\gamma_{sat}$	kN/m³	17
Friction angle	φ'	°	35
Dilatancy angle	ψ'	°	35
Rigid facing (plate element)	**Symbol**	**Unit**	**Mat. Set**
Axial stiffness	EA	kN/m	2 100 000
Bending stiffness	EI	kN m²/m	1750
weight	w	kN/m/m	0
End bearing	-	-	on/off

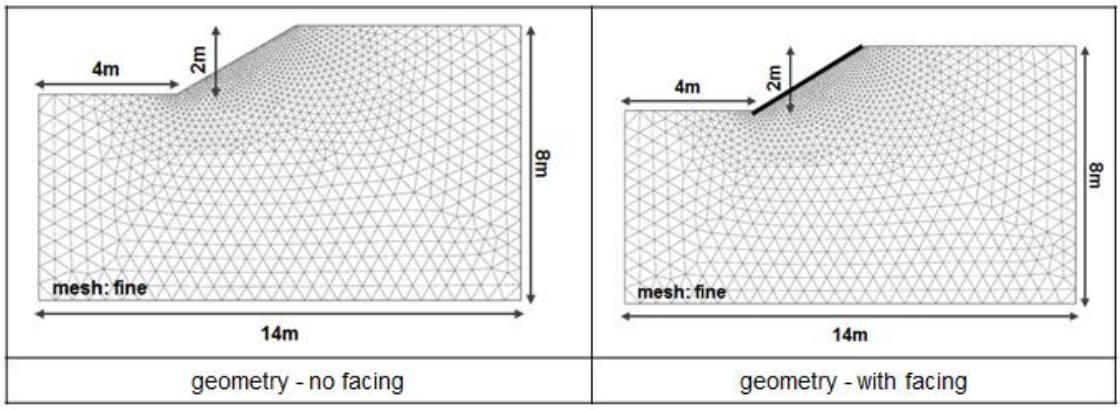

Fig. A 1 Geometry and FEM mesh for case 1 – rigid facing analysis

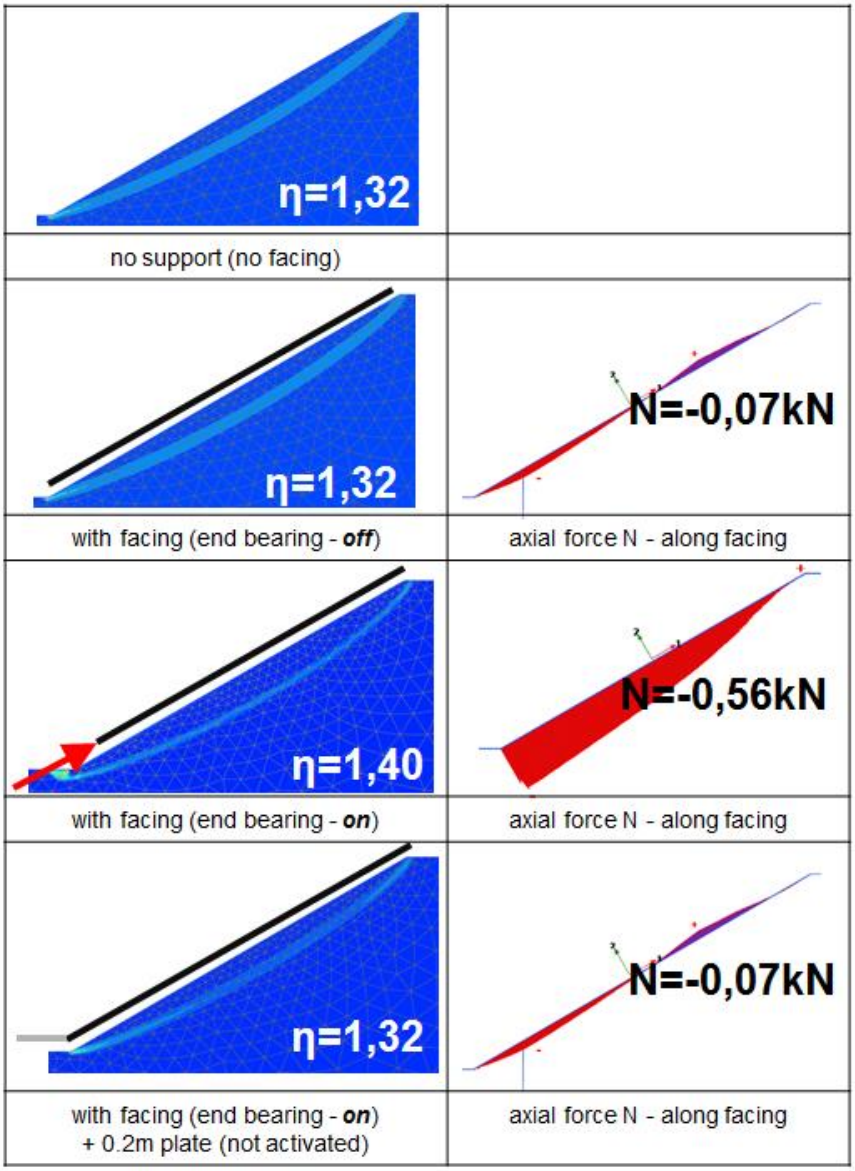

Fig. A 2 Incremental shear strains and axial force distribution case 1 – rigid facing analysis

8.2 Appendix chapter 4.3

This parametric study on mesh discretisation and cohesion relies to case 1.

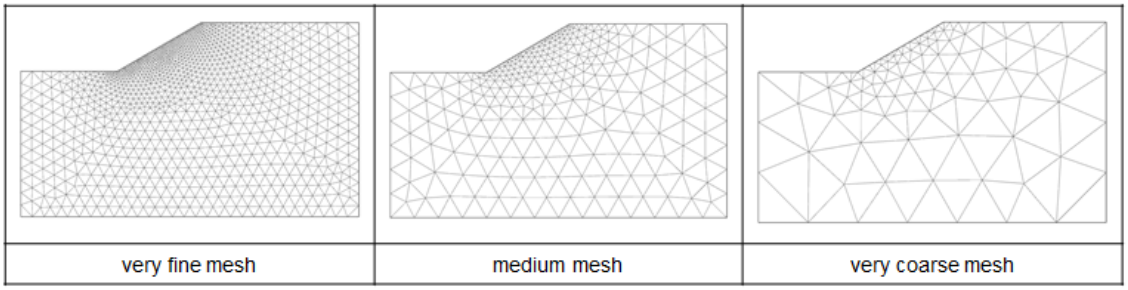

Fig. A 3 Mesh coarseness for case 1

Tab. A 2 FOS_{FE} depending on mesh discretisation and cohesion – case 1

	Case 1 (associated)			Case 1 (non-associated)		
	Very fine	**medium**	**Very coarse**	**Very fine**	**medium**	**Very coarse**
c = 0.01 [kN/m²]	1.24	1.24	1.24	1.13	1.18	1.20
c = 0.1 [kN/m²]	1.32	1.32	1.33	1.21	1.23	1.26
c = 1.0 [kN/m²]	1.72	1.72	1.74	1.60	1.64	1.66
c = 2.0 [kN/m²]	2.04	2.05	2.05	1.95	1.97	2.00
c = 5.0 [kN/m²]	2.81	2.81	2.81	2.76	2.77	2.78
c = 10.0 [kN/m²]	3.91	3.92	3.92	3.88	3.87	3.88

8.3 Appendix chapter 4.6

8.3.1 Plate without facing

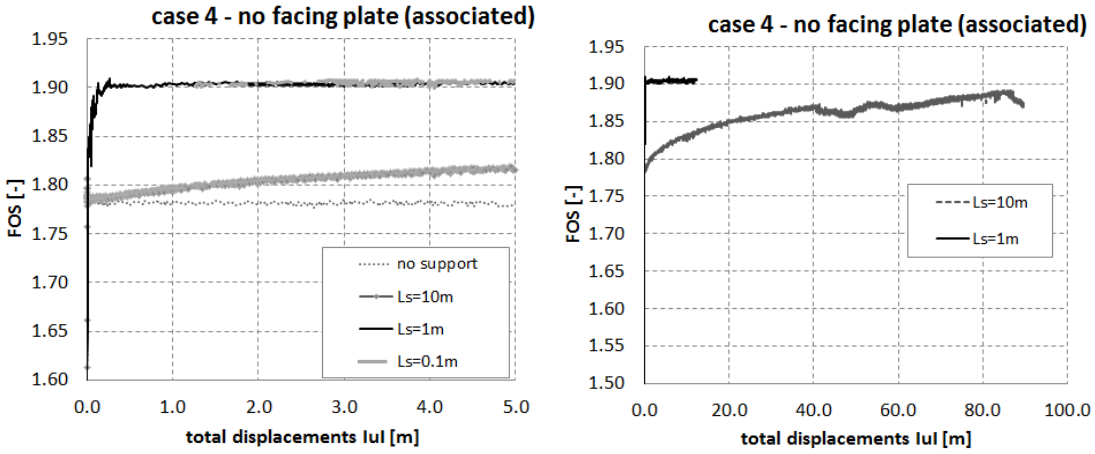

Fig. A 4 FOS-development without facing – plate (associated)

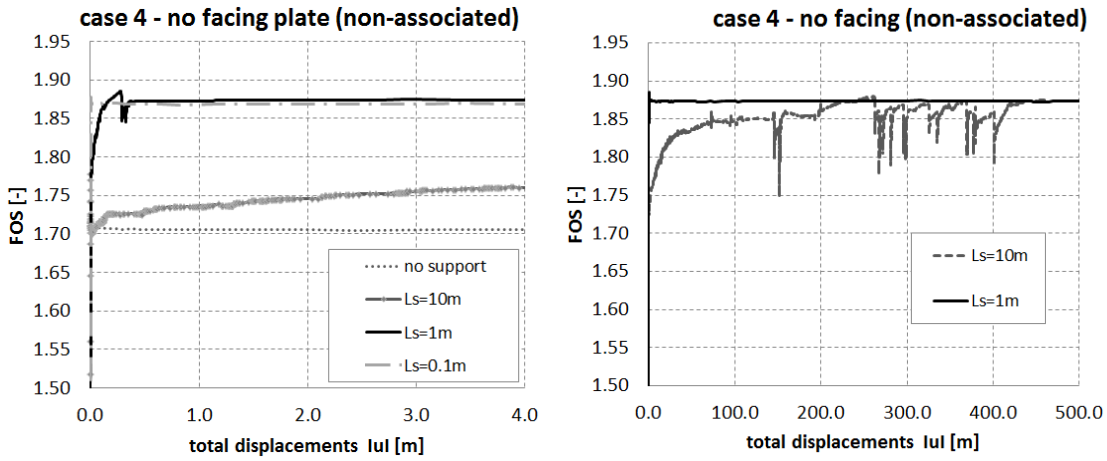

Fig. A 5 FOS-development without facing – plate (non-associated)

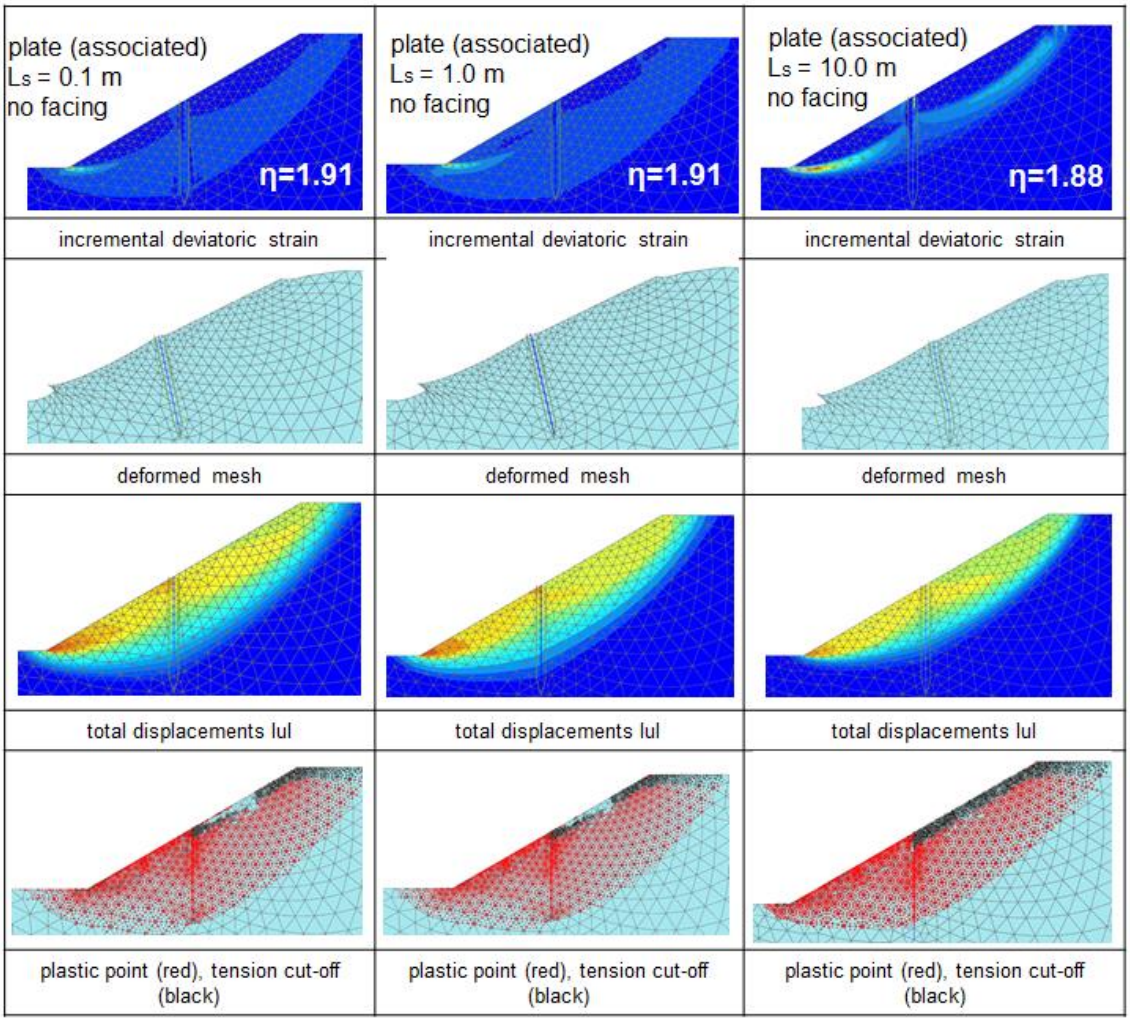

Fig. A 6 Evaluation of failure mechanism without facing - plate (associated)

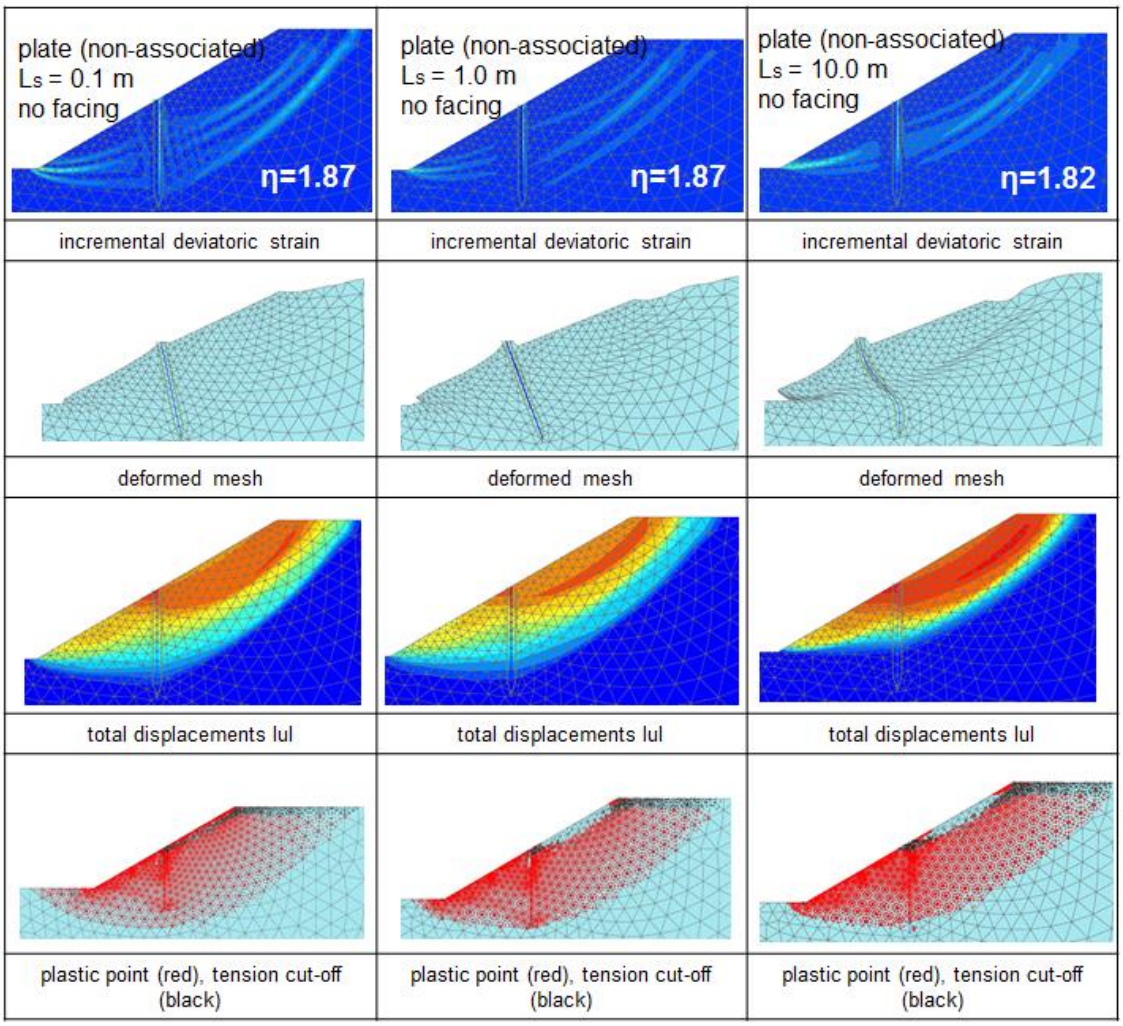

Fig. A 7 Evaluation of failure mechanism without facing -plate (non-associated)

8.3.2 Plate with facing

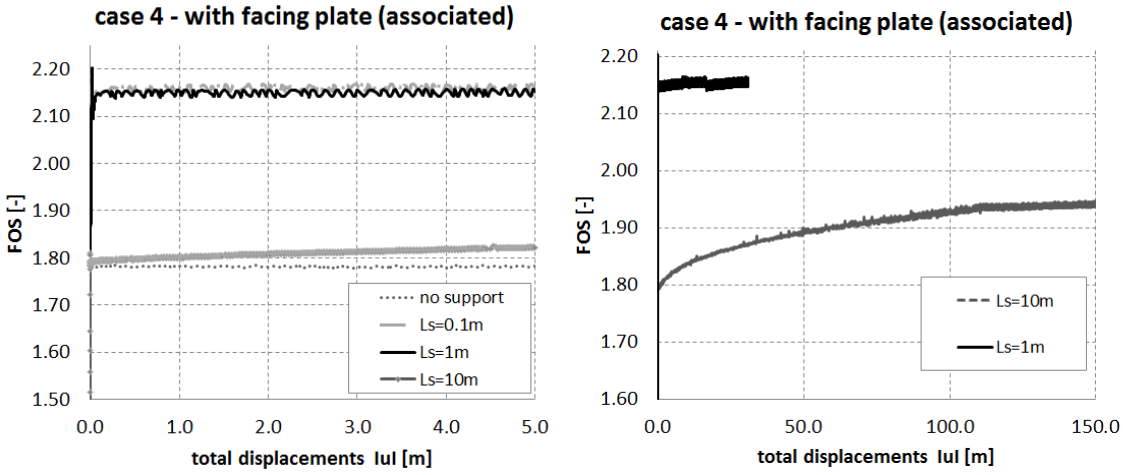

Fig. A 8 FOS-development with facing – plate (associated)

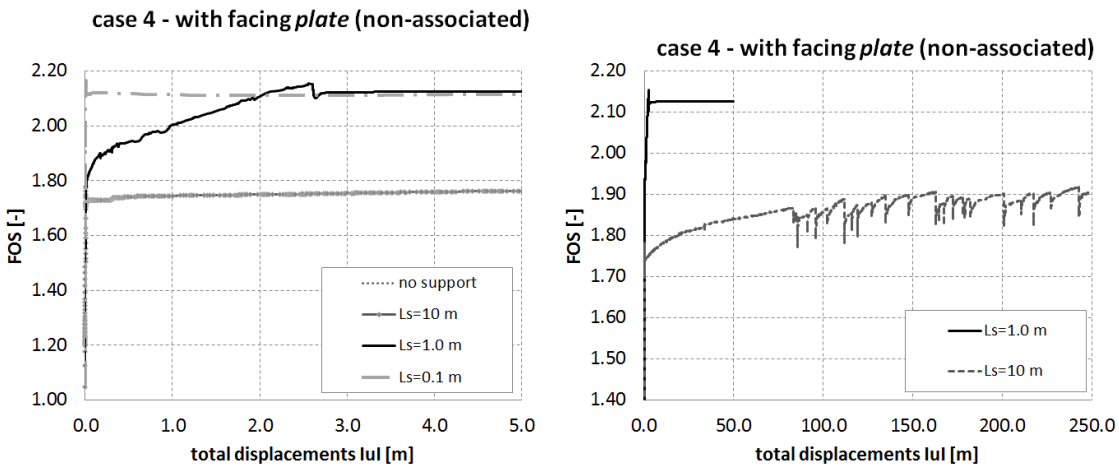

Fig. A 9 FOS-development with facing – plate (non-associated)

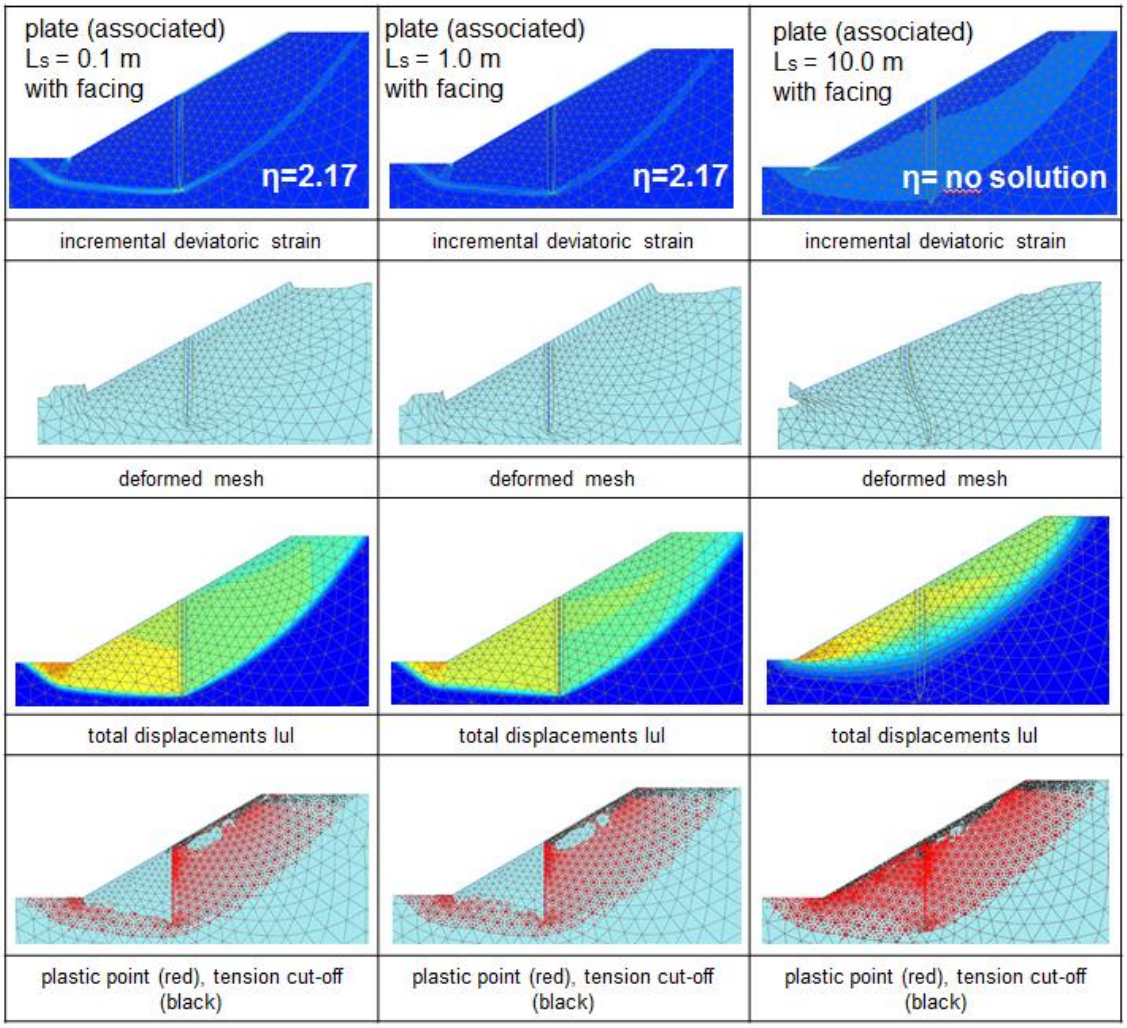

Fig. A 10 Evaluation of failure mechanism with facing -plate (associated)

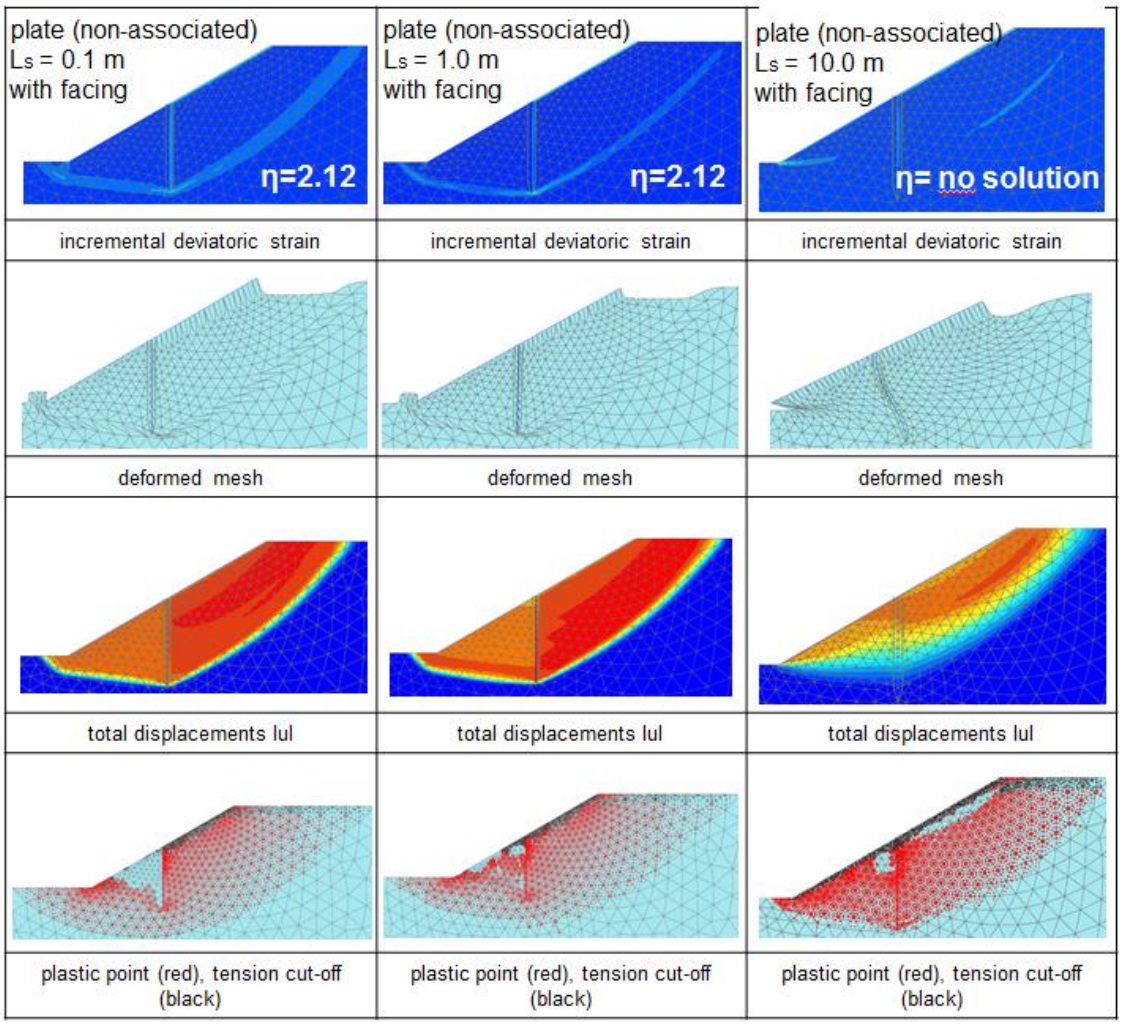

Fig. A 11 Evaluation of failure mechanism with facing -plate (non-associated)

8.4 Appendix chapter 5.3

8.4.1 Results of inclination study (non-associated)

Tab. A 3 FOS_{FE}-results of different nail inclinations for L_s = 1 m (non-associated)

	2D - Case 3 (non-associated)			**3D** - Case 3 (non-associated)	
	Geogrid	**Plate**	**EBR**	**EB**	**Volume element**
No nails	1.38			1.40	
ε = 10°	1.47	1.47	1.48	1.47	1.47
ε = 0°	1.56	1.56	1.56	1.57	1.56
ε = -10°	1.69	1.69	1.70	1.70	1.68
ε = -20°	1.80	1.81	1.82	1.82	1.79

8.4.2 Results of out-of-plane study (non-associated)

Tab. A 4 FOS_{FE}-results of out-of-plane study for ε = -10° (non-associated)

	2D - Case 3 (non-associated)				**3D** - Case 3 (non-associated)	
	EBR					
	T_{skin} = unlimited	T_{skin} = **1.0** [kN/m]	T_{skin} = **5.0** [kN/m]	T_{skin} = **20.0** [kN/m]	**EB**	**Volume element**
	T_{lat} = **1.0** [kN/m]	T_{lat} = unlimited	T_{lat} = unlimited	T_{lat} = unlimited		
No nails	1.38				1.40	
L_s = 0.5 m	1.70	1.57	1.67	1.70	1.72	1.69
L_s = 1.0 m	1.70	1.54	1.64	1.69	1.70	1.68
L_s = 3.0 m	1.70	1.53	1.58	1.65	1.67	1.65
L_s = 12.0 m	1.70	1.53	1.53	1.57	1.56	1.51